STELLAR WINDS

by

MARTIN R. MURCH

B.Sc., University of Sussex, 1968

A THESIS SUBMITTED IN PARTIAL FULFILLMENT

OF THE REQUIREMENTS OF THE DEGREE OF

MASTER OF SCIENCE

in the Department

of

Physics

We accept this thesis as conforming

to the required standard

[redacted]

Accepted by the Faculty of Graduate Studies

on 13 May 1971 by [redacted] Dean of Faculty

UNIVERSITY OF VICTORIA

MAY 1971

Supervisor: Dr J.A. Burke

ABSTRACT

The phenomenon of mass loss from stars is surveyed. It is shown to be of widespread occurrence and, in many cases, to be of sufficient magnitude to alter significantly the course of stellar evolution. A considerable number of different mechanisms appear to be responsible for mass ejection; from these the thermally driven mechanism, believed to be responsible for the solar wind, is chosen for detailed investigation.

The observed characteristics of the solar corona and solar wind are reviewed, and the observational results are used to show, by means of kinetic theory, that the solar wind flow is most appropriately treated by means of hydrodynamics.

Solutions of the hydrodynamic equations are obtained on the assumptions that the only heating effect above the base of the corona is due to thermal conduction, and that the thermal conduction flux tends to zero at infinite distances from the star.

Models corresponding to the solar wind are produced which indicate a rate of mass loss from the sun of about 3.3×10^{-14} $M_{\odot}$/year, in reasonable agreement with space flight observations. There are indications that the non-thermal heating mechanisms responsible for the high coronal temperatures extend for a considerable distance into the solar wind.

Empirical relationships deduced from these models indicate that thermally driven stellar winds from hot, dense coronas may be capable of causing quite considerable rates of mass loss.

ACKNOWLEDGEMENTS

I would like to thank my supervisor, Dr J.A. Burke, for the invaluable help and advice he has given me during the research and the writing of this thesis.

I would also like to express my gratitude to the members of my supervisory committee, Drs J.L. Climenhaga, H.W. Dosso, F.D.A. Hartwick, and J.B. Hutchings for their helpful criticism and comments.

Finally I would like to thank my wife, Rosemary, for her help with the graphs and for doing much of the typing.

TABLE OF CONTENTS

LIST OF TABLES

LIST OF FIGURES

LIST OF SYMBOLS

A	Relation between independent variables x and r. $x = A/r$, $A = GM_{\odot}M/kT_{o}$.
B	Relation between velocity variables u and v. $u = Bv^2$, $B = M/kT_{o}$.
c	Speed of light.
$\vec{D}$	Displacement current.
e	Internal energy of plasma. $e = \gamma P/\rho(\gamma - 1)$.
$\vec{E}$	Electric field.
$\vec{F}_{v}$	Viscous force.
$\vec{g}$	Gravitational force.
$\vec{g}e$	Energy flux vector.
G	Gravitational constant.
$\vec{H}$	Magnetic field.
$\vec{j}$	Current density.
J	Mass flux. (gm/ster/sec.)
J′	Particle flux $J' = J/M$.
k	Boltzmann's constant.
M	Mass of hydrogen atom.
$M_{\odot}$	Mass of the sun.
P	Gas pressure.
r	Heliocentric distance.
R	Reynold's number.
t	Time
T	Temperature.
T_{e}	Electron temperature.
T_{p}	Proton temperature.
u	Dimensionless velocity variable. $u = Bv^2$.
U	Total energy of plasma.
v	Velocity.
x	Dimensionless independent variable. $x = A/r$.
y	Dimensionless temperature variable. $y = \tau^{7/2}$.
γ	Ratio of the specific heats.
κ_{o}	Coefficient of thermal conductivity.
κ	Thermal conductivity.

μ	Molecular weight.
ρ	Density.
ϕ	Gravitational potential.
ξ	Dimensionless independent variable. $\xi = -\ln(x)$.
Ω	Angular velocity of star.

Subscripts.

c	Refers to conditions at the critical point.
E	Refers to conditions occurring at the earth.
r	Radial component of a vector
ϕ	Azimuthal component of a vector.
0	Refers to conditions at the boundary point in the corona.
1	Refers to conditions at the outer boundary point.

CHAPTER 1

INTRODUCTION

It has been known for many years that some stars lose mass in cataclysmic events such as supernovae, but only recently has the importance of the steady outflow of material, which occurs throughout the lifetimes of many stars, been recognised. A considerable number of different mechanisms are thought to be capable of causing these steady outflows.

The theory of the thermally driven mass loss mechanism which is observed to be responsible for the ejection of matter from the sun, in the form of the solar wind, has been developed chiefly by Parker (1958, 1961a,b, 1964a,b). The high coronal temperatures responsible for the solar wind were suggested by Alfvén (1947) and Schwarzschild (1948) to be the result of the dissipation of mechanical energy produced in the sub-photospheric convection zone. Recently Nariai (1968) and de Loore (1970) have shown that the maximum rate of acoustical energy generation in the hydrogen convection zones of main sequence stars occurs at around type F. Consequently all such stars are expected to support a corona and to be losing mass by the solar wind mechanism.

Parker (1963) has suggested, furthermore, that a thermal stellar wind may be produced as the result of heating due to the vigorous turbulence observed in a wide variety of stars. He asserts that most shell stars , and stars with extended atmospheres are likely candidates for the possession of such stellar winds.

Weymann (1963) has considered the possibility that mass ejection from red giants may be due to the solar wind mechanism.

In chapter 2 we survey the theoretical and observational evidence for the widespread occurrence of mass loss from stars. We then select the thermally driven stellar wind mass loss mechanism for more detailed investigation in an attempt to reproduce the conditions occurring in the solar wind, and to estimate its potential for producing high rates of mass loss.

In chapter 3 we survey the results of observations of the solar corona and solar wind on which our calculations will be based. The temperature and density are subject to large, rapid fluctuations, so that the results presented here are necessarily average values taken over a considerable period of time. In the second part of the chapter we use the observational results in order to test, by means of kinetic theory, the applicability of the hydrodynamic approach to the solar wind problem.

We derive, in chapter 4, the basic equation of hydrodynamics which will be solved in chapter 5,as well as the boundary conditions which must be satisfied by the solar wind flow. The importance of the critical point in its relationship to the boundary conditions must be stressed, and we have derived in considerable detail the properties of the flow in relation to it. Numerical models of the solar wind have been produced by a number of authors using a variety of approximations, and in section 3 the methods and results of the work most closely related to our own are discussed. Particular attention is paid to the choice and application of the boundary conditions, but the effects are also noted of refinements, such as the inclusion of the viscosity terms, which we have not treated in our calculations.

The results of our numerical investigation of the solar wind mechanism, and the methods used to obtain them, are discussed in chapter 5. Models of the solar wind are obtained which are in reasonable agreement with observation, but there are indications that the non-thermal heating mechanisms responsible for the high coronal temperatures extend their influence for some considerable distance into the solar wind.

Stellar wind models with rates of mass loss of up to 5.3×10^{-13} $M_{\odot}$/year are computed. They show the rate of mass loss to be a very sensitive function of coronal temperature , but to be practically independent of the coronal density, providing that the density is high enough.

We derive an empirical relatioship between the rate of mass loss and the coronal temperature which allows a tentative extrapolation of

of our results to be made. There are indications that quite considerable rates of mass loss may be produced from a hot, dense corona by means of the thermally driven solar wind mechanism.

Finally the effect of stellar rotation upon the rate of mass loss produced by a stellar wind is briefly considered.

CHAPTER 2

MASS LOSS AS A GENERAL PHENOMENON

THEORETICAL CONSIDERATIONS

2.1 Stellar winds from late-type main sequence stars

The solar corona is known from observation to have a temperature of the order of 2×10^6 °K (Brandt 1970). Parker (1958) pointed out that the coronal gas cannot be retained at so high a temperature by the solar gravitational field, so that in the absence of an external pressure hydrostatic equilibrium cannot be maintained and the corona must expand. The high temperatures which cause the corona to expand and become the solar wind are produced by the deposition of energy in the tenuous gases of the chromosphere and lower corona by magneto-acoustic and gravitational waves generated in the convection zone beneath the solar photosphere. From this model of coronal heating it may be inferred that any star which possesses an extensive sub-photospheric convection zone will also possess a hot corona, and consequently a stellar wind. Current theories of stellar structure predict that main sequence stars of types later than about F4 should possess a convection zone, indicating that the solar wind phenomenon may be of quite general occurrence.

Recently, quantitative estimates have been made of the mechanical energy flux produced in the convection regions of a number of main sequence stars (De Loore 1970). These have shown that the mechanical flux reaches a peak when the effective temperature of the star is about 8000°K, corresponding to that of an F-type star. The computed corona is both hotter and more dense than that of the sun so that the associated stellar wind may be expected to be enhanced correspondingly, and the mass ejection rate to become of some evolutionary significance, particularly with respect to the angular momentum which it removes from the star.

2.2 Requirements of mass loss for stellar evolution

2.2.1 White dwarfs

Theoretical studies of stellar evolution provide some of the most cogent arguments for a belief in the widespread occurrence of the mass loss phenomenon. Any star with an original mass greater than about 1.5M⊖ will exhaust its nuclear material and evolve to a degenerate state in a time shorter than the present age of the galaxy. However, the only stable degenerate configurations available to a star are in the white dwarf state, where the mass of the star must be less than the Chandrasekhar limit of approximately 1.2 $M_\odot$, although rotation of the star may raise this limit considerably (Ostriker and Bodenheimer, 1968), or as a neutron star, in which case the mass must be less than about 2.3 $M_\odot$. It is possible that more massive stars may collapse within their Schwarzchild singularities or into the hypothetical hyperon stars, although there are no definite theoretical conclusions on this subject as yet. If this does not occur, or occurs only rarely, then all the stars whose masses were originally outside the limits mentioned above must lose an appreciable fraction of this mass at some stage during their evolution.

Pre-white dwarf evolution is not clearly resolved since it proceeds at a fast rate accompanied by flashes and instabilities which make computation difficult. Theoretical models of stars approaching the white dwarf region have been produced as the result of mass exchange between the components of a close binary system (Kippenhahn et al. 1967). Recently the evolution of some stars whose original masses were less than 3.5 $M_\odot$ has been followed by Paczynski (1970) through the red supergiant region and a planetary nebula stage to a highly evolved phase approaching a white dwarf. In this model the outer envelope of the red supergiant was lost due to a dynamical instability.

White dwarfs are observed; they are evidence that mass loss has occurred in at least some stars. Stars whose original mass was less than the Chandrasekhar upper limit would have evolved so slowly that during the entire life of the galaxy they would not yet have reached the white dwarf stage.

High rates of mass loss at some phases of evolution are implied

by the existence of white dwarfs in the Hyades cluster whose age is 5.10^8 years, and whose turn-off mass from the main sequence is about 2 $M_\odot$. A white dwarf also occurs in association with Sirius, whose mass is 2.3 $M_\odot$ and whose age is about 4.10^8 years.

2.2.2 Planetary nebulae

Planetary nebulae are very small gaseous emission nebulae which contain a hot blue star emitting ultraviolet radiation that ionises and heats the gas. The velocity of expansion of planetary nebulae is at least one hundred times less than the surface escape velocity of the central star which makes an explosive ejection of the nebulae improbable.

A number of plausible mechanisms for the formation of a planetary nebula have been suggested. Cameron (1970) has suggested that the central stars of planetary nebulae may be highly evolved horizontal branch stars in which the hydrogen burning shell has approached close to the surface. In this situation the luminosity becomes extremely high and radiation pressure may exert a force on the surface layers in excess of the gravitational force. The upper hydrogen rich layers containing about 0.1 $M_\odot$ may be ejected to form the planetary nebula while the stellar remnant, depleted of hydrogen, would contract towards the white dwarf phase (Kutter et al. 1969; Faulkner 1970).

A further attractive suggestion, due to Paczynski and Ziolkowski (1968), is that planetary nebulae are the result of the dynamical instability of the convective envelope of red supergiants with masses less than 4 $M_\odot$ which occurs when their luminosity reaches about 10^4 $L_\odot$. Their idea is that in these stars, which have helium and hydrogen burning shell sources, the total energy of their highly distended envelope may become positive when the ionisation energy of hydrogen and helium, and the dissociation energy of the hydrogen molecule is taken into account, and is sufficient to expel a typical envelope with a speed of up to 30 km/sec. The carbon-oxygen core of the star would then presumably form the central star of a planetary nebula.

2.2.3 RR Lyrae and horizontal branch stars

Further theoretical arguments for the occurrence of mass loss at certain stages of evolution are provided by recent models of stars which have evolved beyond the red giant stage. These are important since all population II stars with masses large enough to start core helium burning are expected to become horizontal branch stars after passing through the helium flash at the red giant tip. Some, or perhaps all, of these will subsequently evolve into the variable RR Lyrae stars.

Models of these stars have been produced by Christy (1966a), and more recently by Iben and Faulkner (1968). These models have shown satisfactory agreement with observation only for masses less than about 0.8 $M_\odot$. Since a longer time than the age of the galaxy would be required for stars of this original mass to evolve to their present states, the implication is that mass has been lost, probably in the red giant phase. From the frequency of occurrence of RR Lyrae stars in globular clusters it appears that they should have evolved from main sequence stars with masses near 1.2 $M_\odot$.

2.2.4 W Virginis stars

An identical argument may be followed in the discussion of the similar W Virginis stars, which are the population II equivalents of the Cepheid variables (Christy 1966b). The model agreeing best with observations has a mass of 0.88 $M_\odot$, a period of 18.5 days, and a normal effective temperature of 5500°K. However, the star, being a variable, has an oscillating atmosphere which was found to produce very strong shock waves that propagate upward through the photosphere. These shock waves transfer momentum to the upper regions of the atmosphere, which are ejected at the rate of about 5.10^{-6} $M_\odot$/year. Thus it may be that W Virginis and RR Lyrae stars are themselves evolutionary phases in which rapid mass loss occurs.

2.3 Mass exchange between components of binary systems

2.3.1 Predictions

Mass loss may be expected from a variety of close binary systems during certain periods of their lifetimes. This may occur in two ways. The first mechanism concerns the ejection of particles from the atmosphere of one of the stars under steady state conditions. Such loss probably occurs in all stars to a small extent but may become quite important during some evolutionary phases. The effect of the companion star is to enhance the flow and to alter its trajectory by means of its gravitational field. The emitted matter may be transferred to the companion star, or may be lost to the system altogether (Prendergast 1960).

The second type of mass loss associated with binary stars arises from the change of stellar radius due to evolution. It is assumed that initially both components are situated on the main sequence and evolve independently. The more massive star, the primary, evolves more rapidly, expands, and eventually fills its Lagrangian surface. This situation occurs during the slow main sequence expansion when hydrogen burning is confined to the core or, in the case of more widely separated binaries, during the phase of rapid expansion when hydrogen burning occurs in a shell and the star is approaching the red giant stage. In binaries where the separation is still larger the primary may not fill its Roche lobe until after the exhaustion of helium in its core, when the star is evolving along the Hayashi track into the supergiant region and expanding rapidly.

Evolutionary models of systems with a wide range of initial masses have been constructed (Kippenhahn et al. 1967; Kippenhahn and Weigert 1967). We consider, for example, the evolution of the primary component of a binary of initial mass 9 $M_\odot$. The Roche limit is reached after 1.2×10^7 years of hydrogen burning, when the star loses mass to its companion at a rate of about 2×10^{-5} $M_\odot$/year. At the end of this phase of rapid mass loss the secondary has become the primary, and the mass of the original primary has decreased to about 3.73 $M_\odot$. The system forms a semi-detached pair with the secondary now filling its Roche lobe and slowly losing mass to the primary.

As we mentioned earlier the formation of white dwarfs in binary systems receives an explanation through the mechanism of mass exchange.

In the model described by Kippenhahn et al. (1967) the initial primary was a 2 $M_\odot$ star which lost mass to its secondary so rapidly that when it reached the white dwarf stage with a mass of about 0.26 $M_\odot$ the new primary was still virtually unevolved but now had a mass of 2.7 $M_\odot$. In these evolutionary calculations it has been assumed that all the ejected material is transferred to the secondary, although this will probably not be true; a substantial fraction will be lost to the system altogether.

2.3.2 Cases where the occurrence of mass loss is implied

Observations of close binary systems reveal many cases in which mass loss must have occurred. Examples are those systems in which one component is a white dwarf, or the Algol-type systems which characteristically consist of a main sequence primary with a later type, less massive, subgiant secondary, over-luminous for its mass and spectral type, and often filling its Roche lobe (Conti 1967). This latter situation can be explained most conveniently by the occurrence of the process of mass exchange described above (Plavec 1968).

2.3.3 'Blue Stragglers'

The evolution of the original secondary component may also be greatly affected by the mass transfer. It was suggested by McCrea (1964) that the 'blue stragglers' above the main sequence turn-off point in old clusters, such as M3 and M67, are the evolved secondaries of semi-detached pairs. Subsequent observations that all, or nearly all, such stars are spectroscopic binaries tend to confirm this view (Cannon 1968; Strom and Strom 1970). These stars may thus be taken as further evidence for the occurrence of mass loss.

OBSERVATIONAL EVIDENCE

2.4 Mass loss from single stars

Although the theoretical arguments that mass loss is a common phenomenon, occurring in a wide variety of stars are persuasive, the number of situations in which the process has been directly observed is rather few. The requirement is to observe an outward flow of gas whose

velocity exceeds the local velocity of escape, or, failing this, to observe an outward flow of gas from a star without a corresponding inward flow to balance it.

2.4.1 Late-type main sequence stars

Mass loss is observed to occur from the sun in the form of the solar wind. Apart from this, no other examples of mass loss have been observed in main sequence stars, even though, as was noted earlier, main sequence stars later than type F4 are expected to support stellar winds, some of which should be much more massive than that of the sun. This is due to the great difficulty of observing the upper atmospheric levels in stars other than the sun.

In many late-type main sequence stars emission lines are detected. Especially prominent are the H and K lines of Ca II which, in the sun are produced in the chromosphere, where their intensity can be correlated with solar activity (Simon and Leighton 1964). The existence of a chromosphere implies the existence of a corona and solar wind, as both are produced by the same mechanism of mechanical energy dissipation. It is therefore reasonable to suppose that the strength of the Ca II H and K emission may also be a measure of the stellar wind strength.

Young stars of types G0-K2 in the Hyades, Praesepe, Coma, and Pleiades clusters were found by Wilson (1963) to show a much higher intensity of H and K emission than do the older field stars. At the 10 A/mm. dispersion he used the H and K emission in the sun, which is thought to be ten to one hundred times older than the clusters, is well below the level of detectability in integrated sunlight. He concluded that chromospheric activity is inversely proportional to the age of the star.

It has been known for a long time that early-type stars have a high rotation rate while late-type stars rotate relatively slowly. The transition is quite sharp and occurs near spectral type F2. The Thickness of the hydrogen convection zone decreases with increasing luminosity until it becomes negligible around type F4 (Kraft 1967), corresponding closely to the point beyond which the chromospheric H and K

emissions are no longer detected (Wilson 1966). The immediate implications are that for some time after reaching the main sequence a solar-type star will support a stellar wind considerably stronger than that of the sun at present, and that this outflow is efficient at reducing the star's angular momentum.

2.4.2 T Tauri stars

One of the most renowned classes of objects from the point of view of mass ejection is the T Tauri stars. These are stars which are believed to be in the process of contraction on to the main sequence. They have high rotation rates and it is thought that mass loss occurs concurrently with the removal of angular momentum necessary to prevent the star from becoming rotationally unstable (Williams 1968).

The mass loss manifests itself in the stellar spectrum by strong wide emission lines of Ca II H and K, and hydrogen, with violet displaced absorption components corresponding to negative velocities of 80-230 km/sec. Red displaced components occur in some of the fainter stars, but in most there is no sign of any returning material, and it may be concluded that it leaves the star entirely (Kuhi 1966). The rate of mass loss as determined from the line strengths is typically in the range $0.3 - 5.8 \times 10^{-7}$ $M_{\odot}$/year (Gahm 1970).

2.4.3 M-type giants and supergiants

There is spectroscopic evidence for the ejection of matter from all giant stars with spectral type later than M0, and also from supergiants of somewhat earlier type. In the M-type giants all strong absorption lines arising from the ground states of ions and atoms consist of two components, the first of which is a broad, fairly shallow absorption line produced in the photosphere, while the second is deep, narrow, and displaced towards the violet with respect to the centre of the photospheric line on which it is superimposed. This second component must be produced in an expanding envelope under conditions of low pressure and excitation temperature. The expansion velocity of the shell indicated by the displacement of the line is always quite small (5 - 25 km/sec), and is much less than the photospheric escape velocity, which

is usually about 100 km/sec (Deutsch 1966). These observations would be consistent with the hypothesis that gas above the photosphere rises slowly and returns to the star in an unobservable state of ionisation but for the fact that many of the circumstellar absorption lines are also observed in the spectra of the companion stars of those red giants which are members of visual binary systems. This implies that the expanding gas reaches a height of several hundred stellar radii above the primary star, at which height its velocity exceeds the escape velocity and it is lost to the system (Weymann 1963).

The strongest circumstellar lines are invariably the Ca II H and K lines, and there appears to be a strong correlation between the strength of these lines and the spectral type of the star. The density of Ca II ions near the surface of the star as determined by the curve of growth method appears to increase by a factor of about 2000 between types M1 and M5. The rate of mass loss is expected to increase by approximately the same factor (Deutsch 1968). Assuming that most calcium is in the singly ionised state the rate of mass loss at type M5, luminosity class (III), is estimated to be about 10^{-8} $M_{\odot}$/year. More luminous M-type stars lose mass at a considerably higher rate and a value of approximately 5×10^{-6} $M_{\odot}$/year for α Orionis M2 (Ib) has been proposed by Weymann (1962).

The high rate of mass loss which occurs during the red giant phase may be extremely important from the evolutionary point of view, due to the considerable length of time which a star spends in this region, and may well account for the apparently low masses of stars at later evolutionary stages.

Unfortunately these estimates of the rates of mass loss from red giant stars are extremely unreliable, due largely to uncertainty about the height above the stellar surface at which the absorption lines are formed. Furthermore the progressive weakening of the circumstellar lines from types M5 to M0, and their total disappearance in the late K stars may be caused by increasing temperature in the gas exciting a large proportion of the calcium to the second and higher ionisation states, where it is less accessible to observation. If this is true then the apparent rate of mass ejection may decrease from types M5 to M0 primarily due to this excitation effect. Deutsch considers it possible

that all giant stars to the right of the Herzprung gap are undergoing mass loss and that it does not set in sharply at type M0, where the circumstellar lines first appear.

The physical processes causing the ejection of matter are not known. It has been suggested that the flow may be analogous to a massive solar wind, but occurring at a much lower temperature, since lines of Fe I and Ca I are observed. Recently,however,radio emission has been detected from α Scorpii M1 (1b) indicating a temperature of 4×10^5 °K (Wade and Hjellming 1971). It is tempting to suppose that the radio emission is due to the corona of α Scorpii and that the absorption lines are produced in the much cooler regions far from the star.

Radiation pressure from strong chromospheric emission in Lyman α has been invoked to explain the ejection of the upper levels of red giant atmospheres (Wilson 1960). This would require a density of radiation such that all the barium in the atmosphere should be doubly ionised. Although there is often a fairly strong core of Ba III in these stars the greater proportion appears to occur in the singly ionised state, indicating that the ultraviolet flux is usually weak. However, the radiation field would be coupled more effectively to the gas if small opaque grains of graphite were formed in the upper atmosphere. This mechanism might also partially explain the apparent increase in the rate of mass loss from type M0 to type M5 (Wickramasinghe 1966).

2.4.4 Supergiants of types A, F, and G

Ejection of matter appears to be very common among the supergiants of types A, F, and G. For example, displaced lines corresponding to expansion velocities approaching escape velocity have been detected in 89 Herculis (F2 Ia) (Sargent and Osmer 1968), as well as in ρ Cassiopeiae F8 Ia (Sargent 1961). In the latter star over a five year period the average rate of mass loss was about 3×10^{-5} $M_\odot$/yr. However this cannot be considered to be a steady outflow, as the ejection rate dropped considerably during the next few years.

Sporadic outbursts are characteristic of the earlier type

supergiants in contrast to the more constant flows from the M-type giants and supergiants. Rapid changes on a time scale of about one month have been noted in the violet displaced emission and absorption features observed in 89 Herculis. Once again the ejection mechanism is unknown but the probable cause is large scale instabilities in the extended atmosphere, perhaps caused by radiation pressure.

2.4.5 Early type supergiants

There is considerable observational evidence that all supergiants of types O and B are ejecting mass (Hutchings 1968a). In these stars Hα is found to have a P Cygni profile, indicating that an extensive, tenuous, expanding envelope is present. Expansion velocities of the shell are often comparable to the photospheric escape velocity. Rocket observations in the far ultraviolet region have shown the presence of strong circumstellar absorption lines in stars of luminosity class III and above. These lines, which are caused by ions of C IV, N V, Si III, and Si IV, are strongly shifted to the violet and indicate velocities of expansion of up to 3000 km/sec which is considerably larger than escape velocity (Morton et al 1969; Morton 1968). Line profiles of some strong lines have been computed by Hutchings (1968b,c) for a number of OB supergiants and indicate that mass loss rates are characteristically about 10^{-6} $M_{\odot}$/yr, the rate generally increasing with the ultraviolet flux of the star, but the extremely luminous star P Cygni (B1 Ia) appears to be losing mass at the rate of 5×10^{-4} $M_{\odot}$/yr (Hutchings 1968d).

The extremely high velocities of mass ejection found in these stars are believed to be due mainly to radiative acceleration in the strong ultraviolet resonance lines, which occur in the wavelength region of maximum emission (Lucy and Solomon 1967). Line profiles of these strong lines have been computed and very close agreement with the observed spectra has been obtained on the assumption that radiation pressure is the accelerating mechanism (Hutchings 1970a).

It is unlikely that these high velocities could be produced by a solar wind type mechanism since a coronal temperature of about 10^7 °K would be required , and at this temperature the ions C IV, N V, and Si IV,

obseved in OB super giant spectra, would be destroyed by collisional ionisation (Lucy and Solomon 1970).

2.4.6 Wolf-Rayet stars

The characteristic spectrum of a Wolf-Rayet star consists of a very faint continuum superimposed on which are wide strong emission lines of neutral and ionised helium, the higher ionised states of carbon, nitrogen, and oxygen, and a few violet displaced absorption lines. These are clear indications of an expanding atmosphere. The velocity of the part of the atmosphere in which most of the emission lines are produced is typically 500 to 800 km/sec, while the extreme upper region of the atmosphere in which the absorption lines are formed expands at 1000 to 2000 km/sec (Morton et al 1969), well above escape velocity. It is estimated that Wolf-Rayet stars may be losing mass at the rate of 10^{-5} to 10^{-6} $M_{\odot}$/yr (Underhill 1968).

A number of Wolf-Rayet stars are seen to be associated with small ring-like nebulae indicating that the interstellar gas is being pushed back by radiation and matter ejected from the star (Smith 1967).

2.4.7 Be stars

Be stars are the subclass of B type stars which show Hα in emission at least some of the time, and in some cases show shell type absorption lines and metallic emission lines as well. About one fifth of B type stars have these spectral characteristics which are caused by an extended atmosphere, and which may arise in a number of ways.

The commonest type of Be stars are rapidly rotating objects occupying a region just above the main sequence in the Hertzsprung-Russell diagram. They are only marginally stable against rotational disruption and are expected gradually to lose the outermost regions of their atmospheres. Their rate of mass loss has been estimated to be about 10^{-7} $M_{\odot}$/yr (Hazlehurst 1967).

From a study of the Hγ emission profile of γ Cassiopeiae, Hutchings (1970b) has concluded that although the extended atmosphere of this Be star is originally caused by the high rotational velocity, it is supported at upper atmospheric levels by radiation pressure.

Rocket observations in the ultraviolet have shown the presence of P Cygni profiles in the C IV resonance lines, which tends to confirm this and to indicate that the mass ejection process is similar to that occurring in the OB supergiants.

Recently an evolutionary model of a Be star has indicated that mass loss occurs in two distinct phases. The first lasts for 2.5×10^7 years when the star is on, or near the main sequence, during which it loses mass at about 10^{-9} $M_\odot$/yr. Subsequently there is a short period (about 10^6 years) when no mass loss occurs, but it recommences when the star starts to expand toward the red giant region. This phase continues for 5×10^4 years when the mean mass loss rate is about 3×10^{-7} $M_\odot$/yr. Mass loss ends after the star is approximately 2.7×10^7 years old during which time it has lost 0.5% of its original mass (Meyer-Hofmeister and Thomas 1970).

Other groups of Be stars are of no particular individual interest. One consists of otherwise normal high-luminosity objects such as β Orionis (B8 Ia) which show no sign of having high rotation rates, but rather lose mass by a mechanism similar to that operative in other OB supergiants.

Another group has the additional complication of a companion star which lowers the surface gravitational field of the B star and so encourages the formation of the extended atmosphere which causes the Be classification. The extended atmosphere is eventually either transferred to the secondary star or lost to the system, as in normal close binaries.

2.5. Mass loss from binary stars

A summary of the theoretical reasons for expecting mass loss to occur in binary systems has previously been given. Spectroscopic observations give evidence of its actually occurring in many cases, either by showing the existence of gaseous streams from one or other of the components, or by showing the existence of an expanding shell surrounding both stars.

The presence of a gaseous stream manifests itself by the appearance in the spectrum of a binary of extra lines, either in emission

or absorption. In the case of β Lyrae these appear just before and after midpoint of the principal eclipse and may be interpreted as being due to two gas streams, one going towards the primary and the other towards the secondary. In the case of the Wolf Rayet binary, V444 Cygni, the streams give rise to a narrow emission line from which the velocity of the stream can be found to be about 700 km/sec.

In some Algol-type systems emission lines occur at certain phases of the cycle which suggests that they arise from concentrations of material between the two stars, presumably at the zero gravity Lagrangian point.

The presence of a circumstellar expanding shell in a binary system is detected, as in the case of single stars, by the existence of violet displaced absorption lines. An example is the system γ^2 Velorum, where the expansion rate is about 1300 km/sec. In many cases Hα is found in emission from the expanding shell (Sahade 1968).

2.6 Mass loss by sudden ejection of matter

2.6.1 Supernovae

The most spectacular example of the phenomenon of mass loss from stars is , of course, the supernovae; at least in this case the observational evidence is incontrovertible.

Type I supernovae occur among population II stars. They are thought to be caused by the detonation of degenerate nuclear material in the interior of a star when the central temperature exceeds about 1.5×10^9 °K. The pre-supernova star is believed to be highly evolved and to have a mass between 1.1 and 1.5 $M_\odot$. During the explosion stellar gas is expelled at velocities of up to 3000 km/sec, heavy nuclei are converted into alpha particles, and nucleosynthesis proceeds by the r process. The expanding envelope contains little or no hydrogen. From studies of the frequency of these supernova events and by comparing them with the rate at which stars in the critical mass range leave the main sequence it appears that most stars lose mass fast enough by other processes to keep the central temperatures below the explosion point (Deutsch 1968; Hoyle and Fowler 1960).

Type II supernovae occur among population I stars, and a considerable number of different mechanisms for their formation have been proposed. Recently Arnett (1969) has suggested that stars with masses in the range $4\ M_\odot < M < 9\ M_\odot$ may ignite the $^{12}C + {}^{12}C$ reaction explosively because of the high degree of electron degeneracy in their central regions. In this model the entire core, with a mass of $1.37\ M_\odot$, would be destroyed, leaving no neutron star as a remnant.

This model has recieved some confirmation from Paczynski (1970), whose calculations have shown that the carbon flash probably will occur explosively for stars in this mass range. He has found that the very dense cores of these stars are dynamically stable, but that instability could result if such effects as crystallization and electron capture were taken into account. If dynamical instability were to occur a thermonuclear explosion would not be produced but the core would collapse into a neutron star before carbon ignition took place.

This collapse may itself result in a supernova, according to a proposal by Ostriker and Gunn (1971). They suggest that some supernovae could be caused by the formation of a pulsar within the core of a highly evolved star. If, as is now generally believed, pulsars are rotating, magnetic neutron stars, these could be produced by the dynamical collapse of the cores of red supergiants envisaged by Paczynski (1970).

2.6.2 Novae

Novae are much less violent outbursts than supernovae and are believed to eject only about 10^{-4} - $10^{-5}\ M_\odot$ of material even though they may increase in luminosity by ten or eleven magnitudes. The pre-nova star is an intrinsically faint object and usually shows this enormous increase in luminosity over a period of about two days. From a study of the line displacements it can be shown that ejection of material takes place by the removal of successive shells of the atmosphere. Ejection velocities are several thousand km/sec. Post-novae stars appear to be of spectral type O or B and to have a mass of about $1\ M_\odot$ (Hazlehurst 1967).

Novae may be caused by the passage of shock waves up through the

star following a sudden liberation of energy in the interior. The shock would strengthen on passing into the less dense atmosphere and could accelerate the outermost shells of the star beyond the escape velocity.

In another model of a nova it is assumed that the pre-nova star is in a hydrogen-exhausted state and is approaching the white dwarf phase with a mass of about 0.75 $M_{\odot}$. It is further assumed that it is a member of a close binary system, and that it is accreting mass at a slow rate (of the order of 7×10^{-3} $M_{\odot}$/yr) from its companion. The accreted material forms a non-degenerate hydrogen-burning shell which eventually becomes thermally unstable and causes the nova outburst (Rose 1967).

CHAPTER 3

OBSERVATIONS OF THE SOLAR WIND

3.1 Observations of the solar corona

3.1.1 Measurements of density

In this chapter we will review the physical properties and the results of observations of the solar corona and solar wind, and discuss briefly the conclusions which can be drawn from them concerning the kinetic properties of the flow.

The light observed from the corona may conveniently be divided into three components. The first of these, known as the K corona, is composed of continuous radiation from the photosphere which has undergone Thompson scattering by free electrons in the corona. The F corona, or inner zodiacal light, consists of photospheric radiation which has been scattered by interplanetary dust. It is not produced in the corona, and has no physical connection with it. The third component is the E corona which consists of the total visible light in the coronal emission lines.

The electron density of the corona may be estimated from photometric determination of the brightness of the K corona. The intensity of this radiation at any point in the corona is proportional to the density of electrons, the Thomson scattering cross-section, and the intensity of radiation from the photosphere. The brightness can be determined observationally as a function of radial distance. The intensity of photospheric radiation can be found by means of radiative transfer theory, allowing the density at any radial distance to be obtained. The density at the base of the corona is found by this method to be a very rapidly changing function of the radial distance, and is in the range 10^7 - 10^8 electrons/cm^3 depending on the latitude under consideration (Allen 1963).

3.1.2 Measurements of temperature

There are a number of methods by which the coronal temperature can be estimated and a considerable variation in the results has been obtained.

A rather crude estimate of the coronal temperature results from the assumption that the corona is isothermal, at temperature T, and in hydrostatic equilibrium. It is well known that the density distribution of such an atmosphere can be expressed as:

$$\frac{N(r)}{N(r_\odot)} = \exp\left\{\frac{GM_\odot M\mu}{R_\odot kT}\left[\frac{1}{r} - \frac{1}{r_\odot}\right]\right\} \qquad (3.1.1)$$

where G is the gravitational constant, $M_\odot$, the mass of the sun, M the mass of a hydrogen atom, μ the molecular weight, $R_\odot$ the solar radius, and k Boltzmann's constant. N(r) represents the density at an altitude r above the base point r_o. Equation 3.1 can be rearranged to give the value of the temperature if the density of distribution is known, presumably from eclipse studies. Temperatures of around 1.5×10^6 °K are deduced from this simple approach.

A more accurate version of this method is to include the possibility of coronal expansion, and to consider the variation of temperature with radial distance. The temperature distribution proves to be quite sensitive to the hydrogen-helium ratio, but temperatures of around 2.0×10^6 °K are implied (Brandt 1970).

Values of the kinetic temperature can be found spectroscopically by measurements of the widths of the coronal emission lines. If we assume the corona to be optically thin and the line to be broadened only by the Doppler effect, the profile is determined by the equation:

$$I = I_o \exp\left\{-\frac{c^2\mu M}{2kT}\left[\frac{\lambda - \lambda_o}{\lambda}\right]^2\right\} \qquad (3.1.2)$$

where I is the intensity, λ the wavelength, c is the velocity of light and subscript zero refers to the line centre.

Since all other quantities in the equation can be measured , the temperature is the only unknown and can readily be determined. The kinetic temperature obtained by this method is found to vary for different lines. The values range between 1.2 - 2.5 x 10^6 °K although most lie in the range 2.0 - 2.5 x 10^6 °K. These values must be regarded as upper limits as the lines will also be broadened by mechanisms other than the Doppler effect, as well as by velocities other than their random thermal velocities.

Turbulent motions in the corona could cause considerable inaccuracies in the observed kinetic temperature (de Jager 1963),and coronal expansion will also contribute significantly to the line width (Parker 1963).

The population of ions in the various stages of ionisation is determined by a balance of the processes of collisional ionisation and radiative or dielectronic recombination between adjacent states. The process is temperature dependent, and the steady state equilibrium point reached in the corona can be inferred from the relative intensities of the coronal emission lines. It is found that dielectronic recombination is the most important process in the corona, and a temperature of about 2 x 10^6 °K is implied.

In summary, it appears that although there is a fair degree of uncertainty in the measurements, a temperature of around 2 x 10^6 °K in the solar corona is in reasonable agreement with observation. It should perhaps be pointed out that it is unlikely that any single temperature can adequately represent the true situation. Over active regions of the sun the temperature can become as high as 3 x 10^6 °K, while over a large flare the temperature may suddenly rise to 5 x 10^6 °K or more.

3,1.3 Measurements of magnetic field

The presence of a solar magnetic field is clearly indicated from photographs of the corona at solar minimum when the orientation of the solar plumes in the polar regions follows quite distinctly the lines of force of a magnetic dipole.

The radial component of the magnetic field near the earth is found from space flight experiments to be on average about 3.5×10^{-5} gauss. Assuming an inverse square law variation of this component with radial distance, a field of about 1.5 gauss near the solar surface is implied. This value is in good agreement with determinations of the solar magnetic field by means of the Zeeman effect.

3.2 Observations of the solar wind

3.2.1 Measurements of velocity

Studies of the solar corona by radar experiments have shown the presence of mass motions in the direction of the earth of about 16 km/sec in the region between 1.5 and 2.0 $R_\odot$, the exact position being unknown because of inhomogeneities in the corona. The solar wind is thus observed in regions of the corona quite close to the sun.

The velocity of the solar wind can be estimated from observations of the extent of comet tails, but systematic measurements have had to await the development of space flight experiments. At the present time the data is still very incomplete and almost all the results have been obtained near the plane of the ecliptic.

Results show that the velocity of the solar wind is very variable, and values between 200 and 1000 km/sec have been measured, with an average of between 400 and 500 km/sec. During periods in which there is little solar activity the velocity is usually in the range 300 to 350 km/sec (Brandt 1970).

Dennison and Hewish (1967) have measured the velocity of the solar wind by observing the interplanetary scintillation of small diameter radio sources. The scintillation is produced by the presence of small-scale irregularities in the electron density, which are presumably moving along with the solar wind. Their results are important as they were able to investigate the flow at high ecliptic latitudes. They obtained the interesting result that the velocity of the solar wind from the polar regions is considerably greater than from the equatorial regions. Near the ecliptic plane they measured an average velocity of about 300 km/sec,

but a mean velocity of nearly 500 km/sec at a latitude of 60°.

3.2.2 Measurements of Density

There is a great range of densities measured for the solar wind in the vicinity of the earth; we will mention just a few of them. Early space flight experiments of Bridge et al. (1961) indicated a proton density of between 7 and 20 particles/cm^3, with a velocity in the range 250 to 400 km/sec at the earth. More recently, results from Pioneer 6 and 7, which were obtained between December 1965 and May 1966, and between August 1966 and March 1967, have shown mean densities of about 4.3 particles/cm^3 and 8.7 particles/cm^3 respectively. At present the results indicate that the density of the solar wind flow in the vicinity of the earth is usually between 5 and 10 protons/cm^3.

3.2.3 Measurements of temperature

The temperature of the solar wind is defined in terms of the distribution of random velocities measured in the frame of reference moving with the bulk velocity of the solar wind. The temperature of the electrons and the protons differs somewhat, for reasons which will be explained in section 3. The mean value of the proton temperature T_p is of the order of 10^5 °K, while the electron temperature T_e is usually three or four times larger than T_p.

3.3 Kinetic properties of the solar wind

3.3.1 Mean free path

Having obtained experimental values of the physical parameters in the solar corona and solar wind we may now use the results of kinetic theory to determine the way in which the dynamics of the expanding corona should be treated. The corona may be considered to be a fluid only if the mean free path of the average thermal ion is short compared with the relevant dynamical lengths such as radial distance and scale height.

The time, t_D, in which a proton with thermal velocity v undergoes an accumulated deflection of about 90° due to Coulomb scattering in

ionised hydrogen of density N, is given by Spitzer (1962) to be

$$t_D \simeq 1.4 \times 10^{-13} \frac{v^3}{N} \text{ seconds} \qquad (3.3.1)$$

The mean free path, λ, is then

$$\lambda = vt_D. \qquad (3.3.2)$$

In the corona at an altitude of 3×10^5 km, where the temperature is about 2×10^6 °K, the root mean squared thermal velocity is approximately 220 km/sec, giving a mean free path $\lambda \simeq 3 \times 10^{17}/N$ cm. For densities of about 3×10^7 cm^{-3} we obtain $\lambda \simeq 1 \times 10^5$km. This is rather a shorter length than the radial distance and should be considerably shorter than the scale height. This situation will persist out to several solar radii at least, indicating that the corona is most appropriately treated by hydrodynamics.

At the orbit of the earth, however, the mean free path will be rather larger than the radial distance, and the hydrodynamic approach is not so easily justified. A magnetic field is observed in the solar wind and Spitzer asserts that this will allow the charged particles to interact over a far larger range than through the Coulomb electrostatic forces, for which the mean free path in equation (3.3.2) is calculated. On this assumption the solar wind can be treated as a fluid even at large radial distances. This is not essential, however, as we will show that the characteristics of the flow are entirely determined at an altitude of only a few solar radii, at which point the hydrodynamic nature of the flow is assured by means of equation(3.3.2). Since the rate of mass loss is determined at this point the behaviour of the flow beyond it is largely immaterial.

3.3.2 Neutrality

The scale of deviation from charge neutrality in the solar wind may be determined from the Debye length, L_D, where:

$$L_D = \left\{\frac{kT}{4\pi Ne^2}\right\}^{\frac{1}{2}} \qquad 3.3.3$$

where e is the electronic charge. Substituting in the coronal values for density and temperature we obtain $L_D \simeq 0.7$ cm, while at earth the Debye length is still only about 2.5 metres, showing that the solar wind is electrically neutral on all except the smallest scales.

3.3.3 Equipartition of energy

The time required for equipartition of energy between protons and electrons, t_E, is longer than the deflection time, t_D, by a factor approximately equal to the square root of the proton-electron mass ratio. At the earth's orbit this is very large and indicates that the electron and proton temperature should be considerably different. This prompted the construction of two fluid models of the solar wind, described in chapter 4 , which do in fact predict that T_e is much greater than the proton temperature T_p. However, observation has shown that the electron temperature is only slightly larger than the proton temperature, implying that interactions other than those due to the Coulomb forces are dominant in the solar wind.

CHAPTER 4

THEORETICAL FORMULATION OF THE SOLAR WIND

4.1 Derivation of equations of motion

4.1.1 General magnetohydrodynamic equations

We have shown that the solar wind may be considered to behave as an electrically neutral, conducting fluid with associated electromagnetic fields. The flow may be described by a set of equations consisting of the hydrodynamic equations, Maxwell's equations, an equation of state, and an equation essentially expressing Ohm's law viz.

a) The Continuity Equation

$$\frac{\partial \rho}{\partial t} + \nabla \cdot (\rho \vec{v}) = 0 \qquad (4.1.1)$$

where ρ is the density, and $\vec{v}$ the velocity of the fluid in a heliocentric frame of reference, stationary with respect to the sun.

b) The Momentum Equation

$$\rho \frac{d\vec{v}}{dt} = -\nabla P + \frac{1}{c}\vec{j} \times \vec{B} + \rho \vec{g} + \vec{F}_v \ , \qquad (4.1.2)$$

where P is the pressure of the fluid, $\vec{j}$ is the current density, $\vec{B}$ the magnetic flux density, and c the speed of light. The derivative with respect to time in (4.1.2) is the convective derivative where

$$\frac{d}{dt} = \frac{\partial}{\partial t} + \vec{v} \cdot \nabla \qquad (4.1.3)$$

The terms on the right hand side of equation (4.1.2) represent the forces acting on the fluid: the pressure forces, the magnetic stresses, and the gravitational and viscous forces. The gravitational forces can be represented as,

$$\vec{g} = - \nabla \phi \qquad (4.1.4)$$

The gravitational potential ϕ is given by,

$$\phi = - \frac{GM_{\odot}}{r} \tag{4.1.5}$$

The viscous forces $\vec{F}_v$ are expressible as,

$$\vec{F}_v = \mu_v \nabla^2 \vec{v} + (\lambda_v + \mu_v/3)\nabla(\nabla \cdot \vec{v}) \tag{4.1.6}$$

where λ_v and μ_v are the coefficients of viscosity.

c) The Energy Equation

$$\frac{\partial U}{\partial t} = - \nabla \cdot \vec{g}_e \tag{4.1.7}$$

where U, the total energy is given by,

$$U = \tfrac{1}{2}\rho v^2 + \frac{B^2}{8\pi} + e\rho + \rho\phi \tag{4.1.8}$$

and where e represents the internal energy per unit mass and is defined by the expression:

$$e = \frac{1}{\gamma - 1} \frac{P}{\rho} \tag{4.1.9}$$

γ is the ratio of the specific heats, taken to be $\frac{5}{3}$ in this work. $\vec{g}_e$ is the energy flux vector, expressed as:

$$\vec{g}_e = \vec{v}(\tfrac{1}{2}\rho v^2 + e\rho + P + \rho\phi) + \frac{c}{4\pi}\vec{E} \times \vec{B} - \kappa\nabla T + \vec{\Phi} \tag{4.1.10}$$

where $\vec{E}$ is the electric field, κ, the thermal conduction term, and $\vec{\Phi}$, the term due to viscosity. The seven terms in equation (4.1.10) represent the transport of kinetic and thermal energy, the work done by the pressure and the gravitational field, the Poynting vector, thermal conduction, and the work done by viscous forces. The thermal conduction term κ is given by

$$\kappa = \kappa_o T^{5/2} \tag{4.1.11}$$

where κ_o, the coefficient of thermal conductivity, is a slowly varying function of density and temperature (Roberts and Potter 1970).

d) Maxwell's Equations

$$\nabla \cdot \vec{D} = 4\pi\rho_e \tag{4.1.12}$$

$$\nabla \times \vec{H} = \frac{4\pi}{c}\vec{j} + \frac{1}{c}\frac{\partial \vec{D}}{\partial t} \tag{4.1.13}$$

$$\nabla \times \vec{E} = -\frac{1}{c}\frac{\partial \vec{B}}{\partial t} \tag{4.1.14}$$

$$\nabla \cdot \vec{B} = 0 \tag{4.1.15}$$

where $\vec{D}$ is the displacement vector, $\vec{H}$ is the magnetic field intensity, and ρ_e is the charge density.

e) Equation of state

The simple ideal gas equation of state is used,

$$P = \frac{\rho k T}{\mu M} . \tag{4.1.16}$$

f) Ohm's law

$$\vec{j} = \sigma(\vec{E} + \frac{1}{c}\vec{v} \times \vec{B}) \tag{4.1.17}$$

where σ is the electrical conductivity.

Thus we have nine equations for the nine variables ($P, \rho, \vec{v}, \vec{B}, \vec{H}, \vec{E}, \vec{D}, T, \vec{j}$). (Jackson 1962; Braginskii 1965; Roberts and Potter 1970).

4.1.2 Steady state equations

The assumption of this simple form for Ohm's Law requires that there be a sufficiently high rate of collisions between ions and electrons for there to be only negligible separation of charge. If, also,

the displacement current is ignored in Maxwell's equations we have the magnetohydrodynamic approximation which will be used throughout.

On neglecting the displacement current the set of four Maxwell's equations becomes reduced to two viz.

$$\nabla \times \vec{E} = - \frac{1}{c} \frac{\partial \vec{B}}{\partial t} \tag{4.1.18}$$

$$\nabla \times \vec{B} = \frac{4\pi \vec{j}}{c} \tag{4.1.19}$$

Equation (4.1.15) can be obtained by taking the divergence of equation (4.1.18) which gives $\frac{\partial}{\partial t} \nabla \cdot \vec{B} = 0$, implying that $\nabla \cdot \vec{B}$ is constant with respect to time. The requirement that $\nabla \cdot \vec{B} = 0$ can be applied as an initial condition.

In the following discussion of the solar wind all phenomena will be assumed to occur in the steady state so that $\frac{\partial}{\partial t} = 0$. The set of solar wind equations then becomes,

$$\nabla \cdot (\rho \vec{v}) = 0 \tag{4.1.20}$$

$$\rho \vec{v} \cdot \nabla \vec{v} = - \nabla P + \frac{1}{c} \vec{j} \times \vec{B} - \rho \nabla \phi + \vec{F}_v \tag{4.1.21}$$

$$\nabla \cdot \left\{ (\tfrac{1}{2} \rho v^2 + e\rho + P + \rho\phi) \vec{v} + \frac{c}{4\pi} \vec{E} \times \vec{B} - \kappa \nabla T + \vec{\Phi} \right\} = 0 \tag{4.1.22}$$

$$\nabla \times \vec{E} = 0 \tag{4.1.23}$$

$$\nabla \times \vec{B} = \frac{4\pi \vec{j}}{c} \tag{4.1.24}$$

$$\vec{j} = \sigma (\vec{E} + \frac{1}{c} \vec{v} \times \vec{B}) \tag{4.1.25}$$

$$P = \frac{\rho k T}{\mu M} \tag{4.1.26}$$

We recall, also, the requirement that,

$$\nabla \cdot \vec{B} = 0 \tag{4.1.27}$$

4.1.3 Derivation of heat equation

In some cases we found it more convenient to use a non-conservative heat equation rather than the conservative energy equation (4.1.7). The heat equation is not independent but can be derived from the momentum and energy equations . To show this we take the scalar product of equation (4.1.21) and $\vec{v}$, subtract it from equation (4.1.22) in order to eliminate the kinetic energy terms. On rearrangement and use of equation (4.1.20) we obtain,

$$\rho \vec{v} \cdot \nabla \left\{ e + \frac{P}{\rho} \right\} - \vec{v} \cdot \nabla P - \nabla \cdot (\kappa \nabla T) = - \frac{c}{4\pi} \nabla \cdot (\vec{E} \times \vec{B}) - \frac{1}{c} \vec{v} \cdot \vec{j} \times \vec{B} + \vec{Q}_v \ , \tag{4.1.28}$$

where we have condensed the heating terms due to viscous dissipation into the single term $\vec{Q}_v$.

The first two terms on the left hand side of equation (4.1.28) become, on the substitution of equation (4.1.9)

$$\frac{1}{\gamma - 1} \vec{v} \cdot \nabla P - \gamma e \vec{v} \cdot \nabla \rho \tag{4.1.29}$$

By using a vector identity the magnetic terms in equation (4.1.28) become,

$$- \frac{c}{4\pi} \vec{B} \cdot \nabla \times \vec{E} + \frac{c}{4\pi} \vec{E} \cdot \nabla \times \vec{B} - \frac{1}{c} \vec{v} \cdot \vec{j} \times \vec{B} = - \frac{j^2}{\sigma} \tag{4.1.30}$$

The right hand side is determined from equations (4.1.23) - (4.1.25). Finally, therefore, the heat equation (4.1.28) can be expressed as,

$$\nabla \cdot (\kappa \nabla T) = \frac{1}{\gamma - 1} \vec{v} \cdot \nabla P - \gamma e \vec{v} \cdot \nabla \rho + \frac{\vec{j}^2}{\sigma} - \vec{Q}_v \tag{4.1.31}$$

4.1.4 Order of magnitude estimates

Although the simplifying assumption of steady state conditions has already been made, the set of equations (4.1.20) - (4.1.27) is still very difficult to solve. Consequently let us consider what further simplifications may be made in order to facilitate solution. At this point it may be useful to conduct an elementary dimensional analysis of the mechanical, electromagnetic, and viscous terms in these equations in order to compare their orders of magnitude, and to justify the omission of some of them.

On substituting equation (4.1.24) into (4.1.21) the equation of motion becomes,

$$\rho\vec{v}\cdot\nabla\vec{v} = -\nabla P + \frac{1}{4\pi}\nabla \times \vec{B} \times \vec{B} - \rho\nabla\phi + \vec{F}_v \qquad (4.1.32)$$

The inertia forces in this equation are equivalent to stresses of order of magnitude $\frac{\rho v^2}{L}$, where L is a characteristic scale length of the system. The magnetic forces are of order $\frac{B^2}{L}$. The ratio of magnetic to inertia forces is thus,

$$S = \frac{B^2}{\rho v^2} \qquad (4.1.33)$$

The number S is the ratio of the magnetic energy (of order B^2) and the kinetic energy per unit volume (of order ρv^2). It measures approximately the effect of the magnetic field upon the motion of the fluid. Near the earth observations indicate the presence of a magnetic field of about 5×10^{-5} gauss, a particle density of 5 - 10 /cm^3, and a velocity of flow during periods of solar quiescence of about 300 - 350 km/sec. These imply a value of $S \simeq 0.03$ showing that the effect of the magnetic field far away from the sun is very small. Near to the sun, however, where the magnetic field may be of the order of 1 gauss, the particle density between 10^7 and 10^8 /cm^3, and the velocity of flow less than 1 km/sec, S may become very large ($\simeq$10), indicating that the fluid flow will in fact be dominated by the influence of the magnetic field. Qualitatively we would expect that near the sun, the expanding corona

would be constrained to move along the solar dipolar magnetic field lines. With increasing heliocentric distance, the flow will become gradually modified by other forces until eventually the influence of the magnetic field is overwhelmed and it is swept along with the fluid in virtually radial expansion.

The relative importance of the inertial forces and the viscous forces in the momentum equation is determined by the Reynold's number R, where,

$$R = \frac{Lv}{\mu_v} \tag{4.1.34}$$

Consequently the ratio of electromagnetic forces and viscous forces is determined by the product RS where,

$$RS = \frac{B^2 L}{\rho \mu_v v} \tag{4.1.35}$$

Since $\mu_v \simeq 1.2 \times 10^{-16}$ both these ratios will be very large in all situations occurring in the solar wind, indicating that the viscous forces are much smaller than both the magnetic and inertial forces.

4.1.5 Non-viscous hydrodynamic equations

It thus appears that there is some justification for ignoring the viscous forces in all regions of the solar wind and for ignoring the electromagnetic effects at large heliocentric distances. However, the electromagnetic terms introduce such great complication into the problem that they will initially be ignored altogether while we attempt to determine the general nature of the flow.

The hydromagnetic equations are now reduced to a set of four,

$$\nabla \cdot (\rho \vec{v}) = 0 \tag{4.1.36}$$

$$\rho \vec{v} \cdot \nabla \vec{v} = - \nabla P - \rho \nabla \phi \tag{4.1.37}$$

$$\nabla \cdot (\kappa \nabla T) = \frac{1}{\gamma - 1} \vec{v} \cdot \nabla P - \gamma e \vec{v} \cdot \nabla \rho \tag{4.1.38}$$

or $$\kappa\nabla T = (\tfrac{1}{2}\rho v^2 + e\rho + P + \rho\phi)\vec{v} + H/r^2 \tag{4.1.39}$$

$$P = \frac{\rho kT}{\mu M} \tag{4.1.40}$$

where H is an integration constant.

Equations (4.1.38) and (4.1.39) are the heat and energy equations, either of which may be used. The constant H in equation (4.1.39) results from the integration of equation (4.1.22) and has to be evaluated from the boundary conditions.

If we ignore the rotational velocity of the sun and assume that the solar wind flow is spherically symmetric, then in heliocentric spherical polar coordinates equations (4.1.36) - (4.1.40) become,

$$\frac{d}{dr}(\rho v r^2) = 0 \tag{4.1.41}$$

$$\rho v \frac{dv}{dr} = -\frac{dP}{dr} - \rho\frac{d\phi}{dr} \tag{4.1.42}$$

$$\frac{1}{r^2}\frac{d}{dr}\left\{\kappa r^2\frac{dT}{dr}\right\} = \frac{1}{\gamma - 1}v\frac{dP}{dr} - \gamma e v\frac{d\rho}{dr} \tag{4.1.43}$$

$$\kappa r^2\frac{dT}{dr} = (\tfrac{1}{2}\rho v^2 + e\rho + P + \rho\phi)vr^2 + H \tag{4.1.44}$$

$$P = \frac{\rho kT}{\mu M} \tag{4.1.45}$$

where v now represents the radial component of velocity .
Equation (4.1.41) may be integrated to give:

$$\rho v r^2 = J \tag{4.1.46}$$

where the quantity $4\pi J$ represents the rate of mass flow from the sun. Eliminating P, ϕ, and e by means of equation (4.1.46),(4.1.5), and (4.1.9) equations (4.1.42) - (4.1.44) become,

$$\frac{dv}{dr} = \frac{\frac{v}{r}\left\{\frac{2kT}{\mu M} - \frac{kr}{\mu M}\frac{dT}{dr} - \frac{GM_\odot}{r}\right\}}{v^2 - \frac{kT}{\mu M}} \tag{4.1.47}$$

$$\frac{d}{dr}\left\{\kappa r^2 \frac{dT}{dr}\right\} = \frac{JkT}{\mu M}\left\{\frac{1}{\gamma - 1}\frac{dT}{dr} + \frac{T}{v}\frac{dv}{dr} + 2\frac{T}{r}\right\} \tag{4.1.48}$$

$$\kappa r^2 \frac{dT}{dr} = J\left\{\tfrac{1}{2}v^2 + \frac{\gamma}{\gamma - 1}\frac{kT}{\mu M} - \frac{GM_\odot}{r}\right\} + H \tag{4.1.49}$$

4.2 Boundary conditions and permissible solutions.

Equations (4.1.46), (4.1.47) and either (4.1.48) or (4.1.49) represent the basic equations of flow for the solar wind problem. The momentum equation (4.1.47) is a first order differential equation, as is equation (4.1.41) from which the continuity equation (4.1.46) is derived. The heat and energy equations are second order differential equations, although the energy equation (4.1.49) has been integrated once to give the integration constant H. It is clearly necessary to specify four boundary conditions, one each for the momentum and continuity equations and two each for the heat and energy equations, in order to arrive at a well defined solution.

The boundary conditions physically most appropriate for the sun are deduced from the requirement that the solar corona should be near hydrostatic equilibrium and tightly bound by the gravitational field, at least during periods of solar minimum. We express this condition by the inequalities:

$$\tfrac{1}{2}v^2(r_o) \ll \frac{kT_o}{\mu M} \ll \frac{GM_\odot}{r_o} \tag{4.2.1}$$

where r_o represents the heliocentric distance of the point in the corona to be considered as the inner boundary of the solar wind.

We obtain the other two boundary conditions from the observation that interstellar space into which the solar wind expands is a cold vacuum compared with conditions near to the sun. The particle density

of the interstellar medium is typically of the order of 1 /cm^3 compared with about 10^7 /cm^3 in the corona, while the temperature of an H I region is about $10^{2°}$K compared with about $10^{6°}$K in the corona. We thus neglect the effects of the interstellar pressure and require that,

$$T(\infty) = 0 \tag{4.2.2}$$

$$\rho(\infty) = 0 \tag{4.2.3}$$

We will now consider qualitatively the effect of these boundary conditions upon the solutions of the solar wind problem, and in particular their effect upon the solution of the momentum equation.

From the requirement that the corona should be near hydrostatic equilibrium we infer that the velocity of the flow in this region must be small. Again, from condition (4.2.1) we expect that near to the corona the dominant terms in the momentum equation (4.1.47) will be the potential energy term $\frac{GM_\odot}{r}$, and the thermal energy term $\frac{kT}{\mu M}$, and consequently that $\frac{dv}{dr} > 0$. This implies that for some distance at least above the base of the corona the velocity of flow will increase. Let the increase in velocity continue until the heliocentric distance r_m, say, is reached, after which, we assume, the velocity will start to decrease. Thus, we assume the solar wind will reach a maximum velocity v_m at the point r_m.

The condition for there to be a maximum velocity in the solar wind flow is for $\frac{dv}{dr} = 0$ at r_m. This will occur if the numerator of equation (4.1.47) vanishes. That is if,

$$\frac{2kT}{\mu M} - \frac{kr}{\mu M}\frac{dT}{dr} - \frac{GM_\odot}{r} = 0 \tag{4.2.4}$$

Equation (4.2.4) can be expressed as,

$$\frac{GM_\odot}{r} = -\, r^3 \frac{d}{dr}\left\{\frac{kT}{\mu M r^2}\right\} \tag{4.2.5}$$

In other words there will be a turning point in the solution to the

momentum equation if there is a root of this equation for a $r_m > r_o$. It will be noted from equation (4.2.5) that this condition depends only upon the temperature. Near to the corona the gas is gravitationally bound and by condition (4.2.1) $\frac{GM_\odot}{r}$ is the dominant term in the numerator of the equation of motion (4.1.47).

Consider now the simple case when the temperature distribution in the solar wind is a monotonically decreasing function of r. Then $\frac{dT}{dr} < 0$ everywhere, and we assume that there exists a minimum positive number N, such that

$$T(r) = T_o/r^N \ . \tag{4.2.6}$$

We note that,

$$- \frac{d}{dr}\left\{\frac{T}{r^2}\right\} = - \frac{1}{r^2}\frac{dT}{dr} + \frac{2T}{r^3} \tag{4.2.7}$$

Since both terms on the right of this equation are positive we have that,

$$- \frac{d}{dr}\left\{\frac{T}{r^2}\right\} > 2T/r^3 > 2T_o/r^{(3 + N)} \tag{4.2.8}$$

which follows from (4.2.6).

Rearranging equation (4.2.5), we have that the condition for a turning point to occur in the solution is for,

$$\frac{GM_\odot \mu M}{kr^4} = - \frac{d}{dr}\left\{\frac{T}{r^2}\right\} \tag{4.2.9}$$

If $N < 1$, $2T_o/r^{(3 + N)}$ must become larger than $\frac{GM_\odot \mu M}{kr^4}$ for some sufficiently large value of r. But at $r = r_o$, $GM_\odot \mu M/kr^4 > - d/dr(T/r^2)$ implying from equation (4.2.8) that at some point $r = r_m$ the equation (4.2.6) will be true. This proves that a sufficient condition for the existence of a turning point in the velocity distribution in the solar wind is that the corona should be tightly bound by the gravitational field and that the temperature should decrease less rapidly than 1/r (Parker 1967).

Thermal conduction in the solar corona is probably sufficient to cause the temperature to decrease slowly enough with increasing radial distance for the above criterion to be fulfilled. It was first shown by Chapman in 1957 that for a static corona where radiative and other losses are negligible, the temperature distribution is determined by the conservation of conductive flux:

$$\nabla\cdot(\kappa\nabla T) = 0 \tag{4.2.10}$$

This is merely the heat equation (4.1.38) where the dissipative terms have been neglected. Equation (4.2.10) is equivalent to

$$\kappa_o T^{5/2} \frac{dT}{dr} r^2 = \text{constant} \tag{4.2.11}$$

which can be integrated to give

$$T(r) = T_o\left[\frac{r_o}{r}\right]^{\frac{2}{7}} \tag{4.2.12}$$

in which case the temperature distribution would certainly satisfy the condition.

From equation (4.1.49) we can approximate that close to the corona

$$\kappa r^2\frac{dT}{dr} = -\frac{GM_\odot J}{r} \tag{4.2.13}$$

On integration this gives that

$$T(r) \propto r^{-\frac{4}{7}} \tag{4.2.14}$$

It thus appears that it is not unreasonable to expect T(r) to vary as $\frac{1}{r^N}$ where $N < 1$ at least in the low velocity region.

Beyond the turning point at r_m the velocity will decrease since the numerator of equation (4.1.47) is now positive.

We will now attempt to estimate the order of magnitude of the

velocity at large heliocentric distances. This can be achieved by a consideration of equation (4.1.42). On rearrangement this becomes,

$$\frac{\mu M}{k}\frac{v}{T}\frac{dv}{dr} = -\frac{1}{P}\frac{dP}{dr} - \frac{\mu M}{k}\frac{1}{T}\frac{d\phi}{dr} \qquad (4.2.15)$$

On integration from the turning point to infinity we have that,

$$\frac{\mu M}{2k}\int_{r_m}^{\infty}\frac{dr}{T}\frac{d}{dr}(v^2) = -[\ln(P)]_{r_m}^{\infty} - \frac{GM_{\odot}M\mu}{k}\int_{r_m}^{\infty}\frac{dr}{Tr^2} \qquad (4.2.16)$$

thus
$$P(\infty) = P(r_m)\exp(A + B) \qquad (4.2.17)$$

where,
$$A = -\frac{M}{2k}\int_{r_m}^{\infty}\frac{dr}{T}\frac{d}{dr}(v^2) \qquad (4.2.18)$$

and
$$B = -\frac{GM_{\odot}M\mu}{k}\int_{r_m}^{\infty}\frac{dr}{Tr^2} \qquad (4.2.19)$$

If v decreases after reaching the turning point, $\frac{d}{dr}(v^2) < 0$ so that $A > 0$. $B < 0$ since T declines less rapidly than $1/r$, and this also implies that B is finite. Thus it is clear from (4.2.17) that $P(\infty)$, the pressure at infinity, is non-vanishing also. Solutions of the type where v decreases after reaching r_m are consequently excluded as they would contravene boundary conditions (4.2.2) and (4.2.3).

In order to find solutions compatible with the boundary conditions we return to a consideration of equation (4.1.47). It will be noted that the denominator vanishes when $v^2 = \frac{kT}{\mu M}$, at which point the velocity gradient will become infinite. As this is obviously not physically possible, solutions of this type are excluded. The velocity gradient can remain finite when $v^2 = \frac{kT}{\mu M}$ only if this occurs at r_m when the numerator of equation (4.1.47) vanishes simultaneously. As this is the only remaining class of solution we determine whether it satisfies the boundary conditions.

From the previous discussion we have that,

$$\frac{GM_\odot}{r} > \frac{2kT}{\mu M} - \frac{kr}{\mu M}\frac{dT}{dr} \quad , \qquad \text{when } r < r_m \ , \tag{4.2.20}$$

and that

$$\frac{GM_\odot}{r} < \frac{2kT}{\mu M} - \frac{kr}{\mu M}\frac{dT}{dr} \quad , \qquad \text{when } r > r_m \ . \tag{4.2.21}$$

In the case of the solution under consideration we have that,

$$v^2 < \frac{kT}{\mu M} \quad , \qquad \text{when } r < r_m \ , \tag{4.2.22}$$

and that

$$v^2 > \frac{kT}{\mu M} \quad , \qquad \text{when } r > r_m \ . \tag{4.2.23}$$

In this situation the velocity gradient will remain positive for all values of r. The point r_m is no longer a turning point but is a singular or critical point of the solution. The heliocentric distance at which this occurs will be denoted r_c. We can demonstrate that this solution satisfies the boundary condition of zero pressure at infinity by considering the continuity equation (4.1.46).

If $\frac{dv}{dr} > 0$ for all values of r, then as $r \to \infty$, v must tend to a constant value greater than zero. Thus the density, ρ, must tend to zero at least as fast as $1/r^2$ as $r \to \infty$, yielding the required zero pressure.

The topology of the solution of the momentum equation has been determined by Parker (1967) and is shown in figure (4.2.1). It constitutes a one parameter family of curves in the (r,v) plane.

The velocity at the critical point,

$$v_c = \left\{\frac{kT(r_c)}{\mu M}\right\}^{\frac{1}{2}} \ , \tag{4.2.24}$$

is close to the velocity of sound $v_s = (\gamma kT/\mu M)^{\frac{1}{2}}$. Velocities at large heliocentric distances are thus supersonic. It is, perhaps, surprising that the solar corona, in which the thermal velocities are typically of the order of 180 km/sec can cause the acceleration of material against the solar gravitational field, where the escape velocity is about

500 km/sec, and give it the velocity of several hundred kilometres per second observed at the earth. The mechanism by which this occurs is analogous to flow through a de Laval nozzle, where the throat constricting the flow in the solar wind case is produced by the restraining gravitational field (Dessler 1967).

4.3 Approaches to the solar wind problem

The four boundary conditions embodied in equations (4.2.1), (4.2.2), and (4.2.3), while being the most reasonable from a physical point of view, are not necessarily the most convenient for a numerical solution of the problem. We have shown that the only solution to the momentum equation consistent with these boundary conditions is the one passing through the critical point from a subsonic to a supersonic region. Conversely any solution passing through this transition point, and obeying the inner boundary requirements, is acceptable as it automatically satisfies the boundary conditions at infinity. Consequently the requirement that the solution pass through the critical point may be used as an alternative, and perhaps simpler boundary condition than equations (4.2.2) and (4.2.3).

4.3.1 Hydrodynamic models

The first attempts at a numerical solution of the equations of motion were by Noble and Scarf (1963). They attempted to produce a model of the solar corona and solar wind in the region between the earth and the sun by integrating the set of equations (4.1.46), (4.1.47) and (4.1.49). their method of solution was to specify as boundary conditions the temperature, velocity, and essentially the constant H in equation (4.1.49), at the earth, where the values were known approximately from space flight experiments. Their fourth condition was obtained from the requirement that the solution should pass through the critical point. This condition was satisfied by the standard numerical methods of two-point boundary value problems: the temperature gradient was specified at the lower boundary point, the earth, and the integration carried out towards the corona. The temperature gradient at the earth was then altered in an iterative process, until the solution passing through the critical point

and down into the solar corona was obtained.

The approach of Whang and Chang (1965) was rather different. They were attempting to produce a numerical solution to equations (4.1.46), (4.1.47), and (4.1.49) for all values of r, and were therefore obliged to treat more thoroughly the condition at infinity.

Their first boundary condition was the requirement that the solution should pass through the critical point, which from equation (4.2.24), fixed the value v_c at the point r_c. Two other boundary conditions were obtained by specifying the coronal values of density and temperature. These were imposed in practice by varying the values of r_c and ρ_c, the density at the critical point, in an iterative manner until the coronal parameters were suitably close to those observed. The final boundary condition was obtained from a consideration of the energy equation (4.1.49). On rearrangement this becomes,

$$H = \kappa r^2 \frac{dT}{dr} - J\left\{\tfrac{1}{2}v^2 + \frac{\gamma}{\gamma - 1}\frac{kT}{\mu M} - \frac{GM_\odot}{r}\right\} \qquad (4.3.1)$$

As $r \to \infty$, $T \to 0$ and $v \to v_\infty$. The first term on the right hand side represents the conductive energy flux; we will consider its limiting value as $r \to \infty$. We assume that the temperature decreases proportional to $1/r^s$. Then $\frac{dT}{dr} \propto -\frac{s}{r^{s+1}}$. Using expression (4.1.11) for the thermal conductivity we find the conductive energy flux F_c varies as

$$F_c \propto - r^{-\frac{7}{2}s + 1} \qquad (4.3.2)$$

Thus $F_c \to 0$ as $r \to \infty$ if $s > 2/7$. If the temperature decrease at large distances as $1/r^{2/7}$, the conductive flux will remain finite, while if it decreases faster than this the conductive flux will vanish. Whang and Chang assumed that the latter case is true. The integration constant H then becomes,

$$H = \tfrac{1}{2}Jv_\infty^2 \qquad (4.3.3)$$

The constant H can be determined from equation (4.3.1) at any point

where all the pertinent quantities are known. Presumably this will be at the critical point. The asymptotic velocity v_∞ can then be evaluated by means of equation (4.3.3).

The final boundary condition is thus obtained: that the computed velocity $v \to v_\infty$ as $r \to \infty$. This condition was applied by the construction of an asymptotic solution which was required to fit smoothly with the exact numerical solution at a certain large distance from the sun.

4.3.2 Hydrodynamic models with viscosity

Numerical solutions of the solar wind problem, including the effects of viscosity, have been obtained by Scarf and Noble (1965) and by Whang, Liu, and Chang (1966), where essentially the same boundary conditions were applied as in the two cases previously discussed.

These have shown that the viscous stresses do, in fact, become large at large distances from the sun and may have an appreciable effect on the flow. Strangely, models including this refinement appear to agree less well with experimental values of the solar wind parameters than those in which the viscous terms were neglected. This anomaly may be due to the alteration of the coefficients of viscosity by the constraining effect of the magnetic field on the flow (Brandt 1970).

4.3.3 Two fluid model

In the approaches to the problems so far described, it has been assumed that a unique temperature could be assigned to the solar wind plasma at any one point, but as we showed in chapter 3, kinetic theory predicts that there should be a considerable difference in temperature between the proton and electron components. Hartle and Sturrock (1968) have thus constructed a model in which the solar wind is regarded as the superimposed flow of two fluids; one consisting of protons and the other of electrons. The density and velocity of the flows must be the same for both electrons and protons in order to preserve charge neutrality.

Consequently although two heat equations are required for a study of the flow only one continuity and one momentum equation is needed. The continuity equation can be represented as,

$$\rho v r^2 = J \tag{4.3.4}$$

which is identical to equation (4.1.46). The momentumequation now becomes,

$$\rho v \frac{dv}{dr} = - \frac{d}{dr}\left\{\frac{\rho k}{M}(T_e + T_p)\right\} - \frac{GM_\odot \rho}{r^2} \tag{4.3.5}$$

where T_e and T_p are the electron and proton temperatures. This equation is analogous to (4.1.42). The two heat equations are,

$$\frac{1}{r}\frac{d}{dr}\left\{\kappa_e r^2 \frac{dT_e}{dr}\right\} = \frac{1}{\gamma - 1}\frac{\rho v k}{M}\frac{dT_e}{dr} - \frac{vkT_e}{M}\frac{d\rho}{dr} + \frac{3}{2}\nu_E \rho \frac{k}{M}(T_e - T_p) \ , \tag{4.3.6}$$

$$\frac{1}{r}\frac{d}{dr}\left\{\kappa_p r^2 \frac{dT_p}{dr}\right\} = \frac{1}{\gamma - 1}\frac{\rho v k}{M}\frac{dT_p}{dr} - \frac{vkT_p}{M}\frac{d\rho}{dr} - \frac{3}{2}\nu_E \rho \frac{k}{M}(T_e - T_p) \ , \tag{4.3.7}$$

where κ_e and κ_p represent the electron and proton thermal conductivities, and ν_E the energy exchange rate. The heat equations reduce to equation (4.1.48) if $T_e = T_p$, as we have previously assumed.

Equations (4.3.6) and (4.3.7) are both second order differential equations requiring two boundary conditions each. Consequently a total of six boundary conditions must be specified in order to define the solution completely; three specify the density and electron and proton temperature at the solar corona; the fourth requires that the solution should pass through the critical point, implying that $\rho \to 0$ as $r \to \infty$; the final two specify that T_e and $T_p \to 0$ as $r \to \infty$. The equations were solved iteratively, rather than simultaneously as in the previous cases described.

The results obtained from this analysis predicted the electron and proton temperatures to be $3.4 \times 10^{5}{}^{\circ}K$ and $4.4 \times 10^{3}{}^{\circ}K$ respectively, near the earth. Space experiments have shown that the average value of T_e is approximately four times the average proton temperature during periods of little solar activity. The discrepancy between theory and observation indicates that a more efficient mechanism of energy exchange between protons and electrons must occur and implies that the single fluid models are a better approximation than kinetic theory predicts.

4.3.4 Magnetohydrodynamic models

We noted earlier that near to the sun the energy density of the magnetic field will be greater than the kinetic energy density of the solar wind. Consequently it will certainly play a significant role in determining the nature of the flow. A considerable number of approximate models have been constructed in order to estimate the magnitude of this effect.

Parker (1963), neglecting the energy considerations, treated the magnetic field in a very simple way by assuming that the field lines follow the streamlines of the solar wind flow. Mestel (1968) has demonstrated the effectiveness of the coupled solar wind and magnetic field at removing angular momentum from the sun, by considering an equation of motion simplified by the assumption of an isothermal corona. Weber and Davis (1967) solved the problem under the restrictive assumption of spherical symmetry by considering flow only near to the equatorial plane of the sun, and with a polytropic representation of the energy equation. More recently Grzedielski (1968) and Brandt, Wolff, and Cassinelli (1969) have solved the set of equations (4.1.20) - (4.1.27) but once again only by considering spherically symmetrical flow near the equator. With these restrictions the equations become,

$$\rho v_r r^2 = J \tag{4.3.8}$$

$$\rho v_r \frac{dv_r}{dr} - \rho\frac{v_\phi^2}{r} + \frac{dP}{dr} + \frac{GM_\odot\rho}{r^2} + \frac{B_\phi}{4\pi r}\frac{d}{dr}(B_\phi r) = 0 \tag{4.3.9}$$

$$\rho v_r \frac{dv_\phi}{dr} + \frac{\rho v_r v_\phi}{r} - \frac{B_r}{4\pi r}\frac{d}{dr}(B_\phi r) = 0 \tag{4.3.10}$$

$$\kappa r^2\frac{dT}{dr} + \frac{1}{4\pi}(B_\phi B_r v_\phi - B_\phi^2 v_r) - J\left\{\tfrac{1}{2}(v_r^2 + v_\phi^2) + \frac{5kT}{M} - \frac{GM_\odot}{r}\right\} = H \tag{4.3.11}$$

$$\frac{d}{dr}\left\{r(B_r v_\phi - v_r B_\phi)\right\} = 0 \tag{4.3.12}$$

$$\frac{d}{dr}(r^2 B_r) = 0 \tag{4.3.13}$$

where H is a constant, and the subscripts r and ϕ represent the radial and azimuthal components of a vector. We have assumed also that the plasma is fully ionised and $\mu = 1/2$. Equation (4.3.13) may be integrated immediately to give,

$$B_r = B_o(r_o/r)^2 \qquad (4.3.14)$$

where B_o is the magnetic flux density at the lower boundary point r_o.

Equation (4.3.12) may be integrated to give,

$$r(B_r v_\phi - v_r B_\phi) = S \ . \qquad (4.3.15)$$

The constant S can be evaluated on the assumption that at the sun the corona is constrained to co-rotate, and that in the frame of reference co-rotating with the sun the velocity is parallel to the magnetic field; that is $\vec{v} \times \vec{B} = 0$. Thus in the non rotating reference frame we have,

$$v_\phi B_r - v_r B_\phi = r\Omega B_r \ . \qquad (4.3.16)$$

Therefore equation (4.3.15) becomes,

$$r(B_r v_\phi - v_r B_\phi) = \Omega r_o^2 B_o \ , \qquad (4.3.17)$$

where Ω represents the angular velocity of the sun.

On rearrangement equation (4.3.10) becomes,

$$\frac{d}{dr}(rv_\phi) - \frac{B_r r^2}{4\pi\rho v_r r^2}\frac{d}{dr}(B_\phi r) = 0 \ . \qquad (4.3.18)$$

From equations (4.3.8) and (4.3.14) we see that the term outside the differential in this equation is a constant, allowing it to be integrated to give,

$$rv_\phi - \frac{B_r}{4\pi\rho v_r}B_\phi r = L \ , \qquad (4.3.19)$$

The constant L, which represents the total angular momentum per unit mass lost by the star can be evaluated by eliminating B_ϕ between equation (4.3.17) and (4.3.19) and substituting:

$$M_A^2 = 4\pi\rho v_r / B_r^2 \tag{4.3.20}$$

where M_A is the Alfvenic Mach number. We then obtain

$$v_\phi = \Omega r \frac{\frac{LM_A^2}{\Omega r^2} - 1}{M_A^2 - 1} \tag{4.3.21}$$

From the discussion of the boundary conditions for the solar wind flow without a magnetic field it was shown that the solution had to pass through a critical point on its way towards supersonic velocities at large distances from the sun. The same analysis will hold true for the case with a magnetic field. Consequently the velocity should exceed the Alfven velocity at some point r_A say. In order for v_ϕ in equation (4.3.21) to remain finite at r_A the numerator must vanish simultaneously with the denominator, since $M_A^2 = 1$ at $r = r_A$. Thus we require that

$$L = \Omega r_A^2 \tag{4.3.22}$$

This equation indicates that the magnetic field causes the same loss of angular momentum as if the corona co-rotated with the sun out as far as the Alfven point r_A. Equation (4.3.22) shows that a stellar wind must be a very effective mechanism for removing angular momentum from a star. Equation (4.3.21) thus becomes,

$$v_\phi = \Omega r \frac{(M_A r_A / r)^2 - 1}{M_A^2 - 1} \tag{4.3.23}$$

From equation (4.3.19) we obtain, after rearrangement,

$$B_\phi = B_r \frac{r\Omega}{v_A r_A^2} \left(\frac{r_A^2 - r^2}{M_A^2 - 1} \right) \tag{4.3.24}$$

where v_A is the velocity of the flow in the radial direction at the Alfven point.

The radial part of the momentum equation becomes, on substitution of equations (4.3.23) and (4.3.24) and some rearrangement

$$\frac{dv_r}{dr} = \frac{\frac{v_r}{r}\left\{ (M_A^2 - 1)^3 \left(\frac{4kT}{Mr} - \frac{GM_\odot}{r} - \frac{2kr}{M}\frac{dT}{dr} \right) + r^2\Omega^2 \left(\frac{v_r}{v_A} - 1 \right) \left(\frac{v_r}{v_A}(M_A^2 - 1) - 3M_A^2 + 1 \right) \right\}}{\left(v^2 - \frac{2kT}{M} \right)(M_A^2 - 1)^3 - \Omega^2 r^2 M_A^4 \left(\frac{r_A^2}{r^2} - 1 \right)^2} \tag{4.3.25}$$

This equation can be simplified to some extent by substituting the propagation velocities of the characteristic disturbances of a plasma. The isothermal speed of sound is given by,

$$v_s^2 = \frac{2kT}{M} \quad . \tag{4.3.26}$$

The Alfven velocity in the radial direction is given by,

$$v_m^2 = \frac{B_r^2}{4\pi\rho} \quad . \tag{4.3.27}$$

The Alfven velocity is given by,

$$v_H^2 = (B_r^2 + B_\phi^2)/4\pi\rho \tag{4.3.28}$$

By using these three equations the denominator of equation (4.3.25) can be reduced to,

$$\left\{ \frac{v_r^2}{v_m^2} - 1 \right\}^2 \left\{ \frac{v_r^2}{v_m^2} \left(v_r^2 - v_s^2 - v_H^2 \right) + v_s^2 \right\} \tag{4.3.29}$$

Critical points of the momentum equation will occur when the denominator becomes equal to zero, at which point the numerator must vanish also. From an inspection of expression (4.3.29) it is obvious that a critical point will occur at the Alfven point, when $v_r(r_A) = v_A = v_m(r_A)$.

Other critical points will occur when,

$$\frac{v_r^2}{v_m^2}\left\{v_r^2 - v_s^2 - v_H^2\right\} + v_s^2 = 0 \quad . \tag{4.3.30}$$

This is a quadratic in v_r^2 which has the solution,

$$v_r^2 = \frac{1}{2}\left\{v_s^2 + v_H^2\right\} \pm \frac{1}{2}\left\{\left\{v_s^2 + v_H^2\right\}^2 - 4v_s^2 v_m^2\right\} \quad . \tag{4.3.31}$$

The plus and minus signs in this expression represent respectively the velocities of the fast and slow magneto-acoustic disturbances in a plasma (Ferraro and Plumpton 1966). The solution of the momentum equation which obeys the boundary condition of vanishing density and temperature at infinity must pass through all three of these critical points.

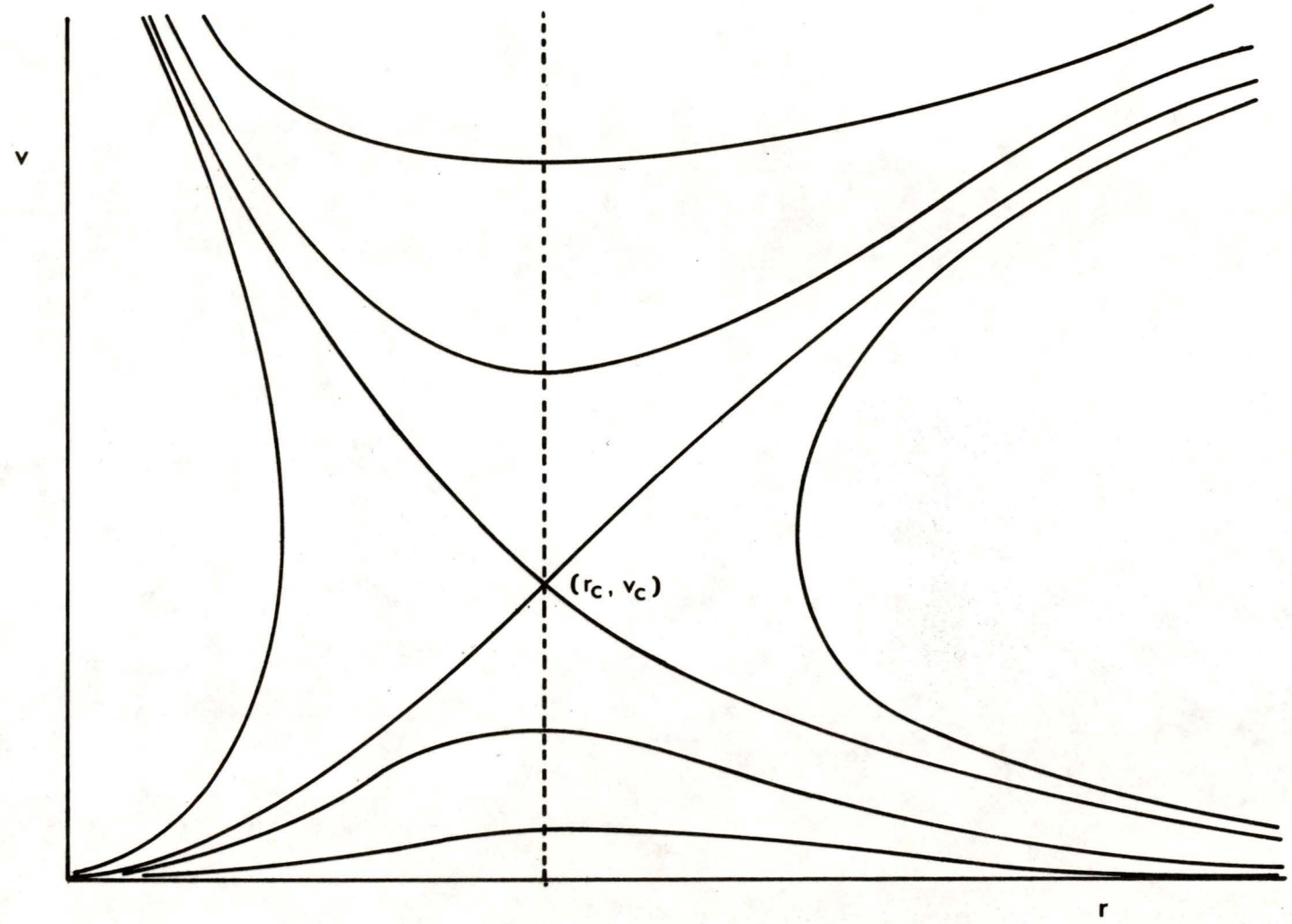

Figure 4.2.1 The solution of the momentum equation

CHAPTER 5

NUMERICAL MODELS

5.1 Introduction

In this chapter we present the results of our numerical investigation of the thermally driven stellar wind as a mechanism for mass loss in stars. We discuss also details of the methods by which the results were obtained.

The methods of solution of the equations of motion differ considerably from previous ones chiefly in the application of the boundary conditions. Their specification constitutes the most difficult part of the problem and was attempted in two different ways.

The first method uses the same basic numerical techniques as Hartle and Sturrock (1968) and solves the equations of motion including a heat equation. However, Hartle and Sturrock were concerned with a two-fluid model of the solar wind, whereas we have assumed throughout that $T_e = T_p$, so that our set of equations is different from theirs. A further difference lies in our more elaborate treatment of the boundary conditions at infinity.

The second approach was necessitated by the greater convenience of specifying the particle flux as a boundary condition when models of stellar winds considerably different from the solar wind were being constructed. The equations of motion, including an energy equation, were solved simultaneously instead of by iteration as before. The method of solution perhaps most resembles that of Whang and Chang (1965) in that the boundary condition at infinity, namely that the thermal conduction flux should vanish, was the same as they used, although applied in a different way. Whang and Chang attempted only to construct models of the solar wind, while our intent is to produce models covering a wider range of circumstances.

5.2 Integration procedures

5.2.1 Integration of the heat equation

Since the sun is the only star in which a thermally driven stellar wind is directly observed it was felt that the inner boundary conditions should initially be chosen to represent approximately the conditions

observed near the solar surface. The approach taken was to solve the set of equations of motion, including a heat equation, on the assumptions that the solar wind is a single fluid flow with a unique temperature at any given radial distance, that the effects of viscosity and the magnetic field are negligible, and that the only heating mechanism above the base of the corona is due to thermal conductivity.

The set of equations to be solved are (4.1.36), (4.1.37), and (4.1.38). These are,

$$Nvr^2 = J' \tag{5.2.1}$$

$$\frac{dv}{dr} = \frac{\frac{v}{r}\left(\frac{GM_\odot}{r} - \frac{2kT}{\mu M} - \frac{kr}{\mu M}\frac{dT}{dr}\right)}{v^2 - \frac{kT}{\mu M}} \tag{5.2.2}$$

$$\frac{d}{dr}\left(\kappa r^2 \frac{dT}{dr}\right) = \frac{J'kT}{\mu}\left(\frac{1}{\gamma - 1}\frac{dT}{dr} + \frac{T}{v}\frac{dv}{dr} + 2\frac{T}{r}\right), \tag{5.2.3}$$

where $J' = J/M$ represents the particle flux.

The equations were solved by an iterative procedure. The temperature distribution satisfying the boundary conditions at the corona and at $r = \infty$ is guessed initially and used to find $v(r)$ from equation (5.2.2). From the first boundary condition, equation (4.2.1), and $v(r)$ the integration constant, J', in equation (5.2.1) is determined. Using the computed values of $v(r)$ and J', the temperature distribution $T(r)$ may be calculated from equation (5.2.3), ensuring that the condition at $r = r_o$ and at infinity are satisfied, by standard techniques of numerical analysis for second order differential equations. Since equation (5.2.3) has end point conditions an iteration procedure, which will be described later, is required in order to ensure that both are satisfied. The new values of $T(r)$ may now be used in the momentum equation (5.2.2) to obtain further estimates of $v(r)$ and $N(r)$. The whole procedure is repeated until changes in the variables from one cycle to the next are less than a small predetermined quantity. The system has then converged to solutions which, in arbitrarily close approximation, simultaneously satisfy the set of equations (5.2.1) - (5.2.3) and the boundary conditions.

In discussing the solutions of the equations of motion it is convenient to transform the independent variable r to a new variable x, where,

$$x = \frac{GM_{\odot}M}{kT_{o}r} = \frac{A}{r} . \qquad (5.2.4)$$

We transform also the dependent variables v, T, to u, τ, where,

$$u = \frac{Mv^2}{kT_{o}} = Bv^2 \qquad (5.2.5)$$

$$\tau = \frac{T}{T_{o}} . \qquad (5.2.6)$$

T_{o} is the temperature at the base of the solar corona, which we take to be 2.0×10^6 °K. Assuming that the solar wind is completely ionised, and that $\mu = \frac{1}{2}$, corresponding to a composition of pure hydrogen, equations (5.2.1) - (5.2.3) become, on transformation,

$$N\left(\frac{u}{B}\right)^{\frac{1}{2}}\left(\frac{A}{x}\right)^2 = J' \qquad (5.2.7)$$

$$\frac{du}{dx} = \frac{\left(1 - 4\frac{\tau}{x} - 2\frac{d\tau}{dx}\right)}{\left(\frac{1}{2} - \frac{\tau}{u}\right)} \qquad (5.2.8)$$

$$\frac{d}{dx}\left(\kappa(\tau)\frac{d\tau}{dx}\right) = \frac{J'k}{A}\left(4\frac{\tau}{x} - \frac{\tau}{u}\frac{du}{dx} - 3\frac{d\tau}{dx}\right) . \qquad (5.2.9)$$

We will use also the energy equation (4.2.39) which transforms to:

$$\frac{d}{dx}\left(\kappa(\tau)\frac{d\tau}{dx}\right) = \frac{d}{dx}\left(\frac{1}{2}x - \frac{1}{4}u - \frac{5\tau}{2}\right)\frac{J'k}{A} \qquad (5.2.10)$$

The condition that the solution of the momentum equation should pass through a critical point is most conveniently satisfied by locating the point and integrating the equations of motion away from it in both directions. This can be achieved by noting that in the integration of

equation (5.2.8) $\tau(x)$ and $\tau'(x)$ are known, either from the initial approximation or from the most recent solution of the heat equation. The critical point will occur when the numerator and the denominator of equation (5.2.8) vanish simultaneously. That is when,

$$1 - 4\frac{\tau}{x} - 2\frac{d\tau}{dx} = 0 \quad . \tag{5.2.11}$$

The value of x satisfying equation (5.2.11) is x_c, and the critical velocity u_c is then given by,

$$u_c = 2\tau_c \quad , \tag{5.2.12}$$

where $\tau_c = \tau(x_c)$.

In order to start the integration an analytical expression for du/dx is required at the critical point. This can be obtained by use of l'Hôpital's rule,

$$\left(\frac{du}{dx}\right)_c = \frac{\lim_{x \to x_c} f'(x)}{\lim_{x \to x_c} g'(x)} \quad , \tag{5.2.13}$$

where,

$$f(x) = 1 - 4\frac{\tau}{x} - 2\frac{d\tau}{dx} \quad , \tag{5.2.14}$$

$$g(x) = \frac{1}{2} - \frac{\tau}{u} \tag{5.2.15}$$

The prime denotes differentiation with respect to x. Equations (5.2.14) and (5.2.15) now yield,

$$\lim_{x \to x_c} f'(x) = -\frac{4}{x_c}\left(\frac{d\tau}{dx}\right)_c + \frac{4\tau_c}{x_c^2} - 2\left(\frac{d^2\tau}{dx^2}\right)_c \tag{5.2.16}$$

$$\lim_{x \to x_c} g'(x) = -\frac{1}{u_c}\left(\frac{d\tau}{dx}\right)_c + \frac{\tau_c}{u_c^2}\left(\frac{du}{dx}\right)_c \quad . \tag{5.2.17}$$

Eliminating $(d\tau/dx)_c$ and τ_c by means of equations (5.2.11) and (5.2.12) we obtain, from equation (5.2.13),

$$\left(\frac{du}{dx}\right)_c = \frac{-\frac{2}{x_c} + 6\frac{u_c}{x_c} - 2\left(\frac{d^2\tau}{dx^2}\right)_c}{-\frac{1}{2u_c} + \frac{1}{x_c} + \frac{1}{2u_c}\left(\frac{du}{dx}\right)_c} . \qquad (5.2.18)$$

On rearrangement this produces a quadratic in $(du/dx)_c$ which has the solution,

$$\left(\frac{du}{dx}\right)_c = \tfrac{1}{2}\left(1 - 2\frac{u_c}{x_c}\right) \pm \tfrac{1}{2}\left\{1 - 20\frac{u_c}{x_c} + 52\frac{u_c^2}{x_c^2} - 16u_c\left(\frac{d^2\tau}{dx^2}\right)_c\right\}^{\frac{1}{2}} . \qquad (5.2.19)$$

There are two curves passing through the critical point, corresponding to the positive and negative signs in equation (5.2.19). One of these is rejected as the velocity decreases outwards and contravenes the boundary condition of zero pressure at infinity. The required solution has $\frac{dv}{dr} > 0$. Since $\frac{dv}{dr} = \frac{dv}{du}\frac{du}{dx}\frac{dx}{dr}$ where $\frac{dx}{dr} < 0$, the critical solution satisfying the correct boundary conditions will have $\frac{du}{dx} < 0$, and is the algebraically smaller of the two. Consequently we select the negative sign in equation (5.2.19). The velocity gradient is then,

$$\left(\frac{du}{dx}\right)_c = \frac{1}{2} - \frac{u_c}{x_c} - \frac{1}{2}\left\{1 - 20\frac{u_c}{x_c} + 52\frac{u_c^2}{x_c^2} - 16u_c\left(\frac{d^2\tau}{dx^2}\right)_c\right\}^{\frac{1}{2}} . \qquad (5.2.20)$$

Having obtained this expression the values of u, $\frac{du}{dx}$, τ, $\frac{d\tau}{dx}$ are all known at x_c and equation (5.2.8) can be integrated as an initial value problem from the critical point by an ordinary predictor-corrector method.

The heat equation is a second order differential equation to which we apply end point conditions. The thermal conductivity is given by,

$$\kappa(\tau) = \kappa_o(T_o\tau)^{\frac{5}{2}} \qquad (5.2.21)$$

On making the substitution $y = \tau^{\frac{7}{2}}$ equation (5.2.9) becomes,

$$\frac{d^2y}{dx^2} = \frac{7J'k}{2A\kappa_o T_o^{\frac{5}{2}}}\left\{4\frac{\tau}{x} - \frac{\tau}{u}\frac{du}{dx} - 3\frac{d\tau}{dx}\right\} , \qquad (5.2.22)$$

which can be expressed as,

$$\frac{d^2y}{dx^2} = F(\tau,\tau',u,u',x) \quad . \qquad (5.2.23)$$

It is obviously impossible to reproduce numerically the condition that $T \to 0$ as $r \to \infty$, and in practice the computation would have to be terminated at some large but finite value of r. On transforming to dimensionless variables the equivalent boundary condition is that $\tau \to 0$ as $x \to 0$. Unfortunately numerical problems again prevent the integration of the equations directly to $x = 0$, as the temperature and velocity gradients, $\frac{d\tau}{dx}$ and $\frac{du}{dx}$, both tend to infinity as $x \to 0$. Consequently integration must be terminated at some small value of x (x_1, say), at which point the temperature is defined to be τ_1. The outer boundary condition is then said to be satisfied when $\tau(x_1) = \tau_1$.

Equation (5.2.23) is linear in y and can be twice numerically integrated to give y(x) and y'(x) for all x in the region $x_0 < x < x_1$. This allows $\tau(x)$ and $\tau'(x)$ to be calculated from the expressions,

$$\tau = y^{2/7} \qquad (5.2.24)$$

and,

$$\frac{d\tau}{dx} = \frac{2}{7} y^{-\frac{5}{7}} \frac{dy}{dx} \quad . \qquad (5.2.25)$$

The integration is started at the inner boundary point, x_0, with $\tau(x_0) = \tau_0$ so that the boundary condition is satisfied automatically. The outer boundary condition, that $\tau(x_1) = \tau_1$, is satisfied by means of an iterative method as we mentioned earlier. The value of the temperature gradient at the corona, $\tau'(x_0)$, is guessed and used as an initial condition for the integration of the heat equation (5.2.23), giving $\tau(x)$ and $\tau'(x)$. In general, $\tau(x_1) \neq \tau_1$, so that $\tau'(x_0)$ must be varied and equation (5.2.23) solved repeatedly until the equality $\tau(x_1) = \tau_1$ is satisfied. When this occurs a temperature distribution satisfying equation (5.2.23) and both the boundary conditions has been obtained.

The value of τ_1 is estimated from a consideration of the energy equation (5.2.10) which, by means of equation (5.2.21), becomes,

$$\frac{A\kappa_o T_o^{\frac{5}{2}}}{J'k}\tau^{\frac{5}{2}}\frac{d\tau}{dx} + \frac{5}{2}\tau + \frac{1}{4}u - \frac{1}{2}x = Z \qquad (5.2.26)$$

The value of Z may be evaluated at the critical point where all the quantities on the left of equation (5.2.26) are known. On substituting for y from equation (5.2.24) we obtain,

$$\frac{dy}{dx} = \left\{Z + \frac{x}{2} - \frac{u}{4} - \frac{5}{2}\tau\right\}\frac{7J'k}{2A\kappa_o T_o^{\frac{5}{2}}}. \qquad (5.2.27)$$

Since $\tau(0) = 0$ we have $y(0) = 0$. Thus if we know all the quantities on the right hand side of equation (5.2.27) it can be numerically integrated to give the values of y by use of the expression

$$y(x_1) = \left\{\left(\frac{dy}{dx}\right)_{x_1} - \left(\frac{dy}{dx}\right)_0\right\}\frac{x_1}{2}, \qquad (5.2.28)$$

which is simply a statement of the trapezium rule. We now assume that $y'(o) = 0$. This requires that $\tau(x) \to 0$ as $x \to 0$ faster than $x^{\frac{2}{7}}$, and is equivalent to the assumption that the thermal conduction flux should vanish at infinity. The reasoning here is similar to that following equation (4.3.1). From equation (5.2.28) we can now obtain the temperature at x_1 :

$$y(x_1) = \tfrac{1}{2}x_1\left(\frac{dy}{dx}\right)_{x_1} \qquad (5.2.29),$$

and,

$$\tau(x_1) = y^{\frac{2}{7}}(x_1) \qquad (5.2.30)$$

Having integrated equation (5.2.22) out as far as x_1 we have an estimate of the temperature at x_1. This is substituted into equation (5.2.27) to obtain a new estimate of the value of $\frac{dy}{dx}$ at x_1. The temperature at the outer boundary was then estimated by using equations (5.2.29) and (5.2.30). This was returned to equation (5.2.27) and the cycle repeated until self consistent values of $y(x_1)$ and $y'(x_1)$ were obtained.

The value of τ obtained in this way is denoted τ_1 and is used as the outer boundary condition at the point x_1. It is appreciated that the method of integration used in equation (5.2.28) represents only a crude approximation, since the parameters of temperature and velocity change rapidly in value for small x. Due to the iteration procedures our results are , however, self consistent and since quite reasonable results were produced the method is vindicated to this extent.

Having solved the heat equation and obtained an improved temperature distribution satisfying the boundary conditions, the parameters at the critical point and its position were determined by means of equation (5.2.11),(5.2.12), and (5.2.13). The momentum equation (5.2.8) was then solved as before and the whole procedure repeated until convergence of all the iterative processes was reached.

Considerable difficulty was found in integrating the equations out to sufficiently small values of x, and it was found to be necessary to transform the independent variable x to ξ where,

$$\xi = - \ln(x). \tag{5.2.31}$$

The momentum and heat equations then become,

$$\frac{du}{d\xi} = \frac{4\tau - e^{-\xi} - 2\frac{d\tau}{d\xi}}{\frac{1}{2} - \frac{\tau}{u}} \tag{5.2.32}$$

$$\frac{d^2y}{d\xi^2} = \frac{7J'k}{2A\kappa_o T_o^{5/2}}\left\{2\tau + \frac{3}{2}\frac{d\tau}{d\xi} + \frac{\tau}{2u}\frac{du}{d\xi}\right\} e^{-\xi} - \frac{7}{2}\tau^{5/2}\frac{d\tau}{d\xi} . \tag{5.2.33}$$

Equations (5.2.32) and (5.2.33) proved more amenable to solution at large radial distances.

5.2.2 Integration of the energy equation

In order to produce models of stellar winds with higher rates of mass loss we found it more convenient to specify as a boundary condition the integration constant J' in equation (5.2.7) rather than the coronal density N_o. Since no attempt was to be made to reproduce the

conditions occuring at the sun it was decided to apply all the boundary conditions at the critical point. This enabled the energy equation (5.2.26) to be used instead of the heat equation, which , since it had been integrated analytically once, had the advantage of being a first order equation and did not require the complicated iterative procedures described earlier to satisfy the boundary conditions.

Having defined the particle flux, J', different models were constructed by varying the position of the critical point x_c. The temperature at the critical point was then fixed by rearranging equation (5.2.11) so that,

$$\tau_c = \tfrac{1}{4}x_c\left\{1 - 2\left(\frac{d\tau}{dx}\right)_c\right\} \qquad (5.2.34)$$

Initially the temperature gradient $(\frac{d\tau}{dx})_c$ must be guessed, but as it is the starting value of an iterative procedure it need not be very accurate. Having τ_c, the critical velocity, u_c, may be then found from equation (5.2.12). Three boundary conditions are thus obtained. The fourth condition is obtained by evaluating the constant Z in equation (5.2.27) at the critical point. The correct value of $\left\{\frac{d\tau}{dx}\right\}_c$ may be chosen by requiring that the thermal conduction flux should tend to zero as $x \to 0$. The constant Z may then be evaluated at $x = 0$ to give,

$$Z = \tfrac{1}{4}u_\infty. \qquad (5.2.35)$$

As $x \to 0$ we then demand that $u \to u_\infty$. In practice we applied this condition by requiring that the temperature distribution should decrease monotonically, and that $u < u_\infty$ out to the limit of integration. This can be achieved by altering $\left\{\frac{d\tau}{dx}\right\}_c$ iteratively until the conditions are obeyed; the procedure converges to one value of $\left\{\frac{d\tau}{dx}\right\}_c$ if the integration is continued to sufficiently small values of x. The boundary conditions applied are thus J', τ_c, u_c, and u_∞. In similar fashion to the earlier method we need an analytical expression for $\frac{du}{dx}$ at the critical point before the integration can proceed. This is obtained as before except that an iterative process between equation (5.2.20) and the heat equation (5.2.9) is necessary to

to produce a self-consistent result.

The system of equations consists now of three first order differential equations with boundary conditions applied at the critical point. They can be solved conveniently as a set of simultaneous initial value equations, the integration starting at the critical point and proceeding in both directions, towards the corona and towards $x = 0$. Only one iteration process is necessary: to ensure that $u \to u_\infty$ as $x \to 0$. The coronal density and temperature appear merely as the values of the parameters N and τ at the value of x at which integration is terminated.

5.3 Results

Figures (5.3.1) and (5.3.2) represent typical results of our calculations and illustrate the topology of the computed solutions. The graphs have been plotted for three different values of coronal density N_o, but the coronal temperature has been kept constant at $\tau(x_o) = 1.0$, corresponding to a temperature of 2×10^6 °K. The position of the critical point is marked throughout by means of a large dot.

Figure (5.3.1) shows the variation of the velocity of the solar wind with radial distance. Near to the corona the velocity tends to zero, satisfying the condition that the corona should be close to hydrostatic equilibrium. On passing through the critical point the rate of increase of velocity becomes very large as the flow becomes highly supersonic. At large radial distances the velocity increases more slowly as it tends to its limiting value u_∞. It will be noted immediately that the qualitative effect of increasing the coronal density is to decrease the velocity of the solar wind.

Figure (5.3.2) shows the variation of the temperature of the solar wind with radial distance. The temperature distribution is a monotonically decreasing function of log r which tends to zero as $r \to \infty$. The result of increasing the density of the corona appears to be that the temperature of the solar wind decreases more rapidly with radial distance, at least as far as the critical point. The reason for this can be deduced by noting that the rate of mass loss also increases with increasing coronal density. We showed in chapter 4 that the rate

of mass loss is completely determined by conditions at the critical point. By the time the critical point has been reached, therefore, a corona with a high density must have done more work in producing its solar wind than a low density corona. Since the acceleration of the solar wind is due to the thermal energy of the corona we may expect that the increased work required will result in the more rapid decrease in the thermal energy, and hence of the temperature, of dense solar winds. Beyond the critical point the temperature of the flow gradually tends to zero as the thermal energy of the solar wind is converted to kinetic energy.

Because the temperature of the dense solar wind flow decreases rapidly close to the corona the velocity of the flow tends to its limiting velocity faster than for a less dense solar wind. This effect can be seen in figure(5.3.1). We may expect that very dense coronas would reach their low limiting velocities virtually immediately after passing through their critical point, after which the expansion velocity would be essentially constant.

Figure (5.3.3) summarizes the effect of coronal density on the rate of mass loss, or the particle flux, J', at constant coronal temperature. For small values of $\log N_o$ the curve is linear and the gradient is equal to unity, indicating that in this region J' is directly proportional to the coronal density, N_o. However, for higher densities the curve flattens out, and the particle flux becomes less dependent upon N_o.

We can elucidate the effect of this behaviour upon the velocity distribution by considering the logarithm of equation (5.2.1), which becomes,

$$\log J' = \log N_o + \log v_o + 2 \log r_o. \qquad (5.3.1)$$

The subscripts have been added as we are concerned with behaviour at the inner boundary point. r_o remains constant by definition. For small N_o $\log J'$ is directly proportional to $\log N_o$ indicating that the velocity remains almost independent of coronal density in this region. At higher

values of N_o this proportionality no longer holds so that the velocity distribution is modified. The particle flux becomes less dependent on the coronal density, which, from equations (5.3.1) must be due to a decrease in the velocity at the coronal boundary point. The rapid decrease of velocity at higher coronal densities can be noted in figure (5.3.1).

The rate of mass loss as a function of coronal temperature at a constant density is shown in figure (5.3.4). The topology of the curves showing velocity and temperature as a function of radial distance are very similar to those in figures (5.3.1) and (5.3.2), and are not shown. It is apparent that the particle flux J' is a quite rapidly increasing function of coronal temperature. At high coronal temperatures the curve appears to become increasingly linear indicating an exponential dependence of the particle flux upon coronal temperature in this region.

Figures (5.3.5) and (5.3.6) show a family of curves which represents the velocity and density of the solar wind as a function of radial distance, with constant particle flux but varying coronal parameters. In the case shown the particle flux was 1.0×10^{35} particles/ster/sec, corresponding to a rate of mass loss of 3.3×10^{-14} $M_\odot$/year.

Figure (5.3.5) shows that for a given rate of mass loss the highest velocities of expansion are obtained from the hottest and least dense coronas.

Figure (5.3.6) shows how the particle density N decreases with increasing radial distance. As the curves were similar in shape only the two models corresponding to the extreme values of the coronal parameters used in figure (5.3.5) are shown. It will be noted that for small values of log r/r_o the density decreases more rapidly if the coronal density is higher. For larger radial distances the dependence of log N upon log r/r_o is almost linear indicating a power law variation of N with r/r_o. The gradient in this region is approximately - 2.09 which shows that $N \propto (r_o/r)^{2.09}$. We expect from the continuity equation that as the velocity tends to its limiting value, the density will decrease proportionately to $(r_o/r)^2$ and that the gradient of the curves in figure (5.3.6) will tend to - 2.0.

Table (5.3.1) shows a grid of models which we computed for a

TABLE 5.3.1

SUMMARY OF STELLAR WIND MODELS

J^-	log N_o	$\tau(x_o)$	u_∞
1.0	6.974	1.083	6.88
	7.087	1.005	5.98
	7.199	0.978	4.38
	7.311	0.957	3.52
2.0	6.837	1.260	9.65
	6.992	1.185	6.41
	7.147	1.128	4.22
	7.234	1.104	3.32
	7.317	1.083	2.60
	7.399	1.068	2.02
	7.475	1.055	1.55
	7.547	1.044	1.27
	7.614	1.037	0.91
	7.677	1.029	0.69
	7.733	1.025	0.52
4.0	7.165	1.289	3.81
	7.284	1.246	2.44
	7.306	1.239	2.24
	7.368	1.222	1.72
	7.392	1.216	1.52
	7.487	1.196	0.94
	7.538	1.188	0.70
8.0	7.169	1.492	4.77
	7.268	1.433	3.03
	7.360	1.392	1.88
	7.408	1.376	1.42
	7.453	1.364	1.07
	7.468	1.360	0.97
16.0	7.411	1.563	2.32
	7.420	1.559	2.20
	7.430	1.554	2.06

number of different rates of mass loss occurring for a range of coronal parameters. The results are plotted in figures (5.3.7) - (5.3.9) which show respectively the loci of constant particle flux, J', in the ($\log N_o$, $\tau(x_o)$) plane, the (u_∞, $\tau(x_o)$ plane, and the (u_∞, $\log N_o$) plane.

5.3.1 Solar wind models

It would be ideal if one solution could be obtained with boundary conditions which could be said to represent the coronal values of temperature and density, and from these predict the velocity, temperature and density at the earth. Unfortunately this is not possible as there is considerable uncertainty in the values observed in the solar corona and great variability in the solar wind parameters at the earth. It is possible then, only to make certain general comments and some order of magnitude estimates. We concluded in chapter 3 that observations generally indicate that the coronal temperature is about 2×10^6 °K and the particle density N_o, a few times 10^7 cm^{-3}. From figure (5.3.7) it will be seen that the particle flux J' corresponding to these values should probably be in the range $1 - 2 \times 10^{35}$ ster/sec.

The solar wind velocity in the vicinity of the earth during periods of minimum solar activity is usually between 300 - 350 km/sec corresponding to values of u in the range 5.45 - 7.42. On consideration of figure (5.3.5) we note that the uppermost curve predicts a velocity at the earth in this range while the second curve corresponds approximately to the lower limit. These curves correspond to points in figure (5.3.7) with coordinates (6.97, 1.04) and (7.09, 1.01).

As it appears that models near the $J' = 1.0$ line in figure (5.3.7) represent most closely the actual solar wind flow we will attempt to estimate from them the range of coronal parameters which produce flows with velocities and temperatures closest to those observed in the vicinity of the earth. Accordingly we assume that in the region near the curve $J' = 1.0$ the flow parameters may be expressed as a linear function of $\log N_o$ and $\tau(x_o)$ only. Thus we assume that the velocity at earth, u_E, can be expressed as,

$$u_E = a \log N_o + b \tau_o, \qquad (5.3.2)$$

where a and b are constants to be determined. These constants can be evaluated by consideration of two particular models in the region in which we are interested, i.e near $J' = 1.0$ and $\log N_o = 7.0$. Expressions similar to (5.3.2) can be formed for the other solar wind parameters. The results can conveniently be expressed in matrix notation

$$\begin{pmatrix} u_E \\ \log N_E \\ \tau_E \end{pmatrix} = \begin{pmatrix} -2.743 & 24.560 \\ 0.240 & -0.517 \\ -0.047 & 0.385 \end{pmatrix} \begin{pmatrix} \log N_o \\ \tau_o \end{pmatrix} \qquad (5.3.3)$$

It is emphasised that this result is only approximate and even at best gives a rough approximation to the actual behaviour of the flow.

In figure (5.3.10) we have shown the general effect of coronal temperature and density upon the parameters in the vicinity of the earth derived from equation (5.3.3). The two velocity limits $u_E = 5.45$ and $u_E = 7.42$ correspond to the range of solar wind velocities usually observed at earth during solar minimum; that is, velocities between 300 km/sec and 350 km/sec. It will be noted from figure (5.3.10) that a rather high coronal temperature is required to produce velocities at the earth as large as the minimum observed velocity, when coronal densities are in excess of $10^7/cm^3$.

The two temperature limits shown in figure (5.3.10) are for $\tau_E = 0.075$ and 0.050, which correspond to temperatures of 1.5×10^5 °K and 1.0×10^5 °K respectively. These are in good agreement with experiment. It will be noted that a higher coronal temperature is required to produce higher temperatures at the earth. The two values of $\log N_E$ shown, correspond to densities at the earth of 13.2 $/cm^3$ and 14.8 $/cm^3$. These are probably rather too high since observation indicates the average density to be between 5 and 10 $/cm^3$. We see that low densities near the earth are produced by high coronal temperatures.

An adequate model of the solar wind should lie between the three pairs of lines shown in figure (5.3.10), and in the region of the $(\log N_o, \tau(x_o))$ plane appropriate to the solar corona. Unfortunately the

dependence of the temperature at the earth upon the coronal parameters is very similar to that of the velocity at the earth. As these lines on figure (5.3.10) are nearly parallel we are not able to exclude many combinations of $\tau(x_o)$ and N_o on the criterion that they do not simultaneously predict suitable values of temperature and density at the earth.

We will choose from our results one model with which to illustrate the parameters of the solar wind and will consider the temperature and density of the corona to be given by $\tau(x_o) = 1.02$ and $\log N_o = 7.04$, which, from figure (5.3.7), can be seen to lie almost exactly on the curve $J' = 1.0$. In this model, therefore, the sun is losing mass at the rate of about 3.3×10^{-14} $M_\odot$/year. From equation (5.3.3) the results at the earth can be expressed as,

$$\begin{pmatrix} u_E \\ \log N_E \\ \tau_E \end{pmatrix} = \begin{pmatrix} -2.743 & 24.560 \\ 0.240 & -0.517 \\ -0.047 & 0.385 \end{pmatrix} \begin{pmatrix} 7.04 \\ 1.02 \end{pmatrix} \qquad (5.3.4)$$

This gives,

$$u_E \simeq 5.74$$
$$\log N_E \simeq 1.16$$
$$\tau_E \simeq 0.06$$

and corresponds to a velocity of 310 km/sec, a density of 14 cm^{-3} and a temperature of 1.2×10^5 °K.

Although these results are in reasonable agreement with observation it seems that an entirely satisfactory model of the solar wind cannot be constructed in this way. A hotter corona would produce parameters near to the earth rather better than the ones adopted here but would not fit so well the observations of the corona itself. The most probable explanation is that our assumption that thermal conduction is the only mechanism of heating in the solar wind above the base of the corona is not valid. Since the high coronal temperatures are known to be produced by the dissipation of energy from magneto-acoustic and shock waves, our results seem to imply that their heating effect is continued for some considerable distance

into the corona and the lower solar wind. This would tend to decrease the temperature gradient in the corona and reproduce the effects of a hotter corona. Thus more accurate models of the solar wind should include a quantitative estimate of the mechanisms for production and damping of these waves.

5.3.2 Stellar winds

We now consider the possibility that a stellar wind may be a mechanism by which a star could lose a considerable fraction of its mass during its evolution . We have shown that the sun loses mass at the rate of about 3.3×10^{-14} $M_\odot$/year. As it stays on the main sequence for a time of the order of 10^9 years it should lose only about 3×10^{-5} $M_\odot$ during this period. It is unlikely that so small a fraction of the total mass would have an appreciable effect upon its evolution.

Since the conditions occurring in the coronae of stars other than the sun are not directly observable it is difficult to make any firm predictions about the associated rate of mass loss. From a consideration of figure(5.3.7) we note that by increasing the temperature of the corona by a factor of about two the rate of mass loss from the corona will be increased by a factor of about 15. An increase of the density further enhances this effect.

An interesting feature of figure (5.3.7) is that it illustrates the perhaps surprising fact, already noted in figures (5.3.3) and (5.3.4), that the rate of mass loss from a corona is a much more sensitive function of coronal temperature than it is of coronal density.

We note also that for a given coronal temperature the particle flux is quite dependent upon density, providing that the coronal densities are low, while at high coronal densities the particle flux is specified almost entirely by the coronal temperature and is nearly independent of density. The curves of constant J^* appear to converge as the density increases, indicating that the particle flux becomes an increasingly sensitive function of coronal temperature, as the coronal density increases.

Although our results certainly allow no definite predictions to be

made, it is interesting to speculate that the rapid fluctuation in the rate of mass ejection observed in the F and G-type supergiants may be due to relatively small fluctuations in the temperature of their upper atmospheres. It would be necessary to postulate that the density of their coronas would be rather higher than that of the sun.

Figure (5.3.8) demonstrates that higher coronal temperatures are required to produce a given asymptotic velocity in increasingly dense mass flows; a not altogether surprising result. It shows that u_∞ is a very sensitive function of the coronal parameters and fluctuations in the temperature will produce sharp changes in the velocity of the flow. Consider for example a corona with log N_o = 7.2 and $\tau(x_o)$ = 0.98. From figure (5.3.7) we see that this corresponds to a particle flux $J' = 1.0 \times 10^{35}$ and from figure (5.3.8) that $u_\infty \simeq 4.95$. If the temperature increases by a factor of 1.13 to $\tau(x_o)$ = 1.11 at constant density the particle flux is doubled and from figure (5.3.8) the asymptotic velocity will decrease to 3.45.

Figure (5.3.8) casts doubts on the hypothesis that mass loss from red giants is due to the stellar wind mechanism. From the discussion in chapter 2 we would expect a red giant to have a high particle flux, a low coronal temperature, and a low asymptotic velocity. Figure (5.3.8) shows, however, that although low asymptotic velocities are possible for high rates of mass loss, high coronal temperatures are required to produce them.

Perhaps the most interesting feature of figure (5.3.8) is the behaviour of the curves as $u_\infty \to 0$. In the region of small asymptotic velocity there appears to be an almost linear dependence of the particle flux J' upon u_∞ and $\tau(x_o)$. This enables us to extrapolate our curves for J' = 2.0, 4.0, and 8.0 with reasonable confidence to determine the value of the abscissa (τ_m, say) at which u_∞ vanishes in each case. The values at which this occurs are shown in table(5.3.2).

We now return to consider figure (5.3.7). Since the asymptotic velocity $u_\infty \to 0$ at a finite value of the coronal temperature the curves of constant J' must approach this limiting value of $\tau(x_o)$ as log $N_o \to \infty$. Consequently, for sufficiently high coronal densities the loci of constant J' will be essentially parallel. In this region the rate of mass ejection

TABLE 5.3.2

TEMPERATURES AT WHICH $u_\infty = 0$

log J′	τ_m
0.30	1.01
0.60	1.16
0.90	1.32

will be determined entirely by the coronal temperature and will be completely independent of the coronal density.

The apparently linear variation of log J′ with τ_m, and the similar shape of the curves in figure (5.3.8) encourages us to suppose that the logarithm of the particle flux and the temperature at which the asymptotic velocity vanishes can be related by means of an equation,

$$\log J' = C\,\tau_m + D, \qquad (5.3.5)$$

where C and D are constants to be determined. C and D can be evaluated by means of the data in table (5.3.2). We obtain,

$$\log J' = 1.94\tau_m - 1.65 \qquad (5.3.6)$$

where we recall that as in figure (5.3.7), (5.3.8) and (5.3.9), J′ is in units of 10^{35} particles/ster/sec.

Equation (5.3.6) fits the data in table (5.3.2) to an accuracy of about 2% and thus allows us to make estimates of the rates of mass ejection from hotter coronas. We must emphasise that equation (5.3.6) represents an upper limit to the rate of mass loss which can occur at any coronal temperature since it has been derived for the case in which $u_\infty = 0$. Real cases, where $u_\infty > 0$, will have rather smaller particle fluxes as some of the coronal thermal energy is required to provide the kinetic energy of the stellar wind flow.

In figure (5.3.11) we show the approximate rates of mass loss from dense stellar coronas as a function of coronal temperature. It will be seen that very high rates of mass loss are probably attainable. We note that a rate of mass ejection of about 10^{-6} $M_{\odot}$/year could be produced from a corona with a temperature of 9.2×10^6 °K providing that equation (5.3.6) holds in this region. This is a rate of mass loss typically observed in the O and B supergiants. Although the stellar wind mechanism thus appears capable of producing these high flux rates its applicability to these stars is doubtful since, as we pointed out in chapter 2, there is observational evidence to indicate that the mass flow occurs at a temperature considerably lower than 10^7 °K, and that radiation pressure must certainly be taken into account.

We should repeat that our predictions of very high rates of mass loss from hot coronas have been obtained from equations (5.3.5) and (5.3.6) by a linear extrapolation of our computed results. They are therefore subject to considerable error, and should be considered only as a general indication of the effects likely to occur.

5.3.3 Models with rotation

We expect that the magnetic field of the sun will result in a sizeable modification of the solar wind flow. In order to make a simple estimate of this we suppose that the only effect of the magnetic field is to enforce co-rotation of the solar wind with the sun, simulating a solid body out as far as the critical point. The effect of the rotation will be to produce a centrifugal force term in the radial momentum equation. Beyond the critical point we assume that the azimuthal velocity decreases so that angular momentum is conserved. This model results in a modification of the solar wind equations. They may be obtained from equation (4.3.8) -(4.3.12) by ignoring the magnetic field terms. These become,

$$\rho v_r r^2 = J, \qquad (5.3.7)$$

$$\rho v_r \frac{dv_r}{dr} - \frac{\rho v_\phi^2}{r} + \frac{dP}{dr} + \frac{GM_\odot \rho}{r^2} = 0 \quad , \tag{5.3.8}$$

$$\rho v_r \frac{dv_\phi}{dr} + \frac{\rho v_r v_\phi}{r} = 0 \quad , \tag{5.3.9}$$

$$\kappa r^2 \frac{dT}{dr} - J\left\{\tfrac{1}{2}(v_r^2 + v_\phi^2) + \frac{5kT}{M} - \frac{GM_\odot}{r}\right\} = H \tag{5.3.10}$$

On transforming these variables to the variable for computation x, τ, u_r, and v_ϕ where u_r is the dimensionless variable $u_r = Bv_r^2$ and $u_\phi = Bv_\phi^2$, equations (5.3.8) - (5.3.10) become,

$$\frac{du}{dx} = \frac{1 - 4\frac{\tau}{x} - 2\frac{d\tau}{dx} - \frac{u_\phi}{x}}{\frac{1}{2} - \frac{\tau}{u}} \quad , \tag{5.3.11}$$

$$\frac{A\kappa_0 T_\odot^{5/2}}{J k r_\odot^{5/2}} \frac{d\tau}{dx} = \frac{1}{2}x + \frac{1}{4}(u_\infty - u_r - u_\phi) - \frac{5}{2}\tau \tag{5.3.12}$$

We allow angular momentum to be conserved beyond the critical point and require there to be solid body rotation inside the critical point. Thus from equation (5.3.9) we have that,

$$\frac{du_\phi}{dx} = \frac{2u_\phi}{x} \quad , \qquad \text{when } x < x_c \tag{5.3.13}$$

or,

$$u_\phi = u_\Phi (x/x_c)^2 \quad , \tag{5.3.14}$$

where,

$$u_\Phi = u_\phi(x_c) \quad . \tag{5.3.15}$$

For solid body rotation,

$$u_\phi = B(\Omega A/x)^2 \quad , \qquad \text{when } x > x_c \tag{5.3.16}$$

where Ω is the angular velocity of the sun.

The introduction of the term u alters the position of the critical point, which is found by the method described for the non-rotating case. Similarily the velocity gradient at the critical point may be found in the same way, although now the expression is more complicated. We obtain:

$$\left(\frac{du}{dx}\right)_c = \frac{1}{2}\left\{1 - 2\frac{u_c}{x_c} - \frac{u_\Phi}{x}\right\} - \frac{1}{2}\left\{\left(1 - \frac{u_\Phi}{x_c}\right)^2 - \left(20 - 12\frac{u_\Phi}{x_c}\right)\frac{u_c}{x_c} + 52\left(\frac{u_c}{x_c}\right)^2 - 16u_c\left(\frac{d^2\tau}{dx^2}\right)_c\right\}^{\frac{1}{2}}$$

(5.3.17)

The expression for $(d^2\tau/dx^2)_c$ is the same as in the non rotating case and may be evaluated by equation (5.1.9).

We computed a number of models for various values of Ω for $J' = 4.0 \times 10^{35}/cm^3$ and compared the results with the non rotating cases. The data is summarized in table (5.3.3) and the results plotted in figure (5.3.12).

TABLE 5.3.3

EFFECT OF ROTATION ON MODELS WITH $J' = 4.0 \times 10^{35}$ ster^{-1} sec^{-1}

Ω ($\times 10^{-6}$ sec^{-1})	log N_o	$\tau(x_o)$
2.887	7.307	1.238
3.464	7.308	1.238
4.157	7.309	1.238
4.988	7.309	1.237
5.986	7.311	1.236
7.184	7.314	1.235
8.620	7.318	1.233
10.000	7.321	1.231
22.500	7.380	1.202

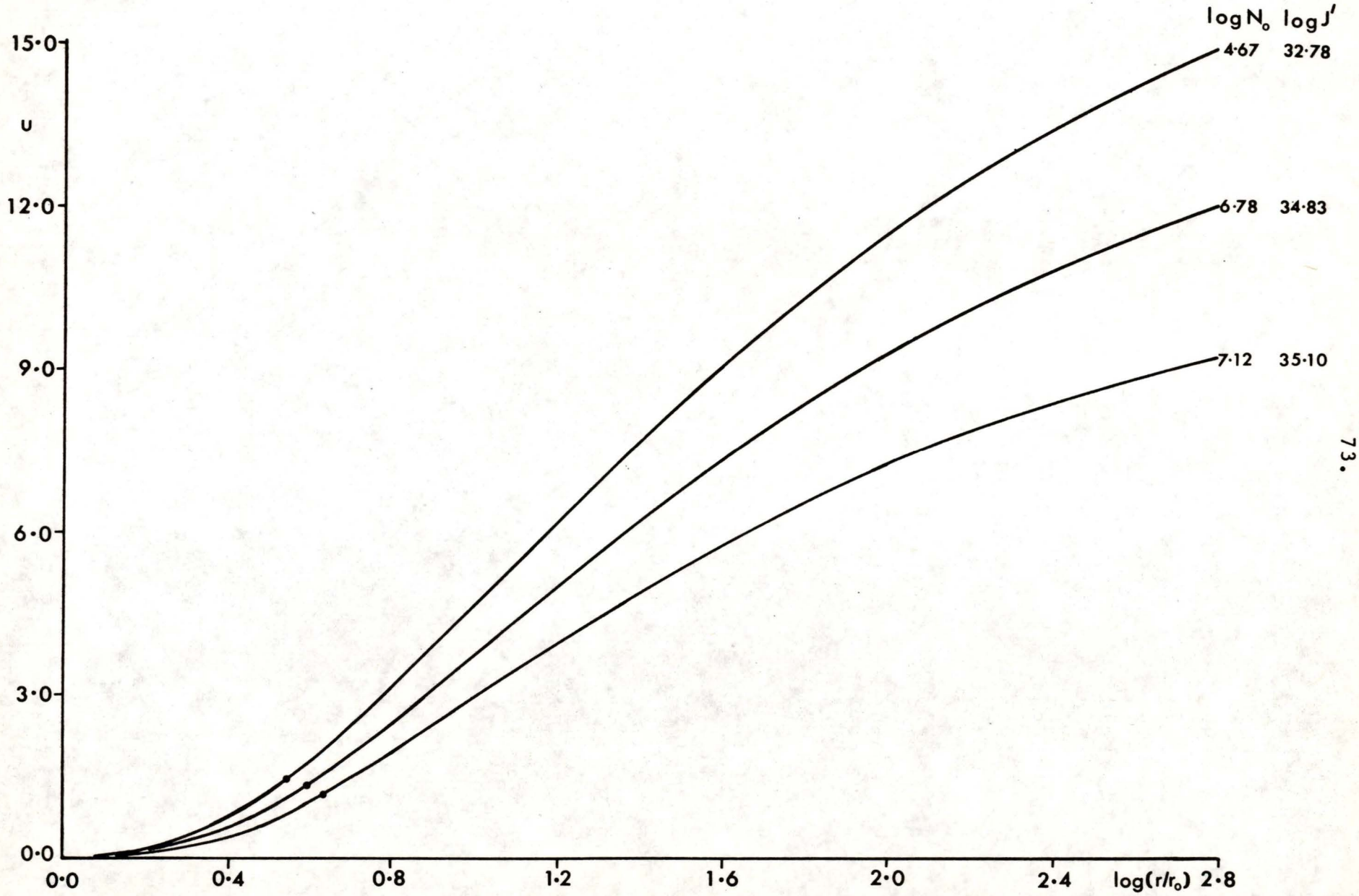

Figure 5.3.1 Velocity u as a function of radial distance for three values of coronal density, N_o, with a coronal temperature $\tau(x_o) = 1{\cdot}0$

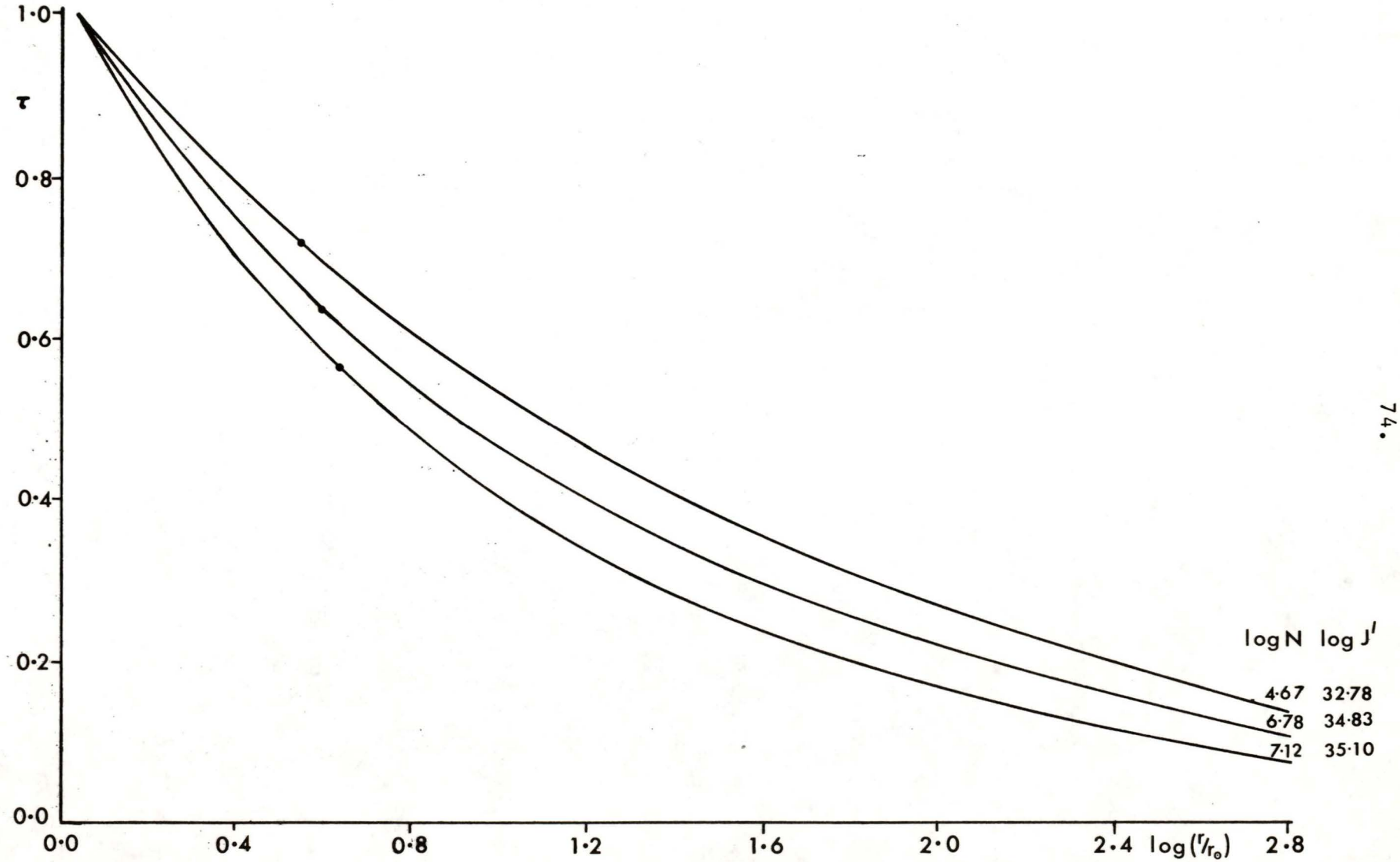

Figure 5.3.2 Temperature τ as a function of radial distance for three values of coronal density, N_o, with a coronal temperature $\tau(x_o) = 1{\cdot}0$

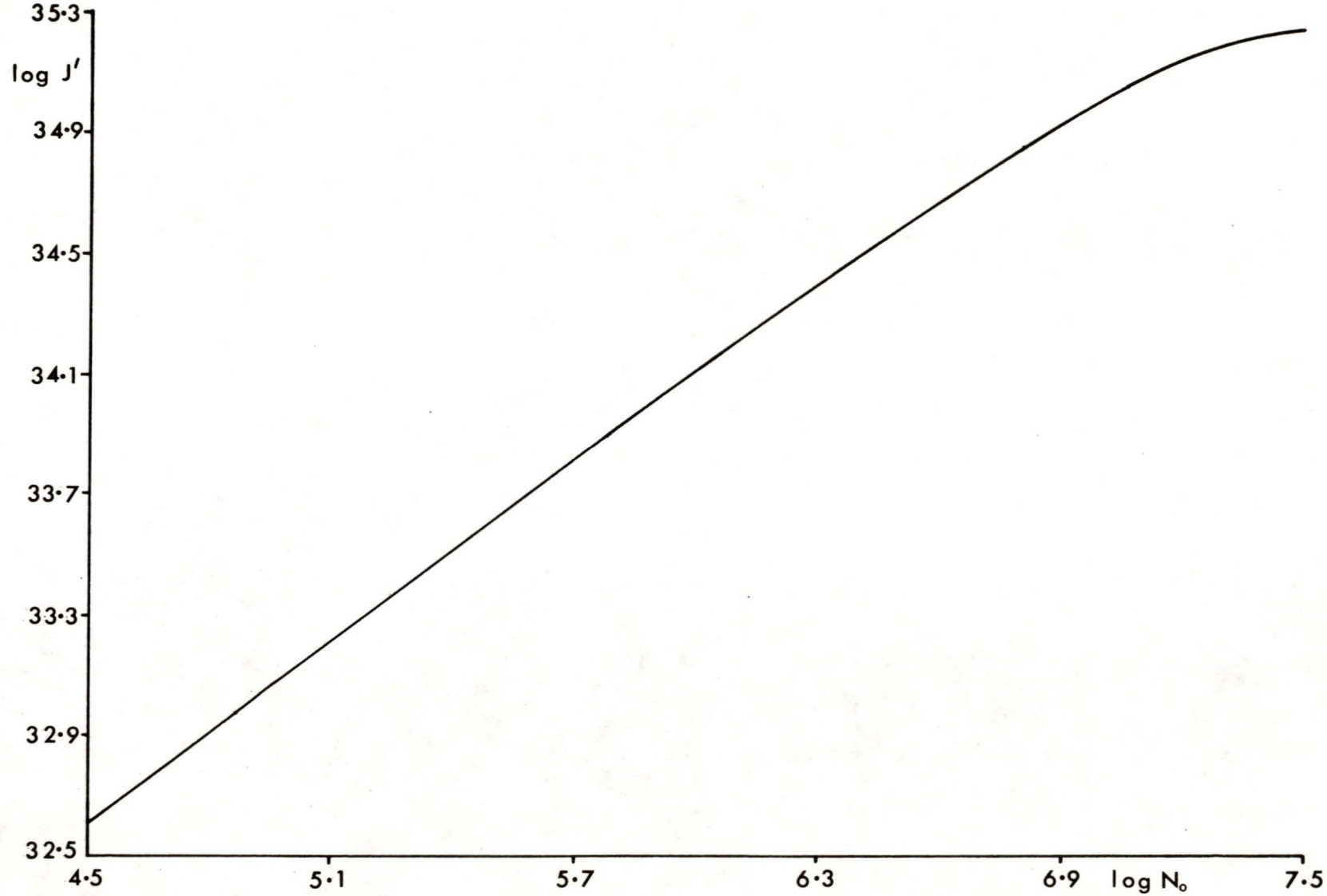

Figure 5.3.3 Particle flux J' as a function of coronal density, N_o, for a coronal temperature $\tau(x_o) = 1{\cdot}0$

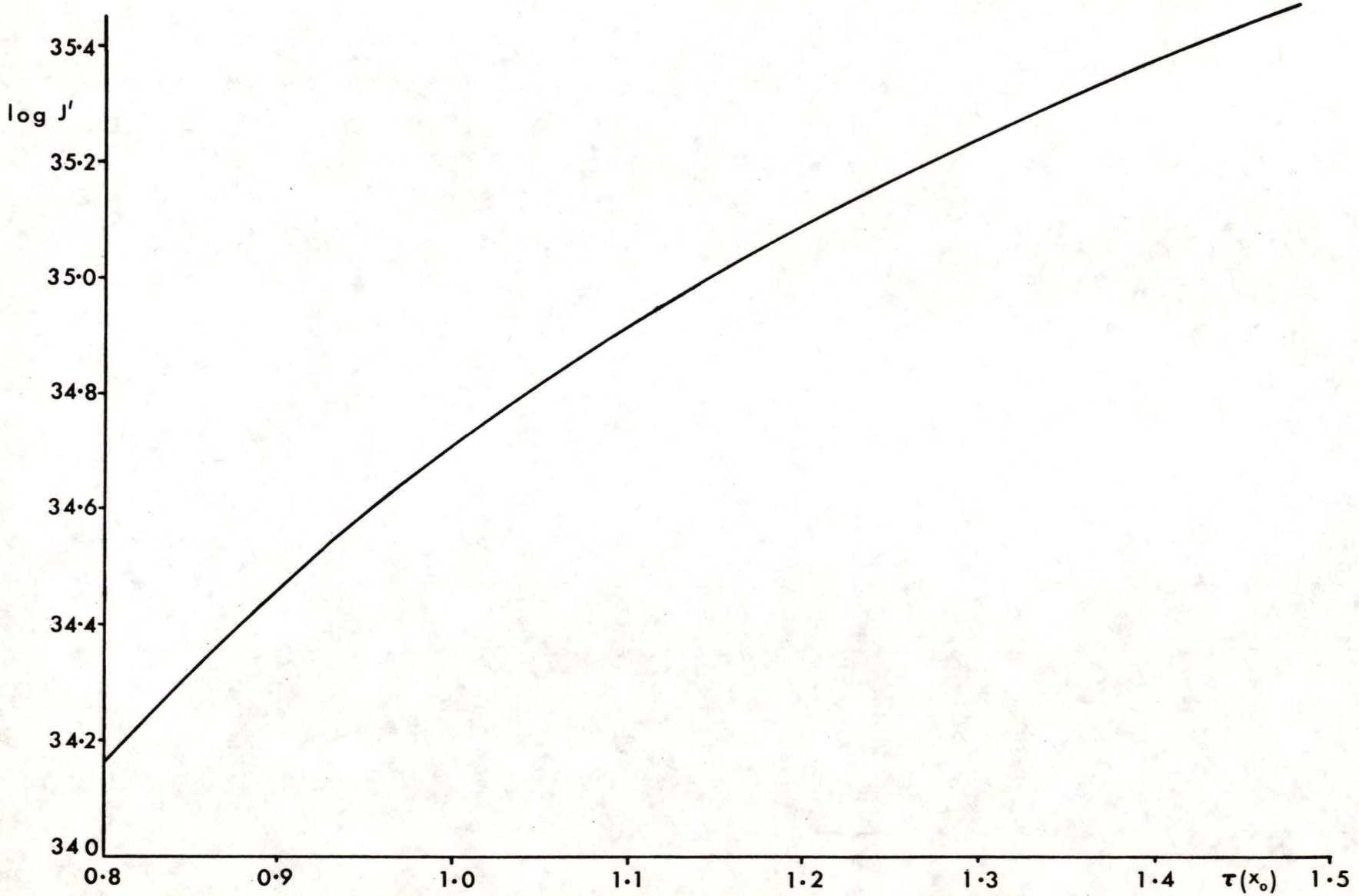

Figure 5.3.4 Particle flux, J', as a function of coronal temperature $\tau(x_0)$, at a coronal density of $\log N_0 = 6{\cdot}7$

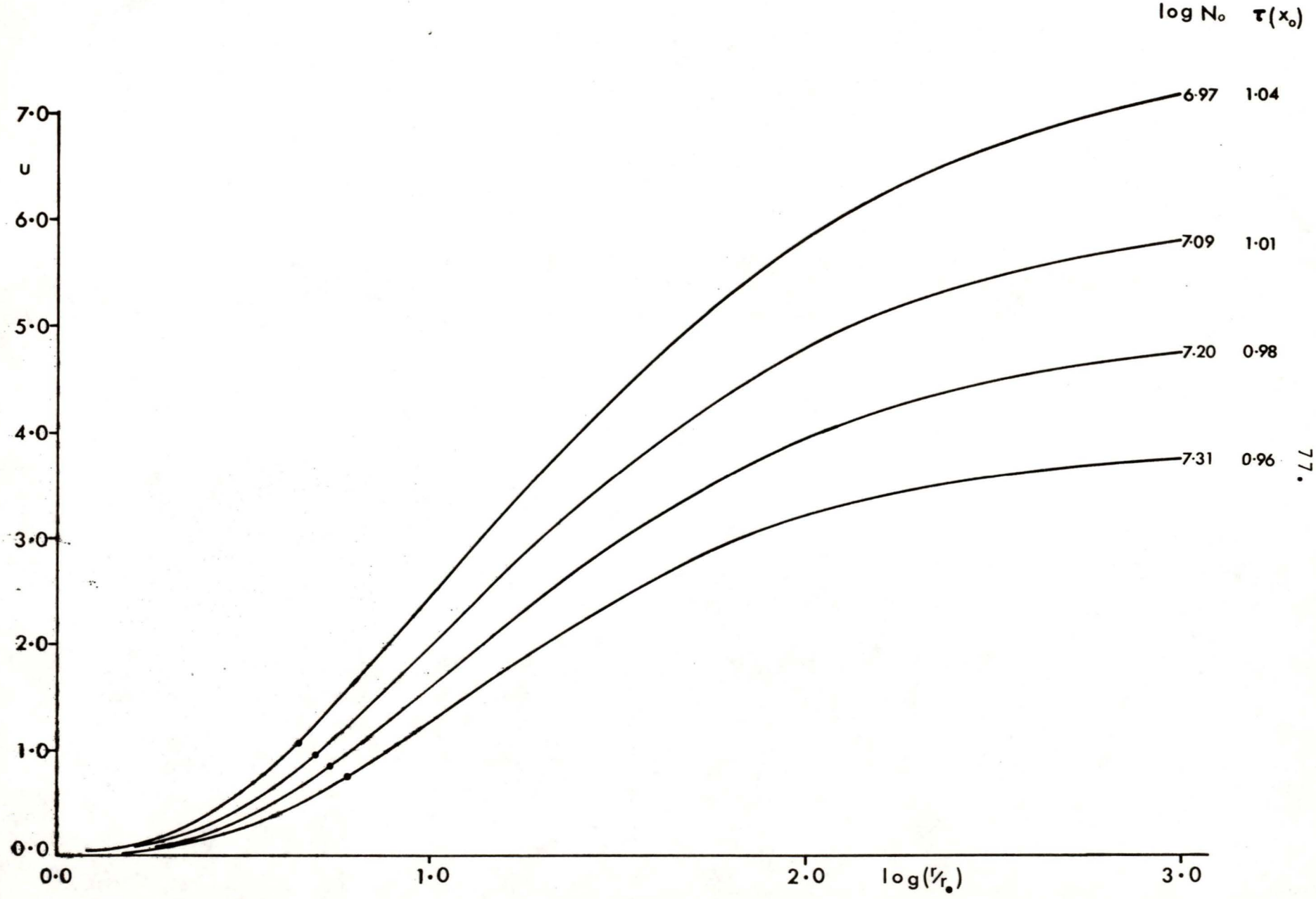

Figure 5.3.5 Velocity u as a function of radial distance at constant particle flux log J' = 35·0.

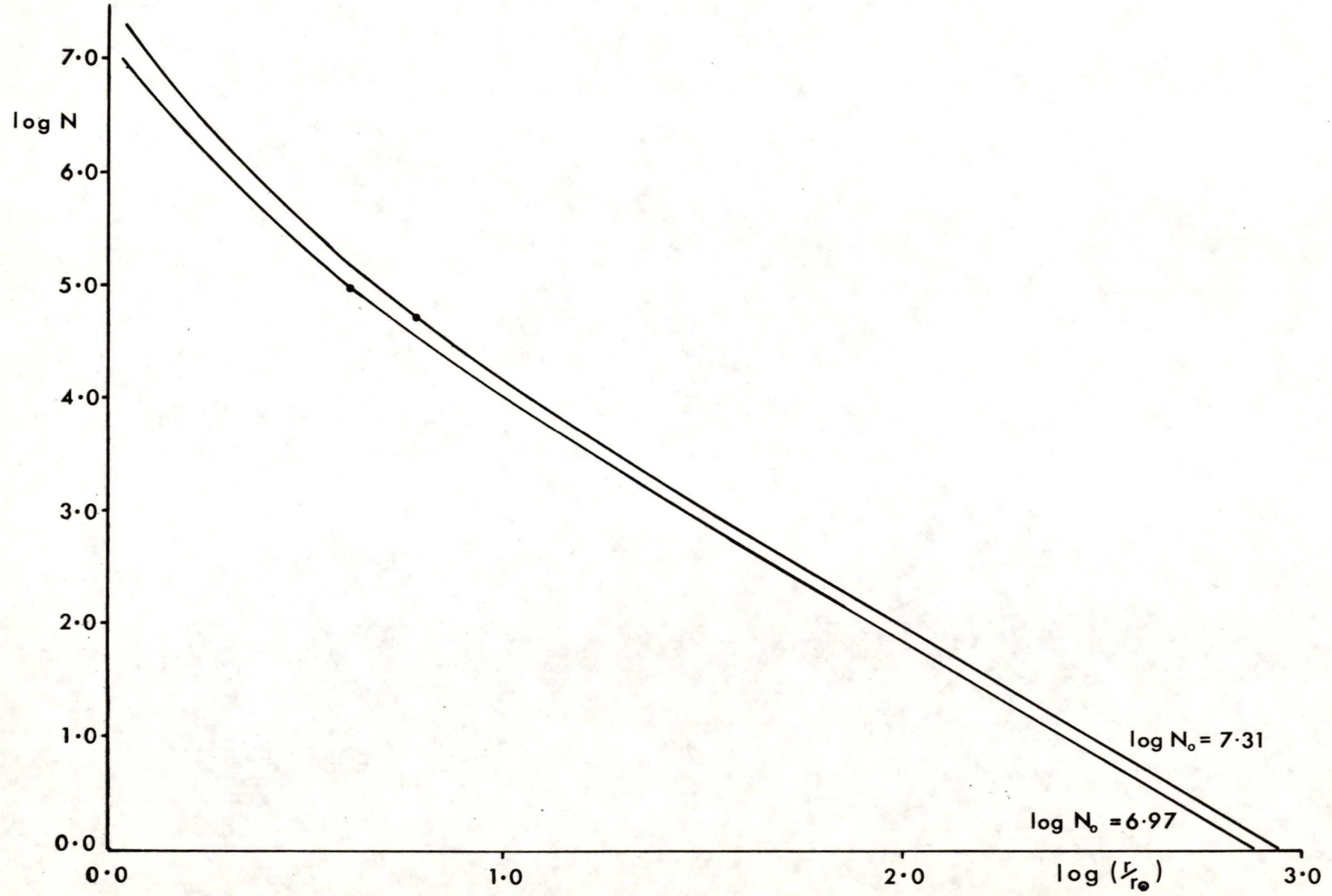

Figure 5.36 Density, log N, as a function of radial distance at constant particle flux, log J = 35·0

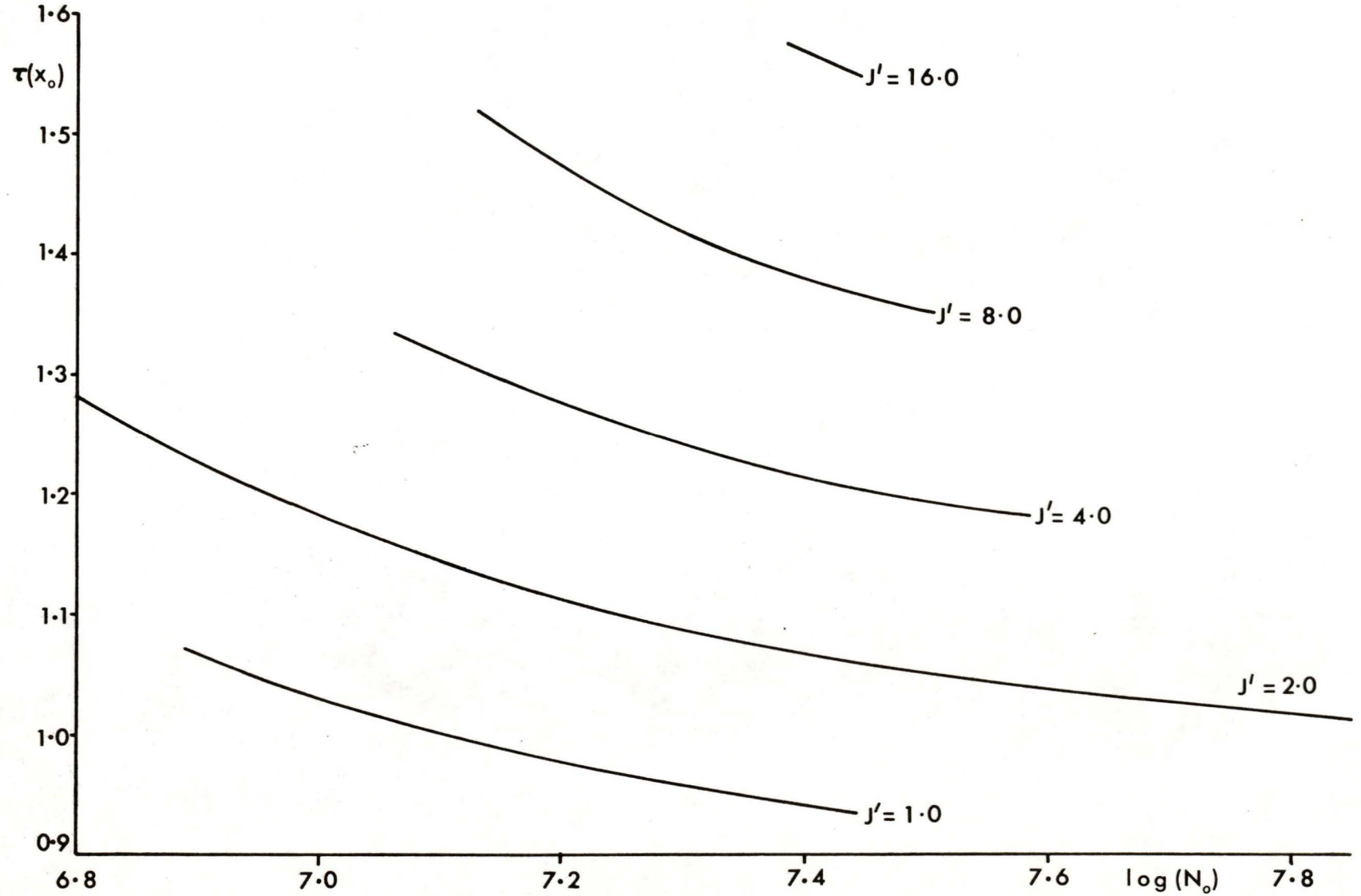

Figure 5.3.7 Loci of constant mass loss related to coronal temperature, $\tau(x_0)$ and density, N_0. J' is measured in units of 10^{35} ster^{-1} sec^{-1}.

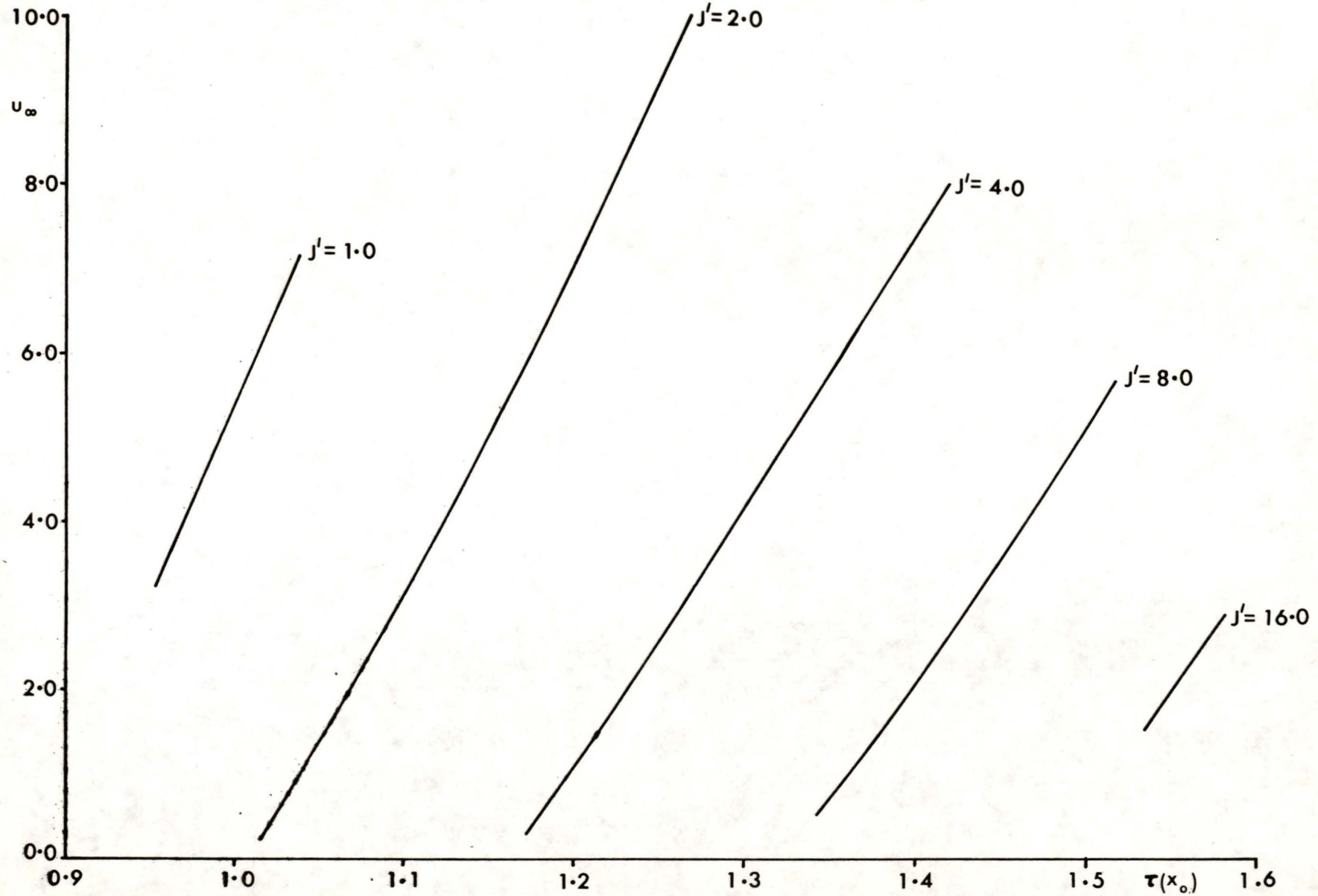

Figure 5·3·8 Loci of constant mass loss, J′, related to asymptotic velocity, u_∞, and coronal temperature, $\tau(x_o)$. J′ is measured in units of 10^{35} ster^{-1}.sec^{-1}.

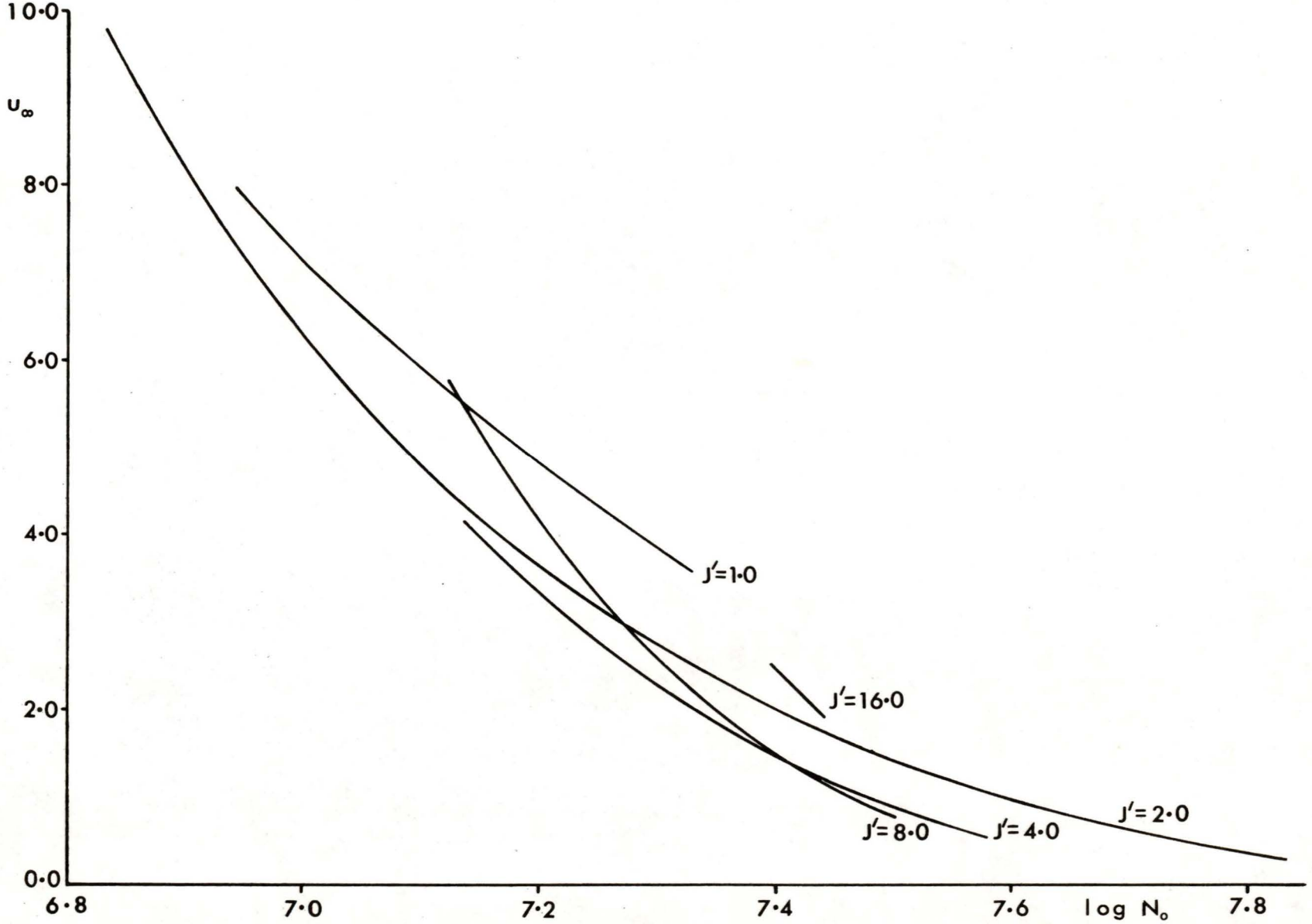

Figure 5.3.9 Loci of constant particle flux, J', related to asymptotic velocity, u_∞ and coronal density N_o. J' is measured in units of 10^{35} ster.$^{-1}$ sec.$^{-1}$

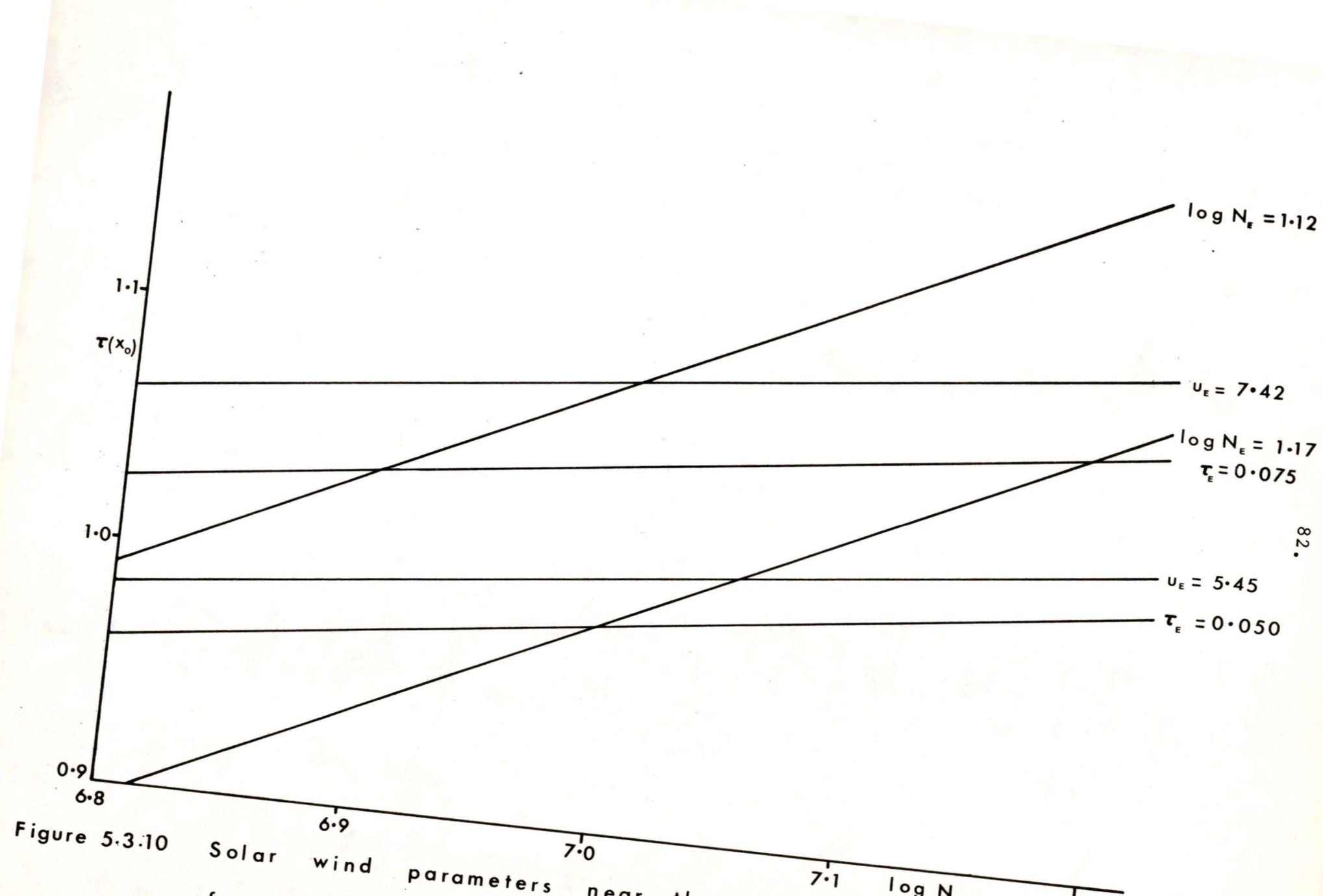

Figure 5.3.10 Solar wind parameters near the earth, u_E, τ_E, $\log N_E$, as a function of coronal parameters $\tau(x_o)$ and $\log N_o$.

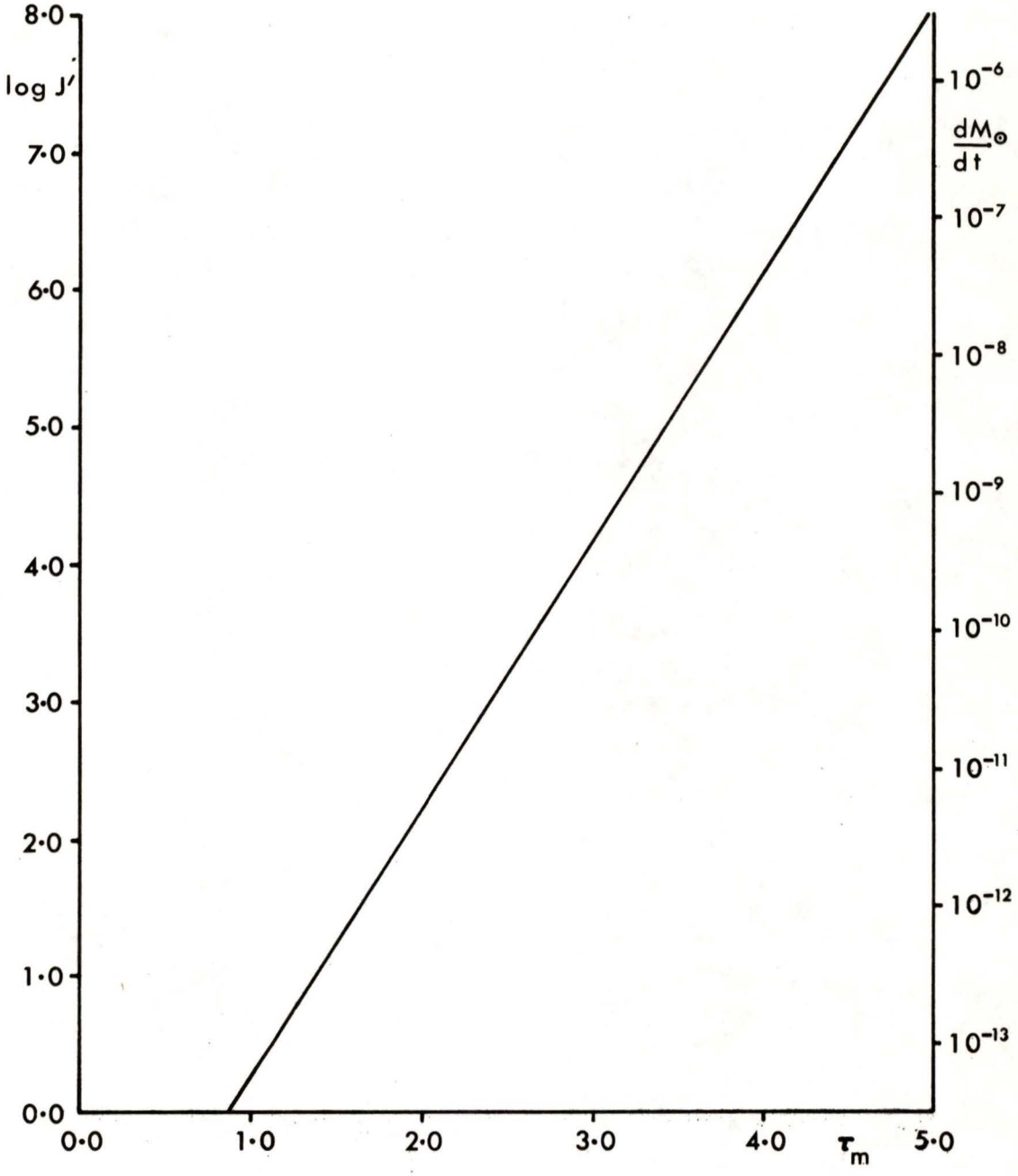

Figure 5·3·11 Rate of mass loss as a function of coronal temperature

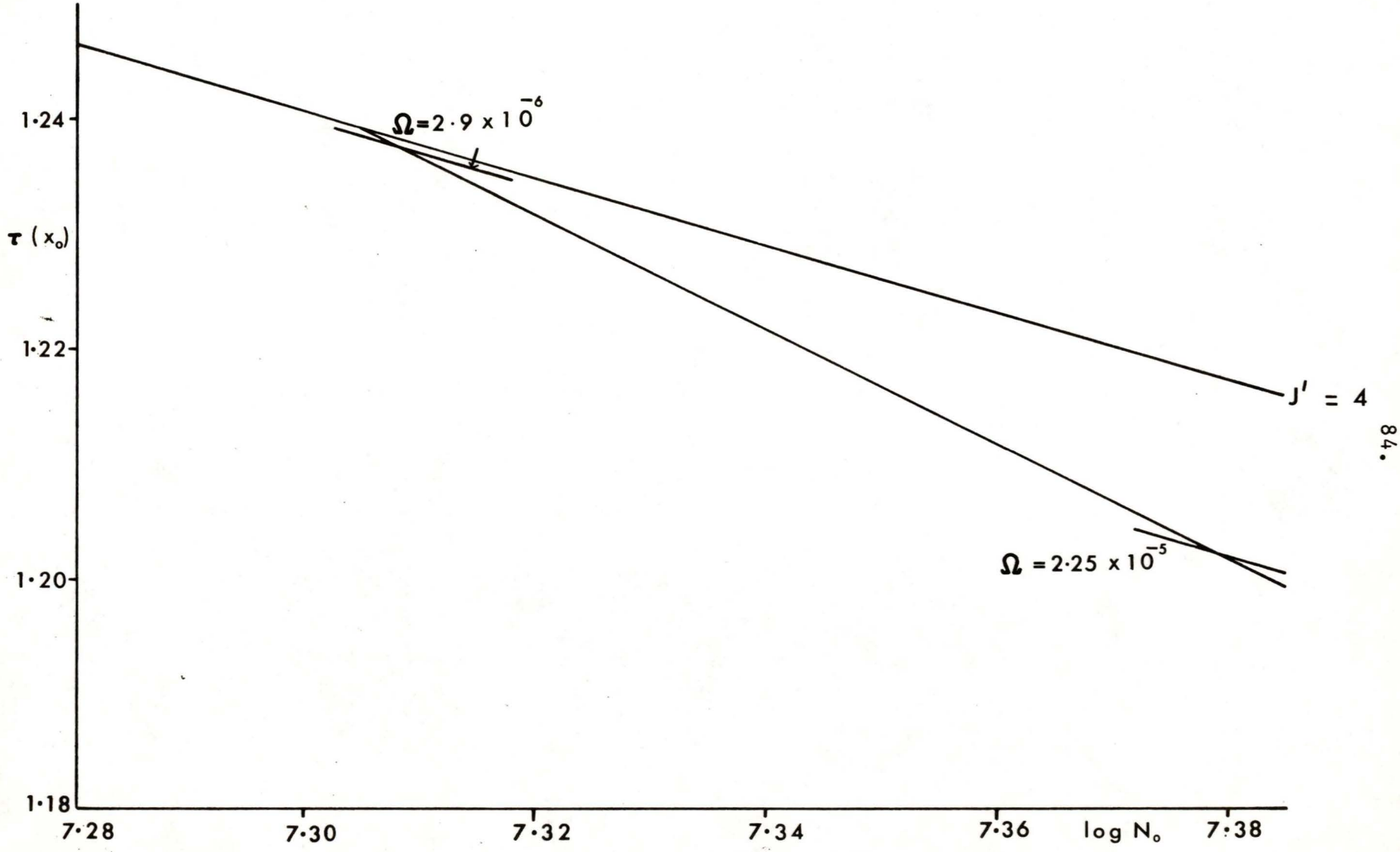

Figure 5.3.12 Effect of increasing stellar rotation upon the particle flux for $J' = 4$

Figure (5.3.12) represents a small part of figure (5.3.7),where the line $\Omega = 0$ is a section of the line $J' = 4.0$. It will be seen that the effect of a rotation rate similar to that of the sun ($\Omega \simeq 2.9 \times 10^{-6}$ sec^{-1}) is quite small. The model similar to the rotating model but with $\Omega = 0$ is presumably the one defined by the intersection of the $\Omega = 0$ line and the line joining the rotating models. This point has the coordinates (7.304, 1.2393) in the (log N_o, $\tau(x_o)$) plane. The effect of the rotation is thus to decrease the coronal temperature and increase the coronal density required to produce a given rate of mass loss.

5.4 Conclusion

We have shown that a hydrodynamic model can reproduce with reasonable accuracy the observed behaviour of the solar wind. If the temperature at the base of the corona is taken to be 2.0×10^6 °K and the density to be 1.1×10^7 protons/cm^3 the sun will be losing mass at the rate of about 3.3×10^{-14} $M_\odot$/yr. This model of the solar wind will produce a velocity at the earth of about 310 km/sec, a density of 14 protons/cm^3, and a temperature of about 1.2×10^5 °K.

There are indications,however, that thermal conductivity, which has been assumed to be the only heating mechanism above the base of the corona, is not sufficient to produce exactly the observed effects, and that other heating mechanisms are operative. It is most likely that the heating effects due to the dissipation of shock and magneto-acoustic waves responsible for the high coronal temperatures, extend for some considerable distance into the solar wind. Theoretical work is necessary to elucidate the damping mechanism of these waves before more accurate solar wind models can be produced.

In order to estimate the importance of a stellar wind as a mechanism for producing mass loss from stars, we have computed models with particle fluxes of up to 1.6×10^{36} protons/ster/sec, corresponding to rates of mass loss of about 5.3×10^{-13} $M_\odot$/year. We have shown that the rate of mass loss is very dependent upon the coronal temperature and that this dependence increases with increasing density. However, the dependence of mass loss upon density is much less and at sufficiently high densities the rate of mass loss is almost independent of density.

at constant temperature.

In the regions of the (log N_o, $\tau(x_o)$) plane for which we have calculated models there was found to be an exponential dependence of the upper limit of the particle flux, J' upon the coronal temperature, $\tau(x_o)$, which can be expressed by means of equation (5.3.6) as,

$$J' = 0.0447 \exp [4.47\ \tau(x_o)] \qquad (5.4.1)$$

This relationship, when applied to coronas with temperatures of about 10^7 °K was found to produce rates of mass loss in excess of 10^{-6} M_o/year. It is appreciated that extrapolation to these regions is quite speculative and this result should be taken to indicate only the general trend of behaviour at high temperatures.

It is interesting to consider the regions in which equation (5.4.1) is likely to hold more accurately. De Loore (1970) has calculated model coronas for main sequence stars and found that the most active occur in the early F region, where the temperature of the corona is around 3.7×10^6 °K and the density log $N_o \simeq 10.5$. From figure (5.3.11) we see that this would correspond to a rate of mass loss, $\frac{dM_\odot}{dt} \lesssim 3 \times 10^{-12}$ $M_\odot$/year.

It is difficult to make firm predictions about giant stars as their surface conditions are not well known. We have shown, however, that the strong dependence of the particle flux upon the coronal temperature in hot, dense coronas could account for the rapid changes in particle flux observed to occur in F and G-type supergiants. It seems reasonable that these stars, with their turbulent atmospheres, should generate sufficient magneto-acoustic energy to support a very dense, hot corona; and furthermore that sporadic small excitations of the corona should occur, leading to rapid increases in the mass flux.

Our calculations also show that it is unlikely that mass ejection from red giants is due to the solar wind mechanism since the high particle fluxes which are observed could only be produced by very high coronal temperatures

Finally we calculated some models in which the rotation of the star was taken into account. It was hoped to approximate in this way the effect of a magnetic field by artificially enforcing co-rotation of the solar wind plasma with the star out as far as the critical point.

We found that only small changes were produced for even large rotation rates. This should perhaps be taken to imply that our model of a magnetic field is unsatisfactory rather than that the effect of a magnetic field upon the solar wind is small.

APPENDIX A

COMPUTER PROGRAM FOR THE SOLUTION OF THE SOLAR WIND EQUATIONS INCLUDING A HEAT EQUATION

Two different computer programs were constructed in order to carry out the numerical integration of the equations of motion for the solar wind problem. The program in Appendix A solves the set of equations (including a heat equation) by iteration. The momentum equation is solved by means of an Adam's Bashforth predictor-corrector method while the heat equation is integrated by means of a Simpson's rule routine.

```
      IMPLICIT REAL*8 (A-H,O-Z)
      REAL*8 NZERO,KZERO
      COMMON/ONE/BK,A,B,PART,TZERO,NZERO,XZERO,H,H1,H2,KUTTA,M,M1,M2,M3
      COMMON /THREE/ RSUN,EMSUN,EMP,G,KZERO
      RSUN=6.95987D1O
      EMSUN=1.9892D33
      EMP=1.672523D-24
      G=6.6705D-8
      BK=1.38O546D-16
      KZERO=5.OD-7
C****SPECIFY BOUNDARY CONDITIONS
      TZERO=2.OD6
      NZERO=5.OD6
      RZERO=1.1*RSUN
      A=G*EMSUN*EMP/(BK*TZERO)
      B=EMP/(BK*TZERO)
      XZERO=A/RZERO
      PART=0.O1
      KUTTA=5
      H=-XZERO/52.O
      H1=O.1*H
      H2=O.1
      M=1OO
      M1=51
      M2=68
      M3=83
C****NEW=O MODEL TO BE COMPUTED APPROXIMATELY, NEW=1 INITIAL MODEL READ
      NEW=1
      NXZ=0
      DO 20 I=1,1O
      IF (I.GT.1) GO TO 1O
      IF (NEW.EQ.1) GO TO 5
      CALL MAIN1 (NXZ)
      GO TO 2O
    5 CONTINUE
      CALL MAIN3 (NXZ)
      GO TO 2O
   1O CONTINUE
      CALL MAIN2 (NXZ)
   2O CONTINUE
      CALL EXIT
      END
```

```
      SUBROUTINE MAIN1 (NXZ)
      IMPLICIT REAL*8 (A-H,O-Z)
      DIMENSION X(100),TAU(100),DTDX(100),U(100),DUDX(100),XX(100),TTAU
     1 (100),DDTDX(100),UU(100),YP(100),TAUI(100),DYDX(100),Y(100),
     2 UA(100),TA(100),D2YDX(100),RLOG(100),T(100),V(100),NUM(5),
     3 XI(100),DTDXI(100),DYDXI(100),D2YDXI(100),DUDXI(100),
     4 DTDXA(100),DTDXIA(100),DUDXA(100),DUDXIA(100)
      EXTERNAL MOTION,MOTB
      COMMON XC,UC,DUDXC,TAUC,DTDXC,ZZ
      COMMON/ONE/BK,A,B,PART,TZERO,NZERO,XZERO,H,H1,H2,KUTTA,M,M1,M2,M3
      COMMON/TWO/X,TAU,DTDX,DUDX,U,HMIN,HPLUS,IMINUS,IPLUS
      COMMON /THREE/ RSUN,EMSUN,EMP,G,KZERO
      REAL*8 NZERO,LOGN(100),MACH(100),KZERO
      M2P1=M2+1
      DO 10 I=1,M1
   10 X(I)=XZERO+H*(I-1)
      DO 11 I=M1,M2
   11 X(I)=X(M1)+H1*(I-M1)
      XI(M2)=-DLOG(X(M2))
      DO 12 I=M2P1,M3
      XI(I)=XI(M2)+H2*(I-M2)
   12 X(I)=DEXP(-XI(I))
      DO 13 I=1,M2
      TAU(I)=DSQRT(X(I)/XZERO)
   13 DTDX(I)=0.5/DSQRT(X(I)*XZERO)
      DO 14 I=M2,M3
      TAU(I)=1.0/(DSQRT(XZERO)*DEXP(XI(I)/2.0))
   14 DTDXI(I)=-0.5*TAU(I)
      XC=25.0/XZERO
      TAUC=DSQRT(XC/XZERO)
      DTDXC=0.5/DSQRT(XC*XZERO)
      D2TDXC=-1.0/(4.0*XC*DSQRT(XC*XZERO))
      UC=2.0*TAUC
      DUDXC=0.5*(1.0-2.0*UC/XC)-0.5*DSQRT(1.0-20.*UC/XC+52.0*(UC/XC)**2-
     1 16.0*UC*D2TDXC)
      DO 20 I=1,M1
      IF (X(I+1).GT.XC) GO TO 20
      HMIN=X(I)-XC
      HPLUS=X(I+1)-XC
      IPLUS=I+1
      IMINUS=I
      GO TO 23
   20 CONTINUE
      ENTRY MAIN3 (NXZ)
      READ (5,705) M1,M2,M3,IMINUS,IPLUS
      READ (5,700) (X(I),TAU(I),DTDX(I),I=1,M2)
      READ (5,700) (X(I),XI(I),TAU(I),DTDXI(I),I=M2,M3)
      READ (5,700) (U(I),DUDX(I),I=1,M2)
```

```
      READ (5,700) (U(I),DUDXI(I),I=M2,M3)
      READ (5,701) HMIN,HPLUS
      READ (5,702) XC,UC,DUDXC,TAUC,DTDXC,D2TDXC
      WRITE (6,601) (X(I),TAU(I),DTDX(I),U(I),DUDX(I),I=1,M2)
      WRITE (6,601) (X(I),TAU(I),DTDXI(I),U(I),DUDXI(I),I=M2,M3)
      WRITE (6,605) XC,UC,DUDXC,TAUC,DTDXC,D2TDXC
  605 FORMAT (6E20.5)
      MMM=0
   23 CONTINUE
      MNC=1
      MODEL=1
      NUM(1)=0
      NUM(2)=1
      NUM(3)=0
      M2P1=M2+1
   25 CONTINUE
      NUMBER=1
   30 CONTINUE
      IF (MNC.EQ.1) GO TO 35
C****CALCULATE CRITICAL POINT PARAMETERS
      CALL CRITIC (M2,&55)
      NUMBER=NUMBER+1
      GO TO 35
      ENTRY MAIN2 (NXZ)
      TAU(1)=1.02*TAU(1)
   35 CONTINUE
      MNC=MNC+1
C****SOLVE MOMENTUM EQUATION FOR U(X) & DUDX(X)
      CALL PIECE (MOTION,HPLUS,U(IPLUS))
      CALL PIECE (MOTION,HMIN,U(IMINUS))
      CALL PREDCO (H,M1,IPLUS,MOTION,X,U,TAU,DTDX,DUDX,KUTTA)
      DO 40 I=1,IMINUS
      XX(IMINUS+1-I)=X(I)
      TTAU(IMINUS+1-I)=TAU(I)
   40 DDTDX(IMINUS+1-I)=DTDX(I)
      HH=-H
      N=1
      UU(1)=U(IMINUS)
      CALL PREDCO (HH,IMINUS,N,MOTION,XX,UU,TTAU,DDTDX,YP,KUTTA)
      DO 50 I=1,IMINUS
      U(IMINUS+1-I)=UU(I)
   50 DUDX(IMINUS+1-I)=YP(I)
      CALL PREDCO (H1,M2,M1,MOTION,X,U,TAU,DTDX,DUDX,C)
      CALL PREDCO (H2,M3,M2,MOTB,XI,U,TAU,DTDXI,DUDXI,C)
  601 FORMAT (5E25.5)
      GO TO 51
      ENTRY MAIN4 (NXZ)
      MMM=1
```

```
      MNC=MNC+1
   51 CONTINUE
C****CALCULATE PARTICLE FLUX J & DENSITY DISTRIBUTION N(X)
      FLUX=NZERO*DSQRT(U(1)/B)*A*A/(XZERO*XZERO)
      LOGN(1)=DLOG10(NZERO)
      DO 52 I=2,M3
      LOGN(I)=DLOG10(FLUX*X(I)*X(I)/(A*A)*DSQRT(B/U(I)))
   52 CONTINUE
      ITER=1
      ZZ=7.0*FLUX*BK/(2.0*A*5.0D-7*TZERO **2.5)*2.0
C****COMPUTE BOUNDARY CONDITION
      UINF=14.0/ZZ*DTDXO*TAUO**2.5+10.0*TAUO+UO-2.0*XO
      IF (UINF.LT.U(M3).AND.NUMBER.GT.1) GO TO 115
      IF (UINF.LT.U(M3))UINF=-14.0/ZZ*DTDXI(M3)*TAU(M3)**2.5/X(M3)+10.0*
     1 TAU(M3)+U(M3)-2.0*X(M3)
      IF (NUMBER.LE.2) GO TO 120
      Y(M3)=TAU(M3)**3.5
   53 CONTINUE
      YEM=Y(M3)
      DYDXM=ZZ*(0.25*(UINF-U(M3))+0.5*X(M3)-2.5*Y(M3)**(1.0/3.5))
      Y(M3)=0.5*DYDXM*X(M3)
      WRITE (6,800) Y(M3),YEM,U(M3),UINF,DYDXM
  800 FORMAT (5E20.5)
      IF (Y(M3).LT.0.0) GO TO 115
      IF (DABS(Y(M3)-YEM).GT.Y(M3)*1.0D-5) GO TO 53
      Y1=Y(M3)
C****SOLVE ENERGY EQUATION FOR TAU(X) & DTDX(X)
   54 CONTINUE
      LL=0
      MM=0
      NN=0
   55 CONTINUE
      DYDX(1)=3.5*DTDX(1)*TAU(1)**2.5
      Y(1)=TAU(1)**3.5
      DO 56 I=1,M2
      TAUI(I)=TAU(I)
      D2YDX(I)=ZZ*(2.0*TAU(I)/X(I)-1.5*DTDX(I)-0.5*TAU(I)*DUDX(I)/U(I))
   56 CONTINUE
      DO 57 I=M2,M3
      TAUI(I)=TAU(I)
      D2YDXI(I)=ZZ*DEXP(-XI(I))*(2.0*TAU(I)+1.5*DTDXI(I)+0.5*TAU(I)*
     1 DUDXI(I)/U(I))-3.5*DTDXI(I)*TAU(I)**2.5
   57 CONTINUE
   60 CONTINUE
      DYDX(1)=3.5*DTDX(1)
      CALL SIMSON (D2YDX,DYDX,H ,M1, 1)
      CALL SIMSON (D2YDX,DYDX,H1,M2,M1)
      DYDXI(M2)=-DYDX(M2)*DEXP(-XI(M2))
```

```
      CALL SIMSON (D2YDXI,DYDXI,H2,M3,M2)
      CALL SIMSON (DYDX,Y,H ,M1, 1)
      CALL SIMSON (DYDX,Y,H1,M2,M1)
      CALL SIMSON (DYDXI,Y,H2,M3,M2)
      CALL BOUND (NN,LL,MM,Y,DTDX(1),Y1,&60,M3,KK,&115)
      LL=0
      MM=0
      NN=0
      DO 70 I=2,M2
      TAU(I)=Y(I)**(2.0/7.0)
   70 DTDX(I)=2.0*DYDX(I)/(7.0*TAU(I)**2.5)
      DO 75 I=M2,M3
      TAU(I)=Y(I)**(2.0/7.0)
      DTDXI(I)=DYDXI(I)/(3.5*TAU(I)**2.5)
   75 CONTINUE
      IF (KK.EQ.1) GO TO 55
      ITER=ITER+1
      IF (NUMBER.EQ.1) GO TO 120
      IF (NUMBER.LE.10) GO TO 100
      IF (ITER.GT.10) GO TO 100
      DO 80 I=1,M3
      IF (DABS(TAU(I)-TAU1(I)).GT.TAU(I)*1.0D-3) GO TO 55
   80 CONTINUE
  100 CONTINUE
C****COMPARE ORIGINAL & CALCULATED VELOCITY & TEMPERATURE DISTRIBUTIONS
      DO 110 I=1,M3
      IF(DABS(UA(I)-U(I)).GT.PART*U(I)) GO TO 120
      IF (DABS(TA(I)-TAU(I)).GT.PART*TAU(I)) GO TO 120
  110 CONTINUE
      GO TO 140
  115 CONTINUE
      FLUX=FLUXA
      ZZ=ZZA
      Y1=Y1A
      DO 116 I=1,M2
      TAU(I)=TA(I)
      DTDX(I)=DTDXA(I)
      U(I)=UA(I)
      DUDX(I)=DUDXA(I)
  116 CONTINUE
      DO 117 I=M2,M3
      TAU(I)=TA(I)
      DTDXI(I)=DTDXIA(I)
      U(I)=UA(I)
      DUDXI(I)=DUDXIA(I)
  117 CONTINUE
      GO TO 54
  120 CONTINUE
```

```
      FLUXA=FLUX
      ZZA=ZZ
      YLA=YL
      DO 127 I=1,M2
      DTDXA(I)=DTDX(I)
      DUDXA(I)=DUDX(I)
  127 CONTINUE
      DO 128 I=M2,M3
      DTDXIA(I)=DTDXI(I)
      DUDXIA(I)=DUDXI(I)
  128 CONTINUE
  129 CONTINUE
      DO 130 I=1,M3
      UA(I)=U(I)
      TA(I)=TAU(I)
  130 CONTINUE
      NOM=NOM+1
      GO TO 30
  140 CONTINUE
      IF (NOM.GT.0) GO TO 145
      YY1=YL
      GO TO 129
  145 CONTINUE
      IF (DABS(YY1-YL).LE.YL*4.0D-4) GO TO 149
      YY1=YL
      GO TO 129
  149 CONTINUE
      DO 150 I=1,M2
      T(I)=TAU(I)*TZERO
      RLOG(I)=DLOG10(A/X(I))
      V(I)=DSQRT(U(I)/B)
  150 MACH(I)=DSQRT(0.5*U(I)/TAU(I))
      DO 160 I=M2P1,M3
      T(I)=TAU(I)*TZERO
      RLOG(I)=DLOG10(A)+XI(I)*0.4343
      V(I)=DSQRT(U(I)/B)
      MACH(I)=DSQRT(0.5*U(I)/TAU(I))
  160 CONTINUE
      WRITE (7,705) M1,M2,M3,IMINUS,IPLUS
      WRITE (7,700) (X(I),TAU(I),DTDX(I),I=1,M2)
      WRITE (7,700) (X(I),XI(I),TAU(I),DTDXI(I),I=M2,M3)
      WRITE (7,700) (U(I),DUDX(I),I=1,M2)
      WRITE (7,700) (U(I),DUDXI(I),I=M2,M3)
      WRITE (7,701) FMIN,FPLUS
      WRITE (7,702) XC,UC,DUDXC,TAUC,DTDXC,D2TDXC
      WRITE (6,790)
      WRITE (6,791) (I,RLOG(I),T(I),V(I),LOGN(I),MACH(I),I=1,M3)
      RC=DLOG10(A/XC)
```

```
      VC=DSQRT(UC/B)
      TC=TAUC*TZERO
      XXX=3.336D-50*FLUX
      VINF=DSQRT(UINF/B)
      WRITE (6,740)
      WRITE (6,750) RC, VC, TC
      WRITE (6,735) NZERO
      WRITE (6,725) VINF
      WRITE (6,780) FLUX
      WRITE (6,770) XXX
      NUM(1)=NUM(1)+1
      CALL PLOT (RLOG,T,M3,NUM)
      NUM(1)=NUM(1)+1
      CALL PLOT (RLOG,V,M3,NUM)
      NUM(1)=NUM(1)+1
      CALL PLOT (RLOG,LOGN,M3,NUM)
      NUM(1)=NUM(1)+1
      CALL PLOT (RLOG,MACH,M3,NUM)
      NUMBER=1
      MNC=1
      IF (NXZ.EQ.0) GO TO 190
      IF (NXZ+M3.GT.M) CALL EXIT
      DO 170 I=1,NXZ
      XI(M3+I)=XI(M3)+H2*I
      X(M3+I)=DEXP(-XI(M3+I))
  170 CONTINUE
      TAU(M3+NXZ)=(3.0*FLUX*BK*X(M3+NXZ)/(A*KZERO*TZERO**2.5))**0.4
      HTAU=(TAU(M3+NXZ)-TAU(M3))/NXZ
      DO 180 I=1,NXZ
      TAU(M3+I)=TAU(M3)+I*HTAU
      DTDXI(M3+I)=DTDXI(M3)+(DTDXI(M3)-DTDXI(M3-1))*I
  180 CONTINUE
      M3=M3+NXZ
      MODEL=MODEL+1
      GO TO 25
  190 CONTINUE
  700 FORMAT (10A8)
  701 FORMAT (2A8)
  702 FORMAT (6A8)
  705 FORMAT (5A4)
  711 FORMAT (T10,'FAILS TO CONVERGE AFTER 20 ITERATIONS')
  720 FORMAT ('1',T22,'TAU(I)',T52,'DTDX(I)',T82,'TAU1(I)',T112,'DTDX1(I
     1)')
  725 FORMAT (////,T10,'ASYMPTOTIC VELOCITY :',E14.5,T47,'CENTIMETRES PE
     1R SECOND')
  730 FORMAT (/,4E30.5)
  735 FORMAT (////,T10,'CORONAL DENSITY :',E14.5,T43,'PARTICLES PER CUBI
     1C CENTIMETRE')
```

```
74C FORMAT (////,T10,'CRITICAL POINT PARAMETERS, RC, VC, TC')
75C FORMAT (////,3E20.5)
76C FORMAT (////,T20,'FAILS TO CONVERGE AFTER 60 ITERATIONS')
77C FORMAT (////,T10,'RATE OF MASS LOSS : ',E14.5,T48,'SOLAR MASSES PE
   1R YEAR')
78C FORMAT (////,T10,'PARTICLE FLUX : ',E14.5,T42,'PER STERADIAN PER S
   1ECOND')
79C FORMAT ('1',T22,'RADIUS',T45,'TEMPERATURE',T71,'VELOCITY',T97,
   1 'DENSITY',T120,'MACH NUMBER')
791 FORMAT (/,I5,5E25.5)
    RETURN
    END
```

```
      REAL FUNCTION MOTB*8 (XI,U,TAU,DTDXI)
      IMPLICIT REAL*8 (A-H,O-Z)
      MOTB=(4.0*TAU-DEXP(-XI)-2.0*DTDXI)/(0.5-TAU/U)
      RETURN
      END


      REAL FUNCTION MOTION*8 (X,U,TAU,DTDX)
      IMPLICIT REAL*8 (A-H,O-Z)
      MOTION=(1.0-4.0*TAU/X-2.0*DTDX)/(0.5*(1.0-2.0*TAU/U))
      RETURN
      END


      SUBROUTINE PIECE (F,H,W)
      IMPLICIT REAL*8 (A-H,O-Z)
      COMMON X,Y,YP,Z1,Z2,ZZ
      H2=H/2.0
      T1=H*YP
      T2=H*F(X+H2,Y+T1/2.0,Z1,Z2)
      T3=H*F(X+H2,Y+T2/2.0,Z1,Z2)
      T4=H*F(X+H,Y+T3,Z1,Z2)
      W=Y+(T1+2.0*T2+2.0*T3+T4)/6.0
      RETURN
      END


      SUBROUTINE SIMSON (Y,Z,H,M,N)
      IMPLICIT REAL*8 (A-H,O-Z)
      DIMENSION Z(M),Y(M)
C****USE SIMPSON'S RULE TO EVALUATE Z(I), THE INTEGRAL OF Y(I), A FUNCTI
C****N IS THE STARTING VALUE OF I AT WHICH BOUNDARY CONDITIONS ARE APPLI
C****M IS FINAL VALUE OF I
      Z(N+1)=Z(N)+H/3.0*(1.25*Y(N)+2.0*Y(N+1)-0.25*Y(N+2))
      N2=N+2
      DO 10 I=N2,M
   10 Z(I)=Z(I-2)+H/3.0*(Y(I-2)+4.0*Y(I-1)+Y(I))
      RETURN
      END
```

```
      SUBROUTINE PREDCO (H,M,N,F,X,Y,Z1,Z2,YP,J)
      IMPLICIT REAL*8 (A-H,O-Z)
C
C   SOLVES Y'=F(X,Y) BY ADAMS BASHFORTH PREDICTOR-CORRECTOR USING RUNGE-
C   METHOD AS STARTER
C****J REPRESENTS NUMBER OF EXTRA STARTING POINTS TO BE CALCULATED BY R-
C
C   SPECIFY INITIAL CONDITIONS Y1=A AT X=X1, NUMBER OF POINTS M, STEPSIZ
C   AND F(X,Y), N REPRESENTS THE VALUE FROM WHICH CALCULATIONS START
C
      DIMENSION X(M),Y(M),Z1(M),Z2(M),YP(M)
C
C   CALCULATE Y(I) AND Y'(I) FOR 1ST FOUR POINTS BY RUNGE-KUTTA
C
      YP(N)=F(X(N),Y(N),Z1(N),Z2(N))
      H2=H/2.0
      MM1=M-1
      NP2=N+2+J
      DO 10 I=N,NP2
      T1=H*F(X(I),Y(I),Z1(I),Z2(I))
      T2=H*F(X(I)+H2,Y(I)+T1/2.0,Z1(I),Z2(I))
      T3=H*F(X(I)+H2,Y(I)+T2/2.0,Z1(I),Z2(I))
      T4=H*F(X(I)+H,Y(I)+T3,Z1(I),Z2(I))
      Y(I+1)=Y(I)+(T1+2.0*T2+2.0*T3+T4)/6.0
      YP(I+1)=F(X(I+1),Y(I+1),Z1(I+1),Z2(I+1))
   10 CONTINUE
C
C   USE ADAMS-BASHFORTH PREDICTOR CORRECTOR FOR REMAINING POINTS.
C
      MM1=M-1
      NP3=NP2+1
      DO 220 I=NP3,MM1
      NUM=0
      Y(I+1)=Y(I)+H/24.0*(55.0*YP(I)-59.0*YP(I-1)+37.0*YP(I-2)-9.0*YP(I-
     13))
      A=Y(I+1)
  278 YP(I+1)=F(X(I+1),Y(I+1),Z1(I+1),Z2(I+1))
      Y(I+1)=Y(I)+H/24.0*(9.0*YP(I+1)+19.0*YP(I)-5.0*YP(I-1)+YP(I-2))
      IF (DABS(DEXP(A)-DEXP(Y(I+1))).LE.DEXP(A)*1.0D-4) GO TO 220
      NUM=NUM+1
      IF (NUM.NE.50) GO TO 200
      WRITE (6,800)
  800 FORMAT (I10,'FAILS TO CONVERGE AFTER 50 ITERATIONS')
      CALL EXIT
  200 CONTINUE
      A=Y(I+1)
      GO TO 278
  220 CONTINUE
      RETURN
      END
```

```
      SUBROUTINE BOUND (NN,LL,MM,Y,DTDX,Y1,*,M,KK,*)
      IMPLICIT REAL*8 (A-H,O-Z)
      DIMENSION Y(M)
C****DTDX=DTDX(1)
      KK=0
      IF (NN.NE.0) GO TO 5
      D1=0.0
      E1=0.0
      A=Y(M)
    5 CONTINUE
      NN=NN+1
      IF (NN.GT.30) RETURN 2
C****SEE IF ALL Y(I) ARE GREATER THAN ZERO
      DO 10 I=1,M
      IF (Y(I).GT.0.0) GO TO 10
      E1=DTDX
      T=Y(1)
      DO 25 J=1,M
      IF (Y(J).GT.0.0) GO TO 25
      IF (Y(J).GT.T) GO TO 25
      T=Y(J)
   25 CONTINUE
      IF (Y(M)-T) 260,30,27
  260 CALL EXIT
   27 CONTINUE
      LL=LL+1
      JO=0
      IF (MM.NE.0) GO TO 28
      DTDX=0.9*DTDX
      NB=1
      WRITE (6,800) NB,NN,D1,E1,DTDX,Y(M),Y1,A
      RETURN 1
   28 CONTINUE
      DTDX=0.5*(D1+E1)
      NB=2
      WRITE (6,800) NB,NN,D1,E1,DTDX,Y(M),Y1,A
      RETURN 1
   30 CONTINUE
      YD2=T
      LL=LL+1
      JO=1
      IF (MM.NE.0) GO TO 20
      DTDX=0.9*DTDX
      NB=3
      WRITE (6,800) NB,NN,D1,E1,DTDX,Y(M),Y1,A
      RETURN 1
   20 CONTINUE
      DTDX=(E1*(Y1-YD1)-D1*(Y1-YD2))/(YD2-YD1)
```

```
      NB=4
      WRITE (6,800) NB,NN,D1,E1,DTDX,Y(M),Y1,A
      RETURN 1
   10 CONTINUE
C****CHECK IF BOUNDARY CONDITIONS ARE OBEYED
      IF(DABS(Y(M)-Y1).LT.Y1*1.0D-3) GO TO 200
C****IF BOUNDARY CONDITIONS NOT OBEYED, ITERATE. IF DYDX(M) IS NEGATIVE
C****Y(M)>Y1 DYDX(1) MUST BE INCREASED. DYDX(1) HERE IS A LOWER BOUND ON
C****REQUIRED VALUE. IF DYDX(M) IS POSITIVE & Y(M)>Y1 DYDX(1) MUST AGAIN
C****INCREASED
      IF (Y(M).LT.Y1) GO TO 120
      MM=MM+1
      D1=DTDX
      YD1=Y(M)
      IF (LL.NE.0) GO TO 110
      DTDX=1.1*DTDX
      NB=6
      WRITE (6,800) NB,NN,D1,E1,DTDX,Y(M),Y1,A
      A=Y(M)
      RETURN 1
  110 CONTINUE
      IF (JO.EQ.1) GO TO 115
      DTDX=0.5*(D1+E1)
      NB=7
      WRITE (6,800) NB,NN,D1,E1,DTDX,Y(M),Y1,A
      GO TO 59
  115 CONTINUE
      DTDX=(E1*(Y1-YD1)-D1*(Y1-YD2))/(YD2-YD1)
      NB=8
      WRITE (6,800) NB,NN,D1,E1,DTDX,Y(M),Y1,A
      GO TO 59
  120 CONTINUE
      LL=LL+1
      E1=DTDX
      YD2=Y(M)
      IF (MM.NE.0) GO TO 125
      DTDX=0.9*DTDX
      NB=5
      WRITE (6,800) NB,NN,D1,E1,DTDX,Y(M),Y1,A
  800 FORMAT (2I5,6E20.5)
      A=Y(M)
      RETURN 1
  125 CONTINUE
      DTDX=(E1*(Y1-YD1)-D1*(Y1-YD2))/(YD2-YD1)
   59 CONTINUE
      IF (NN.EQ.1) RETURN 1
      IF (DABS(A-Y(M)).LT.DABS(Y(M))*4.0D-4) GO TO 180
      A=Y(M)
```

```
      RETURN 1
  18C CONTINUE
      KK=1
  20C CONTINUE
      NB=5
      WRITE (6,800) NB,NN,D1,E1,DTDX,Y(M),Y1,A
      RETURN
      END
```

```
      SUBROUTINE CRITIC (M2,*)
      IMPLICIT REAL*8 (A-H,O-Z)
      DIMENSION X(100),TAU(100),DTDX(100),DUDX(100),U(100)
      COMMON XC,UC,DUDXC,TAUC,DTDXC,ZZ
      COMMON /TWO/ X,TAU,DTDX,DUDX,U,HMIN,HPLUS,J,J1
      D2TDX(X,TAU,DTDX,U,DUDX)=ZZ/3.5*(2.0*TAU/X-1.5*DTDX-0.5*TAU*DUDX/U
     1 )/(TAU**2.5)-2.5*DTDX*DTDX/TAU
      Q(X,TAU,DTDX)=1.0-4.0*TAU/X-2.0*DTDX
      DO 10 I=1,M2
      J=I
      B=Q(X(J),TAU(J),DTDX(J))
      C=Q(X(J+1),TAU(J+1),DTDX(J+1))
      IF (B.LT.0.0.AND.C.GT.0.0) GO TO 20
      IF (B.GT.0.0.AND.C.LT.0.0) GO TO 20
   10 CONTINUE
      WRITE (6,200)
  200 FORMAT (T20,'CRITICAL POINT CANNOT BE DETERMINED')
      CALL EXIT
   20 CONTINUE
      H=B/(B-C)
      XC=X(J)+H*(X(J+1)-X(J))
      TAUC=TAU(J)+H*(TAU(J+1)-TAU(J))
      UC=2.0*TAUC
      DTDXC=0.5*(1.0-4.0*TAUC/XC)
      D2TDXC=D2TDX(X(J),TAU(J),DTDX(J),U(J),DUDX(J))+H*(D2TDX(X(J+1),
     1 TAU(J+1),DTDX(J+1),U(J+1),DUDX(J+1))-D2TDX(X(J),TAU(J),DTDX(J),
     2 U(J),DUDX(J)))
      IF (1.0-20.0*UC/XC+52.0*(UC/XC)**2-16.0*UC*D2TDXC.LT.0.0) RETURN 1
      DUDXC=0.5*(1.0-2.0*UC/XC)-0.5*DSQRT(1.0-20.0*UC/XC+52.0*(UC/XC)**2
     1 -16.0*UC*D2TDXC)
      HMIN=X(J)-XC
      HPLUS=X(J+1)-XC
      J1=J+1
      RETURN
      END
```

APPENDIX B

COMPUTER PROGRAM FOR THE SOLUTION OF THE SOLAR WIND EQUATIONS INCLUDING AN ENERGY EQUATION

The program in Appendix B solves the set of equations of motion, including an energy equation, simultaneously. The method used is Hamming's modified predictor-corrector method which was obtained from the IBM Fortran library subprograms manual and adapted for use in this situation.

```
      IMPLICIT REAL*8 (A-H,O-Z)
      REAL*8 KZERO
      COMMON XC,UC,DUDXC,TAUC,DTDXC,ZZ,UINF,AMIN,AMAX,D2TDXC
      COMMON/ONE/RSUN,EMSUN,EMP,G,BK,KZERO,TZERO,FLUX,RZERO,A,B,XZERO
      RSUN=6.95987D10
      EMSUN=1.9892D33
      EMP=1.6725230-24
      G=6.6705D-8
      BK=1.380546D-16
      KZERO=5.0D-7
      TZERO=2.0D6
      FLUX=2.0D35
      RZERO=1.1*RSUN
      A=G*EMSUN*EMP/(BK*TZERO)
      B=EMP/(BK*TZERO)
      XZERO=A/RZERO
      CALL MAIN2
      CALL EXIT
      END


      SUBROUTINE FCT(DIST,Y,DERY)
      IMPLICIT REAL*8 (A-H,O-Z)
      DIMENSION Y(2),DERY(2)
      COMMON XC,UC,DUDXC,TAUC,DTDXC,ZZ,UINF,AMIN,AMAX,D2TDXC
      COMMON /NINE/ IHLF1
      IF (Y(1).LT.0.0) CALL SUB1(DTDXC,AMIN,AMAX)
      DERY(1)=ZZ/3.5*Y(1)**(-2.5)*(0.5*DIST+0.25*(UINF-Y(2))-2.5*Y(1))
      DERY(2)=(1.0-4.0*Y(1)/DIST-2.0*DERY(1))/(0.5*(1.0-2.0*Y(1)/Y(2)))
      RETURN
      END
```

```
      SUBROUTINE SUB (DT,AMIN,AMAX)
      IMPLICIT REAL*8 (A-H,O-Z)
      AMIN=DT
      IF (AMAX.NE.0.0) GO TO 10
      DT=1.05*DT
      GO TO 30
   10 CONTINUE
      DT=AMIN+0.8*(AMAX-AMIN)
      GO TO 30
      ENTRY SUB1 (DT,AMIN,AMAX)
      AMAX=DT
      IF (AMIN.EQ.0.0) GO TO 20
      DT=0.5*(AMIN+AMAX)
      GO TO 30
   20 CONTINUE
      DT=0.95*DT
   30 CONTINUE
      CALL MAIN1 (DT,AMAX,AMIN)
      RETURN
      END
```

```
      SUBROUTINE OUTP(DIST,Y,DERY,IHLF,NDIM,PRMT)
      IMPLICIT REAL*8 (A-H,O-Z)
      COMMON XC,UC,DUDXC,TAUC,DTDXC,ZZ,UINF,AMIN,AMAX,D2TDXC
      COMMON /SEVEN/X1,TAU,DTDX,DUDX,U,N
      COMMON /EIGHT/ XFAR
      COMMON /NINE/ IHLF1
      DIMENSION Y(2),DERY(2),PRMT(20),X1(100),TAU(100),DTDX(100),DUDX
     1 (100),U(100),XX(100),TT(100),UU(100),DT(100),DU(100)
      WRITE (6,700) DIST,Y(1),DERY(1),Y(2),DERY(2),AMIN,AMAX,PRMT(10),
     1 UINF,IHLF
  700 FORMAT (5E13.5,2E20.10,F6.1,E13.5,I5)
      PRMT(11)=0.0
      IF (PRMT(9).EQ.1.0.AND.DERY(1).LE.DT1) CALL SUB (DTDXC,AMIN,AMAX)
      DT1=DERY(1)
      IF (Y(2).LT.UINF.OR.IHLF.EQ.11) GO TO 200
      IF (PRMT(10).EQ.1.0) GO TO 100
      CALL MAIN5 (DUM)
  200 CONTINUE
      IF (IHLF.LT.5) GO TO 210
      IF (UINF.LE.Y(2)+DERY(2)*PRMT(3)/(2.0**IHLF)) PRMT(11)=1.0
      PRMT(12)=(UINF-Y(2))/DERY(2)
      GO TO 220
  210 CONTINUE
      IF (UINF.LE.Y(2)+DABS(PRMT(3)/(2.0**IHLF))) PRMT(11)=1.0
      PRMT(12)=Y(2)-UINF
  220 CONTINUE
      PRMT(13)=UINF
      IF (IHLF.LT.11) GO TO 5
      IF (XFAR.EQ.0.0) GO TO 2
      IF (DABS(AMAX-AMIN).LT.1.0D-10 .OR.DIST.LE.PRMT(3)) GO TO 5
      IF (PRMT(10).EQ.0.0) GO TO 1
      IF (DIST-DMID) 80,90,100
   80 CONTINUE
      AMIN=AMID
      XFAR=DIST
      GO TO 110
   90 CONTINUE
      IF (DERY(1).LT.DTLAST) GO TO 80
  100 CONTINUE
      PRMT(10)=0.0
      XFAR=DMID
      CALL SUB1 (AMID,AMIN,AMAX)
    1 CONTINUE
      IF (DIST.GT.XFAR) CALL SUB (DTDXC,AMIN,AMAX)
  110 CONTINUE
      PRMT(10)=1.0
      AMID=DTDXC
      DMID=DIST
```

```
      DTLAST=DERY(1)
      DERIV=0.5*(AMID+AMAX)
      CALL MAIN4 (DERIV)
    2 CONTINUE
      XFAR=DIST
      CALL SUB1 (DTDXC,AMIN,AMAX)
    5 CONTINUE
      IF (DERY(1).LT.0.0) CALL SUB (DTDXC,AMIN,AMAX)
      IF (PRMT(8).EQ.1.0) GO TO 10
      XX(N)=DIST
      TT(N)=Y(1)
      UU(N)=Y(2)
      DT(N)=DERY(1)
      DU(N)=DERY(2)
      GO TO 30
   10 CONTINUE
      IF (PRMT(9).EQ.1.0) GO TO 20
      N=N-1
      DO 15 I=1,N
      X1(N+1-I)=XX(I)
      TAU(N+1-I)=TT(I)
      U(N+1-I)=UU(I)
      DTDX(N+1-I)=DT(I)
      DUDX(N+1-I)=DU(I)
   15 CONTINUE
      PRMT(9)=1.0
      GO TO 30
   20 CONTINUE
      X1(N)=DIST
      TAU(N)=Y(1)
      DTDX(N)=DERY(1)
      U(N)=Y(2)
      DUDX(N)=DERY(2)
   30 CONTINUE
      N1=N
      N=N+1
      IF (IHLF.NE.11) RETURN
      CALL MAIN3 (N1)
      RETURN
      END
```

```
      SUBROUTINE MAIN2
      IMPLICIT REAL*8 (A-H,O-Z)
      DIMENSION X(100),TAU(100),DTDX(100),U(100),DUDX(100),UA(100),
     1 TA(100),PRMT(20),Y(2),DERY(2),RLOG(100),T(100),V(100),NUM(5),
     2 YY(2),AUX(16,2)
      EXTERNAL FCT,OUTP
      COMMON XC,UC,DUDXC,TAUC,DTDXC,ZZ,UINF,AMIN,AMAX,D2TDXC
      COMMON/ONE/RSUN,EMSUN,EMP,G,BK,KZERO,TZERO,FLUX,RZERO,A,B,XZERO
      COMMON /SEVEN/ X,TAU,DTDX,DUDX,U,N
      COMMON /EIGHT/ XFAR
      REAL*8 NZERO,LOGN(100),MACH(100),KZERO,NP(100)
      DUCK=0.0
      NUM(1)=0
      NUM(2)=1
      NUM(3)=0
      NUMBER=1
      AMIN=0.0
      AMAX=0.0
      NDIM=2
      XFAR=0.0
      PRMT(10)=0.0
      XC=0.10151D1
      TAUC=0.17360D0
      DTDXC=0.158D0
      D2TDXC=-0.49486D-1
      UC=0.34718D0
      DUDXC=-0.20701D0
      GO TO 80
   35 CONTINUE
      N=1
      ZZ=7.0*FLUX*BK/(A*KZERO*TZERO**2.5)
      UINF=14.0/ZZ*DTDXC*TAUC**2.5+10.0*TAUC+UC-2.0*XC
      L=1
      MNO=MNO+1
      PRMT(1)=XC
      PRMT(2)=10.5
      PRMT(3)=0.4
      PRMT(4)=1.0D-4
      PRMT(6)=0.5
      PRMT(7)=0.5
      PRMT(8)=0.0
      PRMT(9)=0.0
      Y(1)=TAUC
      Y(2)=UC
      DERY(1)=DTDXC
      DERY(2)=DUDXC
      CALL DHPCG(PRMT,Y,DERY,NDIM,IHLF,FCT,OUTP,AUX)
   55 CONTINUE
```

```
      PRMT(2)=0.05*0.2**(NUMBER-1)
      PRMT(3)=-0.2
      PRMT(8)=1.0
      YY(1)=TAUC
      YY(2)=UC
      DERY(1)=DTDXC
      DERY(2)=DUDXC
      CALL DHPCG(PRMT,YY,DERY,NDIM,IHLF,FCT,OUTP,AUX)
      DUCK=DUDXC
      N1=N-1
      IF (TAU(N1).LT.TAU(N1-1).AND.DTDX(N1).GT.DTDX(N1-1)) GO TO 90
      AMIN=DTDXC
      IF (AMAX.EQ.0.0) GO TO 70
      DTDXC=0.5*(AMIN+AMAX)
      GO TO 80
   70 CONTINUE
      DTDXC=1.2*DTDXC
      GO TO 80
      ENTRY MAIN1 (Q,Q1,Q2)
      DTDXC=Q
      AMAX=Q1
      AMIN=Q2
      GO TO 80
      ENTRY MAIN5 (DUM)
      IF (DUCK.EQ.0.0) GO TO 75
      DUDXC=0.5*(DUM+DUCK)
      GO TO 80
   75 CONTINUE
      DUDXC=0.95*DUM
      GO TO 80
      ENTRY MAIN4 (DERIV)
      DTDXC=DERIV
   80 CONTINUE
      TAUC=0.25*XC*(1.0-2.0*DTDXC)
      UC=2.0*TAUC
      GO TO 35
   90 CONTINUE
      IF (AMAX-AMIN.LE.AMIN*1.0D-5) GO TO 100
      NUMBER=NUMBER+1
      GO TO 55
      ENTRY MAIN3 (N1)
  100 CONTINUE
      DO 60 I=1,N1
      NP(I)=FLUX*DSQRT(B/U(I))*X(I)*X(I)/(A*A)
      LOGN(I)=DLOG10(NP(I))
   60 CONTINUE
      WRITE (6,850) (X(I),TAU(I),DTDX(I),U(I),DUDX(I),NP(I),I=1,N1)
      WRITE (6,800) XC,UC,TAUC,DTDXC,DUDXC,D2TDXC
```

```
      WRITE (6,400) UINF,FLUX,ZZ
      WRITE (6,300) AMIN,AMAX
400   FORMAT (//,3E40.5,//)
300   FORMAT (//,2E40.5,//)
800   FORMAT (//,6E20.5,//)
850   FORMAT (6E20.5)
      DO 110 I=1,N1
      RLOG(I)=DLOG10(A/X(I))
110   CONTINUE
      NUM(1)=NUM(1)+1
      CALL PLOT (RLOG,TAU,N1,NUM)
      NUM(1)=NUM(1)+1
      CALL PLOT (RLOG,U,N1,NUM)
      NUM(1)=NUM(1)+1
      CALL PLOT (RLOG,LOGN,N1,NUM)
      N2=N1+1
      TAU(N2)=0.0
      X(N2)=0.0
      NUM(1)=NUM(1)+1
      CALL PLOT (X,TAU,N2,NUM)
      XFAR=0.0
      NUMBER=1
      AMIN=0.0
      AMAX=0.0
      PRNT(10)=0.0
      XC=0.98*XC
      GO TO 80
700   FORMAT (10A8)
701   FORMAT (2A8)
702   FORMAT (6A8)
705   FORMAT (5A4)
      RETURN
      END
```

```
      SUBROUTINE DHPCG(PRMT,Y,DERY,NDIM,IHLF,FCT,OUTP,AUX)
C
C
      DOUBLE PRECISION Y,DERY,AUX,PRMT,X,H,Z,DELT
      DIMENSION PRMT(20),Y(2),DERY(2),AUX(16,2)
      N=1
      IHLF=0
      X=PRMT(1)
      H=PRMT(3)
      PRMT(5)=0.D0
      DO 1 I=1,NDIM
      AUX(16,I)=0.D0
      AUX(15,I)=PRMT(I+5)
    1 AUX(1,I)=Y(I)
      IF(H*(PRMT(2)-X))3,2,4
C
C     ERROR RETURNS
    2 IHLF=12
      GOTO 4
    3 IHLF=13
    4 CONTINUE
C     RECORDING OF STARTING VALUES
      CALL OUTP(X,Y,DERY,IHLF,NDIM,PRMT)
      IF(PRMT(5))6,5,6
    5 IF(IHLF)7,7,6
    6 RETURN
    7 DO 8 I=1,NDIM
    8 AUX(8,I)=DERY(I)
C
C     COMPUTATION OF AUX(2,I)
      ISW=1
      GOTO 100
C
    9 X=X+H
      DO 10 I=1,NDIM
   10 AUX(2,I)=Y(I)
C
C     INCREMENT H IS TESTED BY MEANS OF BISECTION
   11 IHLF=IHLF+1
      X=X-H
      DO 12 I=1,NDIM
   12 AUX(4,I)=AUX(2,I)
      H=.5D0*H
      N=1
      ISW=2
      GOTO 100
C
   13 X=X+H
```

```
      CALL FCT(X,Y,DERY)
      N=2
      DO 14 I=1,NDIM
      AUX(2,I)=Y(I)
   14 AUX(9,I)=DERY(I)
      ISW=3
      GOTO 100
C
C     COMPUTATION OF TEST VALUE DELT
   15 DELT=0.D0
      DO 16 I=1,NDIM
   16 DELT=DELT+AUX(15,I)*DABS(Y(I)-AUX(4,I))
      DELT=.06666666666666667D0*DELT
      IF(DELT-PRMT(4))19,19,17
   17 IF(IHLF-10)11,18,18
C
C     NO SATISFACTORY ACCURACY AFTER 10 BISECTIONS. ERROR MESSAGE.
   18 IHLF=11
      X=X+H
      GOTO 4
C
C     THERE IS SATISFACTORY ACCURACY AFTER LESS THAN 11 BISECTIONS.
   19 X=X+H
      CALL FCT(X,Y,DERY)
      DO 20 I=1,NDIM
      AUX(3,I)=Y(I)
   20 AUX(10,I)=DERY(I)
      N=3
      ISW=4
      GOTO 100
C
   21 N=1
      X=X+H
      CALL FCT(X,Y,DERY)
      X=PRMT(1)
      DO 22 I=1,NDIM
      AUX(11,I)=DERY(I)
   22 Y(I)=AUX(1,I)+H*(.375D0*AUX(8,I)+.7916666666666667D0*AUX(9,I)
     1-.2083333333333333D0*AUX(10,I)+.04166666666666667D0*DERY(I))
   23 X=X+H
      N=N+1
      CALL FCT(X,Y,DERY)
      CALL OUTP(X,Y,DERY,IHLF,NDIM,PRMT)
      IF(PRMT(5))6,24,6
   24 IF(N-4)25,200,200
   25 DO 26 I=1,NDIM
      AUX(N,I)=Y(I)
   26 AUX(N+7,I)=DERY(I)
```

```
      IF(N-3)27,29,200
C
   27 DO 28 I=1,NDIM
      DELT=AUX(9,I)+AUX(9,I)
      DELT=DELT+DELT
   28 Y(I)=AUX(1,I)+.33333333333333333D0*H*(AUX(8,I)+DELT+AUX(10,I))
      GOTO 23
C
   29 DO 30 I=1,NDIM
      DELT=AUX(9,I)+AUX(10,I)
      DELT=DELT+DELT+DELT
   30 Y(I)=AUX(1,I)+.375D0*H*(AUX(8,I)+DELT+AUX(11,I))
      GOTO 23
C
C     THE FOLLOWING PART OF SUBROUTINE DHPCG COMPUTES BY MEANS OF
C     RUNGE-KUTTA METHOD STARTING VALUES FOR THE NOT SELF-STARTING
C     PREDICTOR-CORRECTOR METHOD.
  100 DO 101 I=1,NDIM
      Z=H*AUX(N+7,I)
      AUX(5,I)=Z
  101 Y(I)=AUX(N,I)+.4D0*Z
C     Z IS AN AUXILIARY STORAGE LOCATION
C
      Z=X+.4D0*H
      CALL FCT(Z,Y,DERY)
      DO 102 I=1,NDIM
      Z=H*DERY(I)
      AUX(6,I)=Z
  102 Y(I)=AUX(N,I)+.2969776092477536DD0*AUX(5,I)+.1587596449710C3583D0*Z
C
      Z=X+.4557372542187894300*H
      CALL FCT(Z,Y,DERY)
      DO 103 I=1,NDIM
      Z=H*DERY(I)
      AUX(7,I)=Z
  103 Y(I)=AUX(N,I)+.2181CC38822592047DD0*AUX(5,I)-3.C5C9651486929308D0*
     1AUX(6,I)+3.8328647604670103DC*Z
C
      Z=X+H
      CALL FCT(Z,Y,DERY)
      DO 104 I=1,NDIM
  104CY(I)=AUX(N,I)+.1747602822626903700*AUX(5,I)-.5514806628787329400*
     1AUX(6,I)+1.2055355993965235DC*AUX(7,I)+.1711847812195190300*
     2H*DERY(I)
      GOTO(9,13,15,21),ISW
C
C     POSSIBLE BREAK-POINT FOR LINKAGE
C
```

```
C       STARTING VALUES ARE COMPUTED.
C       NOW START HAMMINGS MODIFIED PREDICTOR-CORRECTOR METHOD.
  200 ISTEP=3
  201 IF(N-8)204,202,204
C
C       N=8 CAUSES THE ROWS OF AUX TO CHANGE THEIR STORAGE LOCATIONS
  202 DO 203 N=2,7
      DO 203 I=1,NDIM
      AUX(N-1,I)=AUX(N,I)
  203 AUX(N+6,I)=AUX(N+7,I)
      N=7
C
C       N LESS THAN 8 CAUSES N+1 TO GET N
  204 N=N+1
C
C       COMPUTATION OF NEXT VECTOR Y
      DO 205 I=1,NDIM
      AUX(N-1,I)=Y(I)
  205 AUX(N+6,I)=DERY(I)
      X=X+H
  206 ISTEP=ISTEP+1
      DO 207 I=1,NDIM
     CDELT=AUX(N-4,I)+1.3333333333333333D0*H*(AUX(N+6,I)+AUX(N+6,I)-
     1AUX(N+5,I)+AUX(N+4,I)+AUX(N+4,I))
      Y(I)=DELT-.9256198347107438D0*AUX(16,I)
  207 AUX(16,I)=DELT
C       PREDICTOR IS NOW GENERATED IN ROW 16 OF AUX, MODIFIED PREDICTOR
C       IS GENERATED IN Y. DELT MEANS AN AUXILIARY STORAGE.
C
      CALL FCT(X,Y,DERY)
C       DERIVATIVE OF MODIFIED PREDICTOR IS GENERATED IN DERY
C
      DO 208 I=1,NDIM
     CDELT=.125D0*(9.D0*AUX(N-1,I)-AUX(N-3,I)+3.D0*H*(DERY(I)+AUX(N+6,I)
     1+AUX(N+6,I)-AUX(N+5,I)))
      AUX(16,I)=AUX(16,I)-DELT
  208 Y(I)=DELT+.07438016528925620D0*AUX(16,I)
C
C       TEST WHETHER H MUST BE HALVED OR DOUBLED
      DELT=0.D0
      DO 209 I=1,NDIM
  209 DELT=DELT+AUX(15,I)*DABS(AUX(16,I))
      IF (PRMT(11).EQ.1.0) GO TO 222
      IF (Y(2).GE.PRMT(13)) GO TO 222
      IF(DELT-PRMT(4))210,222,222
C
C       H MUST NOT BE HALVED. THAT MEANS Y(I) ARE GOOD.
  210 CALL FCT(X,Y,DERY)
```

```
      CALL OUTP(X,Y,DERY,IHLF,NDIM,PRMT)
      IF(PRMT(5))212,211,212
  211 IF(IHLF-11)213,212,212
  212 RETURN
  213 IF(H*(X-PRMT(2)))214,212,212
  214 IF(DABS(X-PRMT(2))-.1D0*DABS(H))212,215,215
  215 IF(DELT-.02D0*PRMT(4))216,216,201
C
C
C     H COULD BE DOUBLED IF ALL NECESSARY PRECEEDING VALUES ARE
C     AVAILABLE
  216 IF(IHLF)201,201,217
  217 IF(N-7)201,218,218
  218 IF(ISTEP-4)201,219,219
  219 IMOD=ISTEP/2
      IF(ISTEP-IMOD-IMOD)201,220,201
  220 H=H+H
      IHLF=IHLF-1
      ISTEP=0
      DO 221 I=1,NDIM
      AUX(N-1,I)=AUX(N-2,I)
      AUX(N-2,I)=AUX(N-4,I)
      AUX(N-3,I)=AUX(N-6,I)
      AUX(N+6,I)=AUX(N+5,I)
      AUX(N+5,I)=AUX(N+3,I)
      AUX(N+4,I)=AUX(N+1,I)
      DELT=AUX(N+6,I)+AUX(N+5,I)
      DELT=DELT+DELT+DELT
  221 AUX(16,I)=8.962962962962963D0*(Y(I)-AUX(N-3,I))
     1-3.361111111111111111D0*H*(DERY(I)+DELT+AUX(N+4,I))
      GOTO 201
C
C
C     H MUST BE HALVED
  222 IHLF=IHLF+1
      IF(IHLF-10)223,223,210
  223 H=.5D0*H
      IF (H.GT.PRMT(12)) PRMT(11)=0.0
      ISTEP=0
      DO 224 I=1,NDIM
     CY(I)=.390625D-2*(8.D1*AUX(N-1,I)+135.D0*AUX(N-2,I)+4.D1*AUX(N-3,I)
     1+AUX(N-4,I))-.1171875D0*(AUX(N+6,I)-6.D0*AUX(N+5,I)-AUX(N+4,I))*H
     CAUX(N-4,I)=.390625D-2*(12.D0*AUX(N-1,I)+135.D0*AUX(N-2,I)+
     1108.D0*AUX(N-3,I)+AUX(N-4,I))-.C234375D0*(AUX(N+6,I)+
     218.D0*AUX(N+5,I)-9.D0*AUX(N+4,I))*H
      AUX(N-3,I)=AUX(N-2,I)
  224 AUX(N+4,I)=AUX(N+5,I)
      X=X-H
```

```
      DELT=X-(H+H)
      CALL FCT(DELT,Y,DERY)
      DO 225 I=1,NDIM
      AUX(N-2,I)=Y(I)
      AUX(N+5,I)=DERY(I)
  225 Y(I)=AUX(N-4,I)
      DELT=DELT-(H+H)
      CALL FCT(DELT,Y,DERY)
      DO 226 I=1,NDIM
      DELT=AUX(N+5,I)+AUX(N+4,I)
      DELT=DELT+DELT+DELT
     CAUX(16,I)=8.962962962962963DC*(AUX(N-1,I)-Y(I))
     1-3.361111111111111111DC*H*(AUX(N+6,I)+DELT+DERY(I))
  226 AUX(N+3,I)=DERY(I)
      GOTO 206
      END
```

REFERENCES

Alfven, H. 1947. M.N.R.A.S. 107, 211.

Allen, C.W. 1963. The Solar Corona, Academic Press, New York, editor Evans.

Arnett, W.D. 1969. Astrophys. Space Sci. 5, 180.

Braginskii, S. 1965. Rev. Plasma Phys. 1, 205.

Brandt, J.C. 1970. Introduction to the Solar Wind. W.H. Freeman, San Francisco.

Brandt, J.C., Wolff, C., and Cassinelli, J.P. 1969. Ap.J. 156, 1117.

Cameron, D.W. 1970. Comments Astrophys. Space Sci. 2, 209.

Cannon, R.D. 1968. Observatory. 88, 206.

Christy, R.F. 1966a. Ap.J. 144, 108.

1966b. Ap.J. 145, 337.

Conti, P.S. 1967. Ap.J. 149, 629.

Dennison, P.A. and Hewish, A. 1967. Nature. 213, 343.

Dessler, A.J. 1967. Rev. Geophys. 5, 1.

Deutsch, A.J. 1966. Stellar Evolution, Plenum Press, New York, editors Stein and Cameron, p. 377.

1968. Mass Loss from Stars, Springer-Verlag Inc., New York, editor Hack, p. 1.

Faulkner, J. 1970. Ap.J. 162, 513.

Ferraro, V.C.A. and Plumpton, C. 1966. Magneto-Fluid Mechanics, O.U.P. London.

Gahm, G.F. 1970. Astron. Astrophys. 8, 73.

Grzedielski, S. 1968. Acta Astron. 18, 479.

Hartle, R.E. and Sturrock, P.A. 1968. Ap.J. 151, 1155.

Hazlehurst, J. 1961. Advances Astron. Astrophys. 1, 1.

1967. Z.Ap. 65, 311.

Hoyle, F. and Fowler, W.A. 1960. Ap.J. 132, 565.

Hutchings, J.B. 1968a. Mass Loss From Stars, p.49.

1968b. M.N.R.A.S. 141, 219.

1968c. M.N.R.A.S. 141, 329.

1968d. M.N.R.A.S. 144, 235.

1970a. M.N.R.A.S. 147, 367.

1970b. M.N.R.A.S. 150, 55.

Iben, I. and Faulkner, J. 1968. Ap.J. 153, 101.

Jackson, J.D. 1962. Classical Electrodynamics. Wiley, New York.

Jager, C.de 1963. Introduction to Solar Terrestrial Relations, editors, Ortner and Maseland, p.26.

Kippenhahn, R., Kohl, K. and Weigert, A. 1967. Z.Ap. 66, 58.

Kippenhahn, R. and Weigert, A. 1967. Z.Ap. 65, 251.

Kraft, R.P. 1967. Ap.J. 150, 551.

Kuhi, L.V. 1966. Stellar Evolution, p. 377.

Kunz, K.S. 1957. Numerical Analysis, McGraw Hill, New York.

Kutter, G.S., Savedoff, M.P. and Schuermann, D.W. 1969. Astrophys. Space Sci. 3, 182.

Loore, C.de 1970. Astrophys. Space Sci. 6,60.

Lucy, L.B. and Solomon, P.M. 1967. Astron.J. 72, 310.
1970. Ap.J. 159, 879.

McCrea, W.H. 1964. M.N.R.A.S. 128, 147

Mestel, L. 1968. M.N.R.A.S. 138, 359.

Meyer-Hofmeister, E. and Thomas, H.C. 1970. Astron.and Astrophys. 5, 490.

Morton, D.C. 1968. Mass Loss from Stars, p.36.

Morton, D.C., Jenins, and Brooks. 1969. Ap.J. 155, 875.

Nariai, K. 1968. Mass Loss from Stars, p.122.

Noble, L.M. and Scarf, F.L. 1963. Ap.J. 138, 1169.

Ostriker, J.P. and Bodenheimer. 1968.

Ostriker, J.P. and Gunn, J.E. 1971. Ap.J. 164, L95.

Paczynski, B. 1970. Acta. Astron. 20, 47.

Paczynski, B. and Ziolkowski, J. 1968. Acta. Astron. 18, 255.

Parker, E.N. 1958. Ap.J. 128, 664.
1961a. Ap.J. 133, 1014.
1961b. Ap.J. 134, 20.
1963 Interplanetary Dynamical Processes, Interscience Publishers, New York.
1964a. Ap.J. 139, 72.
1964b. Ap.J. 139, 93.
1967. Prog.Elem.Part. and Cosmic Ray Phys. 9, 3.

Plavec, M. 1967. Highlights of Astronomy, D. Reidel, Dordrecht, editor,Perek.

Prendergast, K.H. 1960. Ap.J. 132, 162.

Roberts, K.V. and Potter, D.E. 1970. Methods in Comp. Phys. 9, 339.

Rose, J. 1967. Highlights of Astronomy. p.453.

Sahade, J. 1968. Mass Loss from Stars. p. 156.

Sargent, W.L.W. 1961. Ap.J. 134, 142.

Sargent, W.L.W. and Osmer, P.S. 1968. Mass Loss from Stars, p. 57.

Scarf, F.L. and Noble, L.M. 1965. Ap.J. 141, 1479.

Schwarzschild, M. 1948. Ap.J. 107,1.

Simon, G.W. and Leighton, R.B. 1964. Ap.J. 140, 1120.

Smith; L.F. 1967. Astron. J. 72, 829.

Spitzer, L. 1962. Physics of Fully Ionised Gases, Interscience, New York.

Strom and Strom. 1970. Ap.J. 162, 523.

Underhill, A.B. 1968. Mass Loss from Stars. p. 17.

Wade, and Hjellming. 1971. Ap.J. 163, L105.

Weber, E.J. and Davis, L. 1967. Ap.J. 148, 217.

Weymann, R. 1962. Ap.J. 136, 844.

1963. Ann. Rev. Astron. Astrophys. 1, 97.

Whang, Y.C. and Chang, C.C. 1965. J. Geophys. Res. 70, 4175.

Whang, Y.C., Liu, C.K. and Chang, C.C. 1966 Ap.J. 145, 255.

Wickramasinghe, N.C. 1966. Ap.J. 146, 590.

Williams, I.P. 1968. Mass Loss from Stars. p. 139.

Wilson, O.C. 1960. Ap.J. 131, 75.

1963. Ap.J. 138, 832.

1966. Ap.J. 144, 695.

Surname: MURCH Given Names: MARTIN ROBERT

Place of Birth: HARROGATE, ENGLAND

Date of Birth: October 27, 1947

Educational Institutions Attended, with Dates of Entering and Leaving:

UNIVERSITY OF SUSSEX	1965 to 1968
UNIVERSITY OF VICTORIA	1968 to 1971

Degrees, Diplomas, Etc., Awarded, with Dates and Names of Institutions:

B.Sc.	1968	UNIVERSITY OF SUSSEX

Awards:

University of Victoria Scholarship 1968-1970

THE UNIVERSITY OF VICTORIA LIBRARY

MANUSCRIPT DISSERTATION (or THESIS)

AUTHORITY TO DISTRIBUTE

AUTHOR: This dissertation may be lent or microfilm copies made available:

(a) Without restriction [redacted]...

(b) With the restriction that, for a period of five years (until)the written approval of the following is required:

(1) The Chairman, School of Graduate Studies .....

(2) The Author .....

(3) both the Chairman, School of Graduate Studies, and the Author .....

BORROWERS: The borrower undertakes, by signing below, to give proper credit for any use made of the dissertation, and to obtain the consent of the author if it is proposed to make extensive quotations, or to reproduce the dissertation in whole or in part.

Signature of Borrower	Address	Date